Electronic Research Archive

http://www.aimspress.com/journal/MBE

ERA, 33(9): xx–xx.
DOI:
Received: 29 June 2025
Revised: 13 August 2025
Accepted: 13 August 2025
Published: September 2025

Research article

A second-order accurate numerical scheme for Ericksen-Leslie system with penalty terms and defect dynamics in flows of nematic liquid crystals

Tianxin Lv[1], **Cheng Wang**[2,*] **and Zhengru Zhang** [3]

[1] School of Mathematical Sciences, Beijing Normal University, Beijing 100875, China
[2] Department of Mathematics, The University of Massachusetts, North Dartmouth, MA 02747, USA
[3] Laboratory of Mathematics and Complex Systems, Ministry of Education and School of Mathematical Sciences, Beijing Normal University, Beijing 100875, China

* **Correspondence:** Email: cwang1@umassd.edu.

Abstract: In this article, we study a second-order numerical scheme for the Ericksen-Leslie system. A modified Crank-Nicolson temporal discretization is adopted, and the pressure projection approach is used to decouple the Stokes solver. The second-order convex-concave decomposition is applied to the chemical potential vector, in which the convex nonlinear term is updated by a modified Crank-Nicolson approximation, the expansive concave term is computed by an explicit Adams-Bashforth extrapolation, and the surface diffusion part is discretized by the standard Crank-Nicolson interpolation. Meanwhile, semi-implicit second-order approximations are taken for the convection terms, in both the momentum equation and the orientation vector evolutionary equation, as well as the coupled elastic stress terms. In fact, these semi-implicit terms could be represented as a monotone, linear operator of a vector potential, and its combination with the second order convex splitting approximation to the chemical potential yields a closed nonlinear system of equations for the orientation vector function. The unique solvability analysis of the numerical system is established with the help of the Browder-Minty lemma. A combination of the second order convex splitting approximation to chemical potential vector and the semi-implicit discretization for the coupled terms leads to the total energy stability estimate, composed of kinematic energy and internal elastic free energy. Moreover, an optimal rate convergence analysis and error estimate are provided, with second-order accuracy in both time and space. Some numerical simulation results of liquid crystals' molecular dynamics are presented to study the scientific issue of defect annihilation. These results are consistent with the existing literature, and the energy evolution in the defect annihilation process is in agreement with the expectations. In addition, the influence of different parameters on the defect annihilation time instant is tested, and the results also agree with the physical laws.

Keywords: nematic phase liquid crystal model; finite difference spatial discretization; unique solvability; total energy stability; convergence analysis and error estimate; preconditioned steepest descent

iteration algorithm

1. Introduction

A liquid crystal is an intermediate molecular phase between conventional liquids and solids. It can flow like a liquid, while it also exhibits a partial order at the mesoscopic scale normally observed in a solid phase, due to its anisotropic microstructures. Liquid crystal material is widely used in the field of liquid crystal displays, nano science, biophysics [1–5, 45], etc. Since a liquid crystal is a typical complex flow, the related theories and numerical methods may be extended to other areas, such as the interface problem, active matter, polymer and hydrogel.

There are three major classes of liquid crystals [3]: Nematic, cholesteric, and smectic. Three types of models have been used in their description: The vector model, including Oseen-Frank theory [5] and Ericksen's theory [2, 4]; the molecular model [6, 7] proposed by Onsager to characterize the nematic-isotropic phase transition, and the third type is the Q-tensor model including the Landau-de Gennes theory [1]. One simple phase of a liquid crystal is the nematic phase, where the calamitic or rod-shaped molecules have no positional order but demonstrate a long-range orientational order formed by their long axes. In this paper, we study the Ericksen and Leslie dynamic nematic crystal system [2, 4], based on the Oseen-Frank theory [8, 9]:

$$\boldsymbol{u}_t + \boldsymbol{u}\cdot\nabla\boldsymbol{u} + \nabla p - \nu\Delta\boldsymbol{u} - \lambda\nabla\cdot((\nabla\boldsymbol{d})^T(\nabla\boldsymbol{d}) + \beta(\Delta\boldsymbol{d} - f(\boldsymbol{d})^T)\boldsymbol{d}^T + (1+\beta)\boldsymbol{d}(\Delta\boldsymbol{d} - f(\boldsymbol{d}))^T) = 0, \quad (1.1)$$

$$\nabla\cdot\boldsymbol{u} = 0, \quad (1.2)$$

$$\boldsymbol{d}_t + \boldsymbol{u}\cdot\nabla\boldsymbol{d} + (\beta\nabla\boldsymbol{u} + (1+\beta)(\nabla\boldsymbol{u})^T)\boldsymbol{d} = \gamma(\Delta\boldsymbol{d} - f(\boldsymbol{d})), \quad (1.3)$$

with the initial conditions

$$\boldsymbol{u}|_{t=0} = \boldsymbol{u}_0, \quad \boldsymbol{d}|_{t=0} = \boldsymbol{d}_0, \quad \boldsymbol{u}\cdot\boldsymbol{n}|_{\partial\Omega} = \boldsymbol{d}\cdot\boldsymbol{n}|_{\partial\Omega} = 0, \quad \left.\frac{\partial(\boldsymbol{u}\cdot\boldsymbol{\tau})}{\partial\boldsymbol{n}}\right|_{\partial\Omega} = \left.\frac{\partial(\boldsymbol{d}\cdot\boldsymbol{\tau})}{\partial\boldsymbol{n}}\right|_{\partial\Omega} = 0,$$

where $\Omega \subset \mathbb{R}^N (N = 2, 3)$ is a bounded domain with a Lipschitz boundary. The vector $\boldsymbol{u}(t, x) \in \mathbb{R}^N$ is the liquid crystal's velocity, $p(t, x) \in \mathbb{R}$ represents the pressure, and the vector $\boldsymbol{d}(t, x) \in \mathbb{S}^{N-1}$ turns out to be the orientation of the liquid crystal molecules. Moreover, ν, λ, γ are positive parameters: ν is the viscosity constant, λ is the elasticity constant, and γ stands for the time relax constant. The parameter $\beta \in [-1, 0]$ depends on the shape of the crystal molecule; for example, $\beta < -0.5$ for a rod-like liquid crystal molecule, $\beta > -0.5$ for a disc-like liquid crystal molecular, and $\beta = -0.5$ is associated with a spherical liquid crystal molecule. The vector function may be viewed as a penalty function to approximate the constraint $|\boldsymbol{d}| = 1$, since liquid crystal molecules are of asimilar size

$$f(\boldsymbol{d}) = \varepsilon^{-2}(|\boldsymbol{d}|^2 - 1)\boldsymbol{d},$$

in which $\varepsilon > 0$ stands for the interface width parameter. This penalty term is physically meaningful and stands for a possible relaxation of molecules from the strict unit-length constraint. Such an approach could also be viewed as a regularization method, in comparison with the limit system where $|\boldsymbol{d}| = 1$ (as $\varepsilon \to 0$) is rigidly imposed.

The chemical potential $\boldsymbol{\mu} = f(\boldsymbol{d}) - \Delta\boldsymbol{d} = (\mu_1, \mu_2, \mu_3)^T$ is a vector with the following components:

$$\mu_i = \varepsilon^{-2}(|\boldsymbol{d}|^2 - 1)d_i - \Delta d_i, \qquad i = 1, 2, 3.$$

In Eq (1.3), we introduce a term

$$D_\beta(\boldsymbol{u}) = \beta\nabla\boldsymbol{u} + (1+\beta)(\nabla\boldsymbol{u})^T,$$

and rewrite it as

$$D_\beta(\boldsymbol{u}) = -\frac{\nabla\boldsymbol{u} - (\nabla\boldsymbol{u})^T}{2} - (-2\beta - 1)\frac{\nabla\boldsymbol{u} + (\nabla\boldsymbol{u})^T}{2}.$$

In fact, the first term corresponds to the rotation of the liquid crystal molecules, and the second term implies the deformation. It is clear that there is no deformation if $\beta = -0.5$.

On the other hand, the original partial differential equation (PDE) system (1.1)–(1.3) needs to be reformulated to simplify the numerical effort. The following identity is recalled:

$$\nabla\cdot\Big((\nabla\boldsymbol{d})^T\nabla\boldsymbol{d}\Big) = (\nabla\boldsymbol{\mu})^T\boldsymbol{d} + \nabla\pi, \quad \pi := \frac{1}{2}|\nabla\boldsymbol{d}|^2 + \boldsymbol{d}\cdot\Delta\boldsymbol{d} - \frac{1}{4}(|\boldsymbol{d}|^2-1)^2 - \frac{1}{2}|\boldsymbol{d}|^2. \tag{1.4}$$

In turn, the original PDE system (1.1)–(1.3) could be rewritten as

$$\partial_t\boldsymbol{u} + \boldsymbol{u}\cdot\nabla\boldsymbol{u} + \nabla p' - \nu\Delta\boldsymbol{u} + \lambda(\nabla\boldsymbol{\mu})^T\boldsymbol{d} + \lambda\nabla\cdot\Big(\beta\boldsymbol{\mu}\boldsymbol{d}^T + (\beta+1)\boldsymbol{d}\boldsymbol{\mu}^T\Big) = 0, \tag{1.5}$$

$$\nabla\cdot\boldsymbol{u} = 0, \tag{1.6}$$

$$\partial_t\boldsymbol{d} + \boldsymbol{u}\cdot\nabla\boldsymbol{d} + (\beta\nabla\boldsymbol{u} + (1+\beta)(\nabla\boldsymbol{u})^T)\boldsymbol{d} = -\gamma\boldsymbol{\mu}, \tag{1.7}$$

where $p' = p + \lambda\pi$ is introduced as a modified pressure. For simplicity of presentation, we use the modified pressure but drop the prime notation.

In recent years, many theoretical analyses for the coupled Ericksen-Leslie PDE system have been reported. The existence and uniqueness of the solution are established in [10], and the long-term asymptotic behavior of the nematic liquid crystal is presented. The theoretical results on the global classical solution of the Ericksen-Leslie system is studied in [11]. Meanwhile, the regularity and existence of the global solution to the Ericksen-Leslie system in $\mathbb{R}^2$ is studied in [12]. A modified Ericksen-Leslie model is applied to the research on the mixture of liquid crystals and viscous flow [13–15] and some related biological phenomena [16].

The free energy for the orientation vector $\boldsymbol{d}$ is introduced as

$$E(\boldsymbol{d}) = \int_\Omega \Big(\varepsilon^{-2}(\frac{1}{4}|\boldsymbol{d}|^4 - \frac{1}{2}|\boldsymbol{d}|^2) + \frac{1}{2}|\nabla\boldsymbol{d}|^2\Big)\,\mathrm{d}\boldsymbol{x}.$$

It is observed that $\mathrm{d}_t E(\boldsymbol{d}) = \int_\Omega \partial_t\boldsymbol{d}\cdot\boldsymbol{\mu}\,\mathrm{d}\boldsymbol{x}$. Taking the inner products with (1.1) by $\boldsymbol{u}$, with (1.3) by $\lambda\boldsymbol{\mu}$, we obtain the total energy dissipation law:

$$\frac{\mathrm{d}}{\mathrm{d}t}\Big(\frac{1}{2}\|\boldsymbol{u}\|^2 + \lambda E(\boldsymbol{d})\Big) = -\nu\|\nabla\boldsymbol{u}\|^2 - \gamma\|\boldsymbol{\mu}\|^2 \le 0.$$

Other than the total energy dissipation law, there is no other physical property preservation for the orientation vector $\boldsymbol{d}$. Because of an L^2 type gradient flow structure in Eq (1.7), a mass conservation

for $\boldsymbol{d}$ is not available. Moreover, although the limit PDE system of (1.5)–(1.7) preserves a point-wise constraint $|\boldsymbol{d}| \equiv 1$ as $\varepsilon \to 0$, such a normalization is not valid for a fixed $\varepsilon > 0$.

There have been extensive numerical works on the Ericksen-Leslie system. The following essential issues of the PDE system have to be considered: (i) Total energy dissipation, (ii) the incompressibility of the flow ($\nabla \cdot \boldsymbol{u} = 0$), (iii) the treatment on the coupled term, (iv) and the nonlinearity of the penalty function. To simplify the computation, there are many simplified models, such as the $1+2$ model [17,18] and the ones omitting Leslie stress D_β. Actually, the reduced models are physically incorrect for flows of liquid crystal, since they do not obey the frame-invariant principle, and the elastic stress is not included in the system, either. One may argue that the reduced models may be acceptable when the velocity gradient is small and the elastic stress is weak at the same time. However, these two effects can rarely be weak simultaneously, in general. Hence, the reduced models have very limited applicability to real liquid crystal flows; see the related simulations in [19]. Therefore, the elastic stress has to be included in the Ericksen-Leslie system. A C^0 finite element method was proposed in [20], and a mixed finite element algorithm was designed in [21]. A more recent work [22] develops a fully discrete finite difference scheme, based on the first order accurate convex splitting of the free energy functional; the unique solvability, total energy stability, and convergence analysis were provided. A second order backward differentiation formula (BDF2) numerical scheme is studied in [23], where external interpolation such as $2\boldsymbol{d}^n - \boldsymbol{d}^{n-1}$ is used for explicit terms, and the pressure gradient is decoupled with the velocity vector in the Navier-Stokes equation. Meanwhile, the pressure correction with a rotational form is adopted in [24], which avoids the difficulty associated with the artificial Neumann boundary condition. Furthermore, an observation on the liquid crystal defects is reported in [23]. In addition, a second-order Crank-Nicolson scheme is reported in [19], where the energy stability estimate has been derived, while no convergence analysis is available. More recent works can be found in [25,26], etc.

In this paper, we will propose a second-order accurate, Crank-Nicolson type numerical scheme, and provide a theoretical analysis on the unique solvability, total energy stability, and convergence. Similar to [19], the Crank-Nicolson interpolation is used to handle the implicit approximation, while the Adams-Bashforth extrapolation is applied to the explicit one. Regarding the chemical potential vector μ, the idea of second order accurate convex splitting is adopted: The nonlinear polynomial expansion is discretized by a modified Crank-Nicolson approximation, which comes from its convexity; the expansive and linear concave term is computed by an explicit Adams-Bashforth extrapolation; and the surface diffusion part is updated by the standard Crank-Nicolson method. For the convection terms, semi-implicit second order approximations are applied in both the momentum equation and the orientation vector's evolutionary equation. Again, a combination of second-order Adams-Bashforth explicit extrapolation and Crank-Nicolson interpolation has to be used in the semi-implicit discretization. Moreover, the coupled elastic stress terms are also computed by semi-implicit approximation. In the unique solvability analysis, it is observed that these semi-implicit terms could be represented as a monotone, linear operator of a vector potential, and its combination with the second-order convex splitting approximation to chemical potential yields a closed nonlinear system of equations for the orientation vector's function. In turn, a careful application of the Browder-Minty lemma implies the unique solvability of the numerical system. Moreover, a careful analysis reveals a modified total energy stability estimate, composed of the kinematic energy and internal elastic free energy.

The optimal rate convergence analysis and error estimate contains more technical details. An $\ell^\infty(0,T;H_h^1) \cap \ell^2(0,T;H_h^2)$ error estimate for the orientation vector variable $\boldsymbol{d}$, combined with an

$\ell^\infty(0,T;\ell^2)\cap\ell^2(0,T;H_h^1)$ error estimate for the velocity vector, is needed in the convergence analysis. In other words, the error estimate in the total energy forms leads to the cancellation of three nonlinear coupled inner products, with an appropriate error test function, between the momentum and orientation error equations. This technique has been used in theoretical analyses for various coupled physical systems, such as Cahn-Hilliard-Hele-Shaw [27, 30, 32], Cahn-Hilliard-Navier-Stokes [29, 31], Cahn-Hilliard-Stokes-Darcy [28], MHD [33–35] equations; meanwhile, the technical details for Eriksen-Leslie system turn out to be more complicated, due to the fact that the orientation variable is a vector instead of a scalar function. With the help of the discrete L^6 bounds of the numerical solution, the second-order convergence rate is derived in both time and space.

This paper is organized as follows. In Section 2, we propose the fully-discrete Crank-Nicolson style numerical scheme. In Section 3, the unique solvability is proved for the numerical system, and a modified energy stability analysis is established. Moreover, an optimal rate convergence analysis is provided in Section 4. Subsequently, some numerical experiments are presented in Section 5. Finally, some concluding remarks are made in Section 6.

2. The fully discrete Crank-Nicolson style numerical scheme

Consider $\Omega=(0,1)^2\subset\mathbb{R}^2$ and let $h=1/N$ be the spatial size. An extension to the three-dimensional domain would be straightforward, and all the theoretical analysis is expected to proceed in the same manner. The orientation vector $\boldsymbol{d}$, the pressure p, and the chemical potential vector $\boldsymbol{\mu}$ are defined at the mesh center $((i+\frac{1}{2})h,(j+\frac{1}{2})h)$, while the related gradients are evaluated at $((ih,(j+\frac{1}{2})h),((i+\frac{1}{2})h,jh)$ as follows:

$$(D_x d_k)_{i,j+\frac{1}{2}}=\frac{(d_k)_{i+\frac{1}{2},j+\frac{1}{2}}-(d_k)_{i-\frac{1}{2},j+\frac{1}{2}}}{h},\quad (D_y d_k)_{i+\frac{1}{2},j}=\frac{(d_k)_{i+\frac{1}{2},j+\frac{1}{2}}-(d_k)_{i+\frac{1}{2},j-\frac{1}{2}}}{h},\ k=1,2.$$

The discrete Laplacian operator Δ_h is given by the standard centered-difference approximation:

$$(\Delta_h d_k)_{i+\frac{1}{2},j+\frac{1}{2}}=\frac{(d_k)_{i+\frac{3}{2},j+\frac{1}{2}}+(d_k)_{i-\frac{1}{2},j+\frac{1}{2}}+(d_k)_{i+\frac{1}{2},j+\frac{3}{2}}+(d_k)_{i+\frac{1}{2},j-\frac{1}{2}}-4(d_k)_{i+\frac{1}{2},j+\frac{1}{2}}}{h^2}.$$

The gradient of chemical potential $\boldsymbol{\mu}$ is approximated at the mesh center as

$$(\widetilde{D}_x\mu_k)_{i+\frac{1}{2},j+\frac{1}{2}}=\frac{(\mu_k)_{i+\frac{3}{2},j+\frac{1}{2}}-(\mu_k)_{i-\frac{1}{2},j+\frac{1}{2}}}{2h},\qquad (\widetilde{D}_y\mu_k)_{i+\frac{1}{2},j+\frac{1}{2}}=\frac{(\mu_k)_{i+\frac{1}{2},j+\frac{3}{2}}-(\mu_k)_{i+\frac{1}{2},j-\frac{1}{2}}}{2h}.$$

The components v^x, v^y of the velocity $\boldsymbol{v}$ are evaluated at the staggered grids $(ih,(j+\frac{1}{2})h),((i+\frac{1}{2})h,jh)$. The discrete divergence of the velocity is defined at the mesh centers $((i+\frac{1}{2})h,(j+\frac{1}{2})h)$:

$$(\nabla_h\cdot\boldsymbol{v})_{i+\frac{1}{2},j+\frac{1}{2}}:=(D_x v^x)_{i+\frac{1}{2},j+\frac{1}{2}}+(D_y v^y)_{i+\frac{1}{2},j+\frac{1}{2}}.$$

A cell-centered function ϕ is said to satisfy the homogeneous Neumann boundary condition if

$$\phi_{-1/2,j+1/2}=\phi_{1/2,j+1/2},\quad \phi_{N+1/2,j+1/2}=\phi_{N-1/2,j+1/2},$$

$$\phi_{i+1/2,-1/2}=\phi_{i+1/2,1/2},\quad \phi_{i+1/2,N+1/2}=\phi_{i+1/2,N-1/2}.$$

In this case, we assume $\boldsymbol{n}\cdot\nabla_h\phi = 0$. A cell-centered function $\boldsymbol{f} = (f^x, f^y)^T$ is said to have a zero normal component, namely $\boldsymbol{n}\cdot\boldsymbol{f} = 0$, if we have

$$f^x_{-1/2,j+1/2} + f^x_{1/2,j+1/2} = 0, \quad f^x_{N+1/2,j+1/2} + f^x_{N-1/2,j+1/2} = 0,$$
$$f^y_{i+1/2,1/2} + f^y_{i+1/2,-1/2} = 0, \quad f^y_{i+1/2,N+1/2} + f^y_{i+1/2,N-1/2} = 0.$$

Subsequently, the evaluation of the coupled terms is given by the following formulas:

$$\nabla_h\cdot\left(\boldsymbol{v}\boldsymbol{u}^T\right) = \begin{pmatrix} \widetilde{D}_x\left(u^x v^x\right)_{i,j+1/2} + \widetilde{D}_y\left(\mathcal{A}_{xy}u^y v^x\right)_{i,j+1/2} \\ \widetilde{D}_x\left(\mathcal{A}_{xy}u^x v^y\right)_{i+1/2,j} + \widetilde{D}_y\left(u^y v^y\right)_{i+1/2,j} \end{pmatrix},$$
$$\left(\nabla_h\boldsymbol{\mu}\right)^T\boldsymbol{d} = \begin{pmatrix} \left(D_x\mu^x\cdot\mathcal{A}_x d^x\right)_{i,j+1/2} + \left(D_x\mu^x\cdot\mathcal{A}_x d^y\right)_{i,j+1/2} \\ \left(D_y\mu^x\cdot\mathcal{A}_y d^x\right)_{i+1/2,j} + \left(D_y\mu^y\cdot\mathcal{A}_y d^y\right)_{i+1/2,j} \end{pmatrix},$$
$$\nabla_h\cdot\left(\boldsymbol{\mu}\boldsymbol{d}^T\right) = \begin{pmatrix} D_x\left(\mu^x d^x\right)_{i,j+1/2} + \mathcal{A}_x\widetilde{D}_y\left(\mu^x d^y\right)_{i,j+1/2} \\ \mathcal{A}_y\widetilde{D}_x\left(\mu^y d^x\right)_{i+1/2,j} + D_y\left(\mu^y d^y\right)_{i+1/2,j} \end{pmatrix},$$
$$\nabla_h\cdot\left(\boldsymbol{d}\boldsymbol{\mu}^T\right) = \begin{pmatrix} D_x\left(\mu^x d^x\right)_{i,j+1/2} + \mathcal{A}_x\widetilde{D}_y\left(\mu^y d^x\right)_{i,j+1/2} \\ \mathcal{A}_y\widetilde{D}_x\left(\mu^x d^y\right)_{i+1/2,j} + D_y\left(\mu^y d^y\right)_{i+1/2,j} \end{pmatrix},$$
$$\nabla_h\cdot\left(\boldsymbol{d}\boldsymbol{u}^T\right) = \begin{pmatrix} D_x\left(\mathcal{A}_x d^x u^x\right)_{i+1/2,j+1/2} + D_y\left(\mathcal{A}_y d^x u^y\right)_{i+1/2,j+1/2} \\ D_x\left(\mathcal{A}_x d^y u^x\right)_{i+1/2,j+1/2} + D_y\left(\mathcal{A}_y d^y u^y\right)_{i+1/2,j+1/2} \end{pmatrix},$$
$$\left(\nabla_h\boldsymbol{u}\right)\boldsymbol{d} = \begin{pmatrix} \left(D_x u^x\cdot d^x\right)_{i+1/2,j+1/2} + \left(\mathcal{A}_x\widetilde{D}_y u^x\cdot d^y\right)_{i+1/2,j+1/2} \\ \left(\mathcal{A}_y\widetilde{D}_x u^y\cdot d^x\right)_{i+1/2,j+1/2} + \left(D_y u^y\cdot d^y\right)_{i+1/2,j+1/2} \end{pmatrix},$$
$$\left(\nabla_h\boldsymbol{u}\right)^T\boldsymbol{d} = \begin{pmatrix} \left(D_x u^x\cdot d^x\right)_{i+1/2,j+1/2} + \left(\mathcal{A}_y\widetilde{D}_x u^y\cdot d^y\right)_{i+1/2,j+1/2} \\ \left(\mathcal{A}_x\widetilde{D}_y u^x\cdot d^x\right)_{i+1/2,j+1/2} + \left(D_y u^y\cdot d^y\right)_{i+1/2,j+1/2} \end{pmatrix},$$

in which the following average operators are introduced:

$$\mathcal{A}_{xy}u^x_{i+1/2,j} = \frac{1}{4}\left(u^x_{i,j-1/2} + u^x_{i,j+1/2} + u^x_{i+1,j-1/2} + u^x_{i+1,j+1/2}\right),$$
$$\left(\mathcal{A}_x\widetilde{D}_y\mu^x\right)_{i,j+1/2} = \frac{1}{2}\left(\widetilde{D}_y\mu^x_{i-1/2,j+1/2} + \widetilde{D}_y\mu^x_{i+1/2,j+1/2}\right),$$
$$\mathcal{A}_x d^y_{i,j+1/2} = \frac{1}{2}\left(d^y_{i-1/2,j+1/2} + d^y_{i+1/2,j+1/2}\right),$$
$$\left(\mathcal{A}_x\widetilde{D}_y u^x\right)_{i+1/2,j+1/2} = \frac{1}{2}\left(\widetilde{D}_y u^x_{i,j+1/2} + \widetilde{D}_y u^x_{i+1,j+1/2}\right).$$

Meanwhile, the following notations are introduced to simplify the presentation:

$$\boldsymbol{d}^{n+\frac{1}{2}} = \frac{1}{2}(\boldsymbol{d}^{n+1} + \boldsymbol{d}^n), \quad \tilde{\boldsymbol{d}}^{n+\frac{1}{2}} = \frac{1}{2}(3\boldsymbol{d}^n - \boldsymbol{d}^{n-1}),$$
$$\boldsymbol{u}^{n+\frac{1}{2}} = \frac{1}{2}(\boldsymbol{u}^{n+1} + \boldsymbol{u}^n), \quad \tilde{\boldsymbol{u}}^{n+\frac{1}{2}} = \frac{1}{2}(3\boldsymbol{u}^n - \boldsymbol{u}^{n-1}).$$

The chemical potential vector is computed by a second-order convex splitting approach:

$$\boldsymbol{\mu}^{n+\frac{1}{2}} = (\mu_1^{n+\frac{1}{2}}, \mu_2^{n+\frac{1}{2}})^T = \varepsilon^{-2}\Big(\frac{|\boldsymbol{d}^{n+1}|^2 + |\boldsymbol{d}^n|^2}{2}\boldsymbol{d}^{n+\frac{1}{2}} - \tilde{\boldsymbol{d}}^{n+\frac{1}{2}}\Big) - \Delta_h \boldsymbol{d}^{n+\frac{1}{2}},$$
$$\text{with} \quad \mu_i^{n+\frac{1}{2}} = \varepsilon^{-2}\Big(\frac{|\boldsymbol{d}^{n+1}|^2 + |\boldsymbol{d}^n|^2}{2} d_i^{n+\frac{1}{2}} - \tilde{d}_i^{n+\frac{1}{2}}\Big) - \Delta_h d_i^{n+\frac{1}{2}}, \quad i = 1, 2.$$

In turn, the full discrete Crank-Nicolson style numerical scheme is proposed as follows:

$$\frac{\overline{\boldsymbol{u}}^{n+1} - \boldsymbol{u}^n}{\Delta t} + \frac{1}{2}(\tilde{\boldsymbol{u}}^{n+\frac{1}{2}} \cdot \nabla_h \overline{\boldsymbol{u}}^{n+\frac{1}{2}} + \nabla_h \cdot (\tilde{\boldsymbol{u}}^{n+\frac{1}{2}} \overline{\boldsymbol{u}}^{n+\frac{1}{2}})) + \nabla_h p^n - \nu \Delta_h \overline{\boldsymbol{u}}^{n+\frac{1}{2}} + \lambda(\nabla_h \boldsymbol{\mu}^{n+\frac{1}{2}})\tilde{\boldsymbol{d}}^{n+\frac{1}{2}}$$
$$+ \lambda \nabla_h \cdot (\beta \boldsymbol{\mu}^{n+\frac{1}{2}}(\tilde{\boldsymbol{d}}^{n+\frac{1}{2}})^T + (\beta + 1)\tilde{\boldsymbol{d}}^{n+\frac{1}{2}}(\boldsymbol{\mu}^{n+\frac{1}{2}})^T) = 0, \tag{2.1}$$
$$\frac{\boldsymbol{u}^{n+1} - \overline{\boldsymbol{u}}^{n+1}}{\Delta t} + \frac{1}{2}\nabla_h(p^{n+1} - p^n) = 0, \tag{2.2}$$
$$\nabla_h \cdot \boldsymbol{u}^{n+1} = 0, \tag{2.3}$$
$$\frac{\boldsymbol{d}^{n+1} - \boldsymbol{d}^n}{\Delta t} + \nabla_h \cdot (\tilde{\boldsymbol{d}}^{n+\frac{1}{2}} \overline{\boldsymbol{u}}^{n+\frac{1}{2}}) + (\beta \nabla_h \overline{\boldsymbol{u}}^{n+\frac{1}{2}} + (1 + \beta)(\nabla_h \overline{\boldsymbol{u}}^{n+\frac{1}{2}})^T)\tilde{\boldsymbol{d}}^{n+\frac{1}{2}} = -\gamma \boldsymbol{\mu}^{n+\frac{1}{2}}, \tag{2.4}$$
$$\varepsilon^{-2}\Big(\frac{|\boldsymbol{d}^{n+1}|^2 + |\boldsymbol{d}^n|^2}{2}\boldsymbol{d}^{n+\frac{1}{2}} - \tilde{\boldsymbol{d}}^{n+\frac{1}{2}}\Big) - \Delta_h \boldsymbol{d}^{n+\frac{1}{2}} - \boldsymbol{\mu}^{n+\frac{1}{2}} = 0, \tag{2.5}$$

and the corresponding boundary conditions are

$$(\overline{\boldsymbol{u}}^{n+\frac{1}{2}} \cdot \boldsymbol{n})|_{\partial\Omega} = (\boldsymbol{d}^{n+\frac{1}{2}} \cdot \boldsymbol{n})|_{\partial\Omega} = (\boldsymbol{u}^{n+\frac{1}{2}} \cdot \boldsymbol{n})|_{\partial\Omega} = 0,$$
$$(\boldsymbol{n} \cdot \nabla_h(\overline{\boldsymbol{u}}^{n+\frac{1}{2}} \cdot \boldsymbol{\tau}))|_{\partial\Omega} = (\boldsymbol{n} \cdot \nabla_h(\boldsymbol{d}^{n+\frac{1}{2}} \cdot \boldsymbol{\tau}))|_{\partial\Omega} = 0.$$

According to the given initial data $\boldsymbol{u}^0, \boldsymbol{d}^0$, the initial chemical potential can vector is computed as

$$\boldsymbol{\mu}^0 = \varepsilon^{-2}(|\boldsymbol{d}^0|^2 \boldsymbol{d}^0 - \boldsymbol{d}^0) - \Delta_h \boldsymbol{d}^0.$$

On the other hand, the initial pressure is determined via the following equation:

$$-\Delta_h p^0 = \nabla_h \cdot \Big(\frac{1}{2}(\boldsymbol{u}^0 \cdot \nabla_h \overline{\boldsymbol{u}}^0 + \nabla_h \cdot (\boldsymbol{u}^0 \overline{\boldsymbol{u}}^0)) + \lambda(\nabla_h \boldsymbol{\mu}^0)\boldsymbol{d}^0 + \lambda \nabla_h \cdot (\beta \boldsymbol{\mu}^0 (\boldsymbol{d}^0)^T + (\beta + 1)\boldsymbol{d}^0 (\boldsymbol{\mu}^0)^T)\Big),$$
$$(\boldsymbol{n} \cdot \nabla_h p^0)|_{\partial\Omega} = 0.$$

3. Unique solvability and energy stability analysis

Since the staggered mesh is adopted, we need to introduce the corresponding inner products.

Definition 3.1. *For any pair of variables u^a, u^b(such as u, $D_x\boldsymbol{d}$, $D_x\boldsymbol{\mu}$, $D_x p$, etc.), which are evaluated at the mesh points $(i, j + 1/2)$, the discrete L_h^2-inner is defined as:*

$$\langle u^a, u^b \rangle_A = h^2 \sum_{j=0}^{N-1} \sum_{i=0}^{N} \gamma_i^{(0)} u^a_{i,j+1/2} u^b_{i,j+1/2}; \quad \gamma_i^{(0)} = \begin{cases} \frac{1}{2}, & \text{if } i = 0 \text{ or } i = N, \\ 1, & \text{otherwise}, \end{cases}$$

for any pair of variables v^a, v^b which are evaluated at the mesh points $(i+1/2, j)$, (such as $v, D_y\boldsymbol{d}, D_y\boldsymbol{\mu}, D_y p$, etc.), the discrete L_h^2-inner product is defined as

$$\langle v^a, v^b\rangle_B = h^2 \sum_{j=0}^{N}\sum_{i=0}^{N-1} \gamma_j^{(1)} v^a_{i+1/2,j} v^b_{i+1/2,j}; \quad \gamma_j^{(1)} = \begin{cases} \frac{1}{2}, & \text{if } j=0 \text{ or } j=N, \\ 1, & \text{otherwise}, \end{cases}$$

for any pair of variables μ^a, μ^b which are evaluated at the mesh points $(i+1/2, j+1/2)$ (such as $\boldsymbol{\mu}$, $\boldsymbol{d}$, p, etc.), the discrete L_h^2-inner product is defined as

$$\langle \mu^a, \mu^b\rangle_C = h^2 \sum_{j=0}^{N-1}\sum_{i=0}^{N-1} \mu^a_{i+1/2,j+1/2}\mu^b_{i+1/2,j+1/2}.$$

In addition, for two velocity vectors $\boldsymbol{u} = (u^x, u^y)^T$ and $\boldsymbol{v} = (v^x, v^y)^T$, their vector inner product is defined as

$$\langle \boldsymbol{u}, \boldsymbol{v}\rangle_1 = \langle u^x, v^x\rangle_A + \langle u^y, v^y\rangle_B,$$

The corresponding L_h^2-norms, namely the $\|\cdot\|_2$ norm, are based on the inner product above. Of course, all the associated discrete L_h^2 inner products are second-order accurate. In addition to the standard L_h^2 norm, we need to introduce the discrete L_h^p, $1 \le p \le \infty$ and L_h^∞ norms for the grid functions

$$\|\boldsymbol{f}\|_\infty := \max_{i,j} \left|f_{i+1/2,j+1/2}\right|, \quad \|\boldsymbol{f}\|_p := \Big(h^2 \sum_{i,j=0}^{N-1} \left|f_{i+1/2,j+1/2}\right|^p\Big)^{\frac{1}{p}}, \quad 1 \leqslant p < \infty.$$

Lemma 3.1. *[22] For discrete grid functions $\boldsymbol{u}$, $\boldsymbol{v}$ (with the two components evaluated at $(x_i, y_{j+1/2})$ and $(x_{i+1/2}, y_j)$, respectively), $\boldsymbol{\mu}$, p, and $\boldsymbol{d}$ (evaluated at$(x_{i+1/2}, y_{j+1/2})$) satisfying the discrete boundary conditions*

$$(\boldsymbol{u}\cdot\boldsymbol{n})|_{\partial\Omega} = (\boldsymbol{v}\cdot\boldsymbol{n})|_{\partial\Omega} = (\boldsymbol{d}\cdot\boldsymbol{n})|_{\partial\Omega} = 0, \quad (\boldsymbol{n}\cdot\nabla_h(\boldsymbol{v}\cdot\boldsymbol{\tau}))|_{\partial\Omega} = (\boldsymbol{n}\cdot\nabla_h(\boldsymbol{d}\cdot\boldsymbol{\tau}))|_{\partial\Omega} = 0,$$

we have the following summation-by-parts identities:

$$\begin{aligned} \langle \boldsymbol{v}, \boldsymbol{u}\cdot\nabla_h\boldsymbol{v}\rangle_1 + \left\langle \boldsymbol{v}, \nabla_h\cdot\left(\boldsymbol{v}\boldsymbol{u}^T\right)\right\rangle_1 &= 0, \qquad (3.1)\\ \langle \boldsymbol{u}, \nabla_h p\rangle_1 &= 0, \quad \text{if } \nabla_h\cdot\boldsymbol{u} = 0, \text{and } (\boldsymbol{n}\cdot\boldsymbol{u})|_{\partial\Omega} = 0,\\ -\langle \boldsymbol{v}, \Delta_h\boldsymbol{v}\rangle_1 &= \|\nabla_h\boldsymbol{v}\|_2^2 := \|\nabla_h v^x\|_1^2 + \|\nabla_h v^y\|_2^2,\\ \langle \boldsymbol{v}, (\nabla_h\boldsymbol{\mu})^T\,\boldsymbol{d}\rangle_1 &= -\left\langle \boldsymbol{\mu}, \nabla_h\cdot\left(\boldsymbol{d}\boldsymbol{v}^T\right)\right\rangle_C,\\ \left\langle \boldsymbol{v}, \nabla_h\cdot\left(\boldsymbol{\mu}\boldsymbol{d}^T\right)\right\rangle_1 &= -\langle \boldsymbol{\mu}, (\nabla_h\boldsymbol{v})\,\boldsymbol{d}\rangle_C,\\ \left\langle \boldsymbol{v}, \nabla_h\cdot\left(\boldsymbol{d}\boldsymbol{\mu}^T\right)\right\rangle_1 &= -\langle \boldsymbol{\mu}, (\nabla_h\boldsymbol{v})^T\,\boldsymbol{d}\rangle_C. \qquad (3.2) \end{aligned}$$

For any cell-centered, vector grid function $\boldsymbol{d}$, the discrete version of the energy functional turns out to be

$$E_h(\boldsymbol{d}) := \varepsilon^{-2}\Big(\frac{1}{4}\|\boldsymbol{d}\|_4^4 - \frac{1}{2}\|\boldsymbol{d}\|_2^2\Big) + \frac{1}{2}\|\nabla_h\boldsymbol{d}\|_2^2. \qquad (3.3)$$

To simplify the unique solvability analysis, we need to introduce a linear operator $\mathcal{L}_h$. Assume that $\tilde{\boldsymbol{u}}^{n+\frac{1}{2}}$, $\tilde{\boldsymbol{d}}^{n+\frac{1}{2}}$ are given by p^n. For any vector $\boldsymbol{\mu}$, $\boldsymbol{v} = \mathcal{L}_h(\boldsymbol{\mu})$ is defined as the unique solution of the following convection-diffusion type equation:

$$\begin{aligned}\frac{2\boldsymbol{v} - 2\boldsymbol{u}^n}{\Delta t} + \frac{1}{2}(\tilde{\boldsymbol{u}}^{n+\frac{1}{2}} \cdot \nabla_h \boldsymbol{v} + \nabla_h \cdot (\tilde{\boldsymbol{u}}^{n+\frac{1}{2}} \boldsymbol{v})) + \nabla_h p^n - \nu \Delta \boldsymbol{v} + \lambda(\nabla_h \boldsymbol{\mu})\tilde{\boldsymbol{d}}^{n+\frac{1}{2}} \\ + \lambda \nabla_h \cdot (\beta \boldsymbol{\mu}(\tilde{\boldsymbol{d}}^{n+\frac{1}{2}})^T + (\beta+1)\tilde{\boldsymbol{d}}^{n+\frac{1}{2}}\boldsymbol{\mu}^T) = 0. \end{aligned} \tag{3.4}$$

In other words, for any given $(\tilde{\boldsymbol{u}}^{n+\frac{1}{2}}, \tilde{\boldsymbol{d}}^{n+\frac{1}{2}}, p^n)$, we write $\overline{\boldsymbol{u}}^{n+\frac{1}{2}} = \mathcal{L}_h(\boldsymbol{\mu}^{n+\frac{1}{2}})$. Moreover, the velocity at the next time step turns out to be $\boldsymbol{u}^{n+1} = \mathcal{P}_h \overline{\boldsymbol{u}}^{n+1}$, the Helmholtz projection of $\overline{\boldsymbol{u}}^{n+1}$. In turn, a substitution of $\overline{\boldsymbol{u}}^{n+\frac{1}{2}} = \mathcal{L}_h(\boldsymbol{\mu}^{n+\frac{1}{2}})$ into (2.4) gives the equations for $\boldsymbol{d}$ and $\boldsymbol{\mu}$

$$\frac{\boldsymbol{d}^{n+1} - \boldsymbol{d}^n}{\Delta t} = -\nabla_h \cdot (\tilde{\boldsymbol{d}}^{n+\frac{1}{2}} \mathcal{L}_h(\boldsymbol{\mu}^{n+\frac{1}{2}})) - (\beta \nabla_h \mathcal{L}_h(\boldsymbol{\mu}^{n+\frac{1}{2}})) - (1+\beta)(\nabla_h \mathcal{L}_h(\boldsymbol{\mu}^{n+\frac{1}{2}}))^T)\tilde{\boldsymbol{d}}^{n+\frac{1}{2}} - \gamma \boldsymbol{\mu}^{n+\frac{1}{2}}, \tag{3.5}$$

$$\boldsymbol{\mu}^{n+\frac{1}{2}} = \varepsilon^{-2}\Big(\frac{|\boldsymbol{d}^{n+1}|^2 + |\boldsymbol{d}^n|^2}{2}\boldsymbol{d}^{n+\frac{1}{2}} - \tilde{\boldsymbol{d}}^{n+\frac{1}{2}}\Big) - \Delta_h \boldsymbol{d}^{n+\frac{1}{2}}. \tag{3.6}$$

Of course, Eq (3.5) could be rewritten as

$$\frac{\boldsymbol{d}^{n+1} - \boldsymbol{d}^n}{\Delta t} = -\mathcal{G}_h(\boldsymbol{\mu}^{n+\frac{1}{2}}), \tag{3.7}$$

$$\mathcal{G}_h(\boldsymbol{\mu}) := \nabla_h \cdot (\tilde{\boldsymbol{d}}^{n+\frac{1}{2}} \mathcal{L}_h(\boldsymbol{\mu})) + (\beta \nabla_h \mathcal{L}_h(\boldsymbol{\mu}) + (1+\beta)(\nabla_h \mathcal{L}_h(\boldsymbol{\mu}))^T)\tilde{\boldsymbol{d}}^{n+\frac{1}{2}} + \gamma \boldsymbol{\mu}. \tag{3.8}$$

It is clear that $\mathcal{G}_h : (\mathbb{R}^{N^2})^2 \to (\mathbb{R}^{N^2})^2$ is a linear operator, prescribed with discrete boundary condition. In the following lemma, we prove that $\mathcal{G}_h$ is invertible.

Lemma 3.2. *The linear operator $\mathcal{G}_h$ satisfies the monotonicity condition:*

$$\langle \mathcal{G}_h(\boldsymbol{\mu}^{(1)}) - \mathcal{G}_h(\boldsymbol{\mu}^{(2)}), \boldsymbol{\mu}^{(1)} - \boldsymbol{\mu}^{(2)} \rangle_C \geq \gamma \|\boldsymbol{\mu}^{(1)} - \boldsymbol{\mu}^{(2)}\|^2 \geq 0, \tag{3.9}$$

for any $\boldsymbol{\mu}^{(1)}$, $\boldsymbol{\mu}^{(2)}$, and the equality holds if and only if $\boldsymbol{\mu}^{(1)} = \boldsymbol{\mu}^{(2)}$. As a result, the operator $\mathcal{G}_h$ is invertible.

Proof. Define $\tilde{\boldsymbol{\mu}} = \boldsymbol{\mu}^{(1)} - \boldsymbol{\mu}^{(2)}$. Since $\mathcal{G}_h$ is a linear operator, it is observed that

$$\mathcal{G}_h(\boldsymbol{\mu}^{(1)}) - \mathcal{G}_h(\boldsymbol{\mu}^{(2)}) = \nabla_h \cdot (\tilde{\boldsymbol{d}}^{n+\frac{1}{2}} \mathcal{L}_h(\tilde{\boldsymbol{\mu}})) + (\beta \nabla_h \mathcal{L}_h(\tilde{\boldsymbol{\mu}}) + (1+\beta)(\nabla_h \mathcal{L}_h(\tilde{\boldsymbol{\mu}}))^T)\tilde{\boldsymbol{d}}^{n+\frac{1}{2}} + \gamma \tilde{\boldsymbol{\mu}}. \tag{3.10}$$

Subsequently, its discrete inner product with $\tilde{\boldsymbol{\mu}}$ gives

$$\begin{aligned}\langle \mathcal{G}_h(\tilde{\boldsymbol{\mu}}), \tilde{\boldsymbol{\mu}} \rangle_C = &- \langle \nabla_h \tilde{\boldsymbol{\mu}} \tilde{\boldsymbol{d}}^{n+\frac{1}{2}}, \mathcal{L}_h(\tilde{\boldsymbol{\mu}}) \rangle_1 + \beta \langle \tilde{\boldsymbol{d}}^{n+\frac{1}{2}} \tilde{\boldsymbol{\mu}}^T, \nabla_h \mathcal{L}_h(\tilde{\boldsymbol{\mu}}) \rangle_C \\ &+ (1+\beta)\langle \tilde{\boldsymbol{d}}^{n+\frac{1}{2}} \tilde{\boldsymbol{\mu}}^T, \nabla_h \mathcal{L}_h(\tilde{\boldsymbol{\mu}}) \rangle_C + \gamma \|\tilde{\boldsymbol{\mu}}\|^2. \end{aligned} \tag{3.11}$$

By the linearity of the operator $\mathcal{L}_h$, we introduce $\boldsymbol{v}^{(1)} = \mathcal{L}_h(\boldsymbol{\mu}^{(1)})$, $\boldsymbol{v}^{(2)} = \mathcal{L}_h(\boldsymbol{\mu}^{(2)})$ and write $\tilde{\boldsymbol{v}} := \boldsymbol{v}^{(1)} - \boldsymbol{v}^{(2)} = \mathcal{L}_h \tilde{\boldsymbol{\mu}}$. A substitution of $\boldsymbol{v}^{(1)}$ and $\boldsymbol{v}^{(2)}$ into (3.4) leads to

$$\frac{2\tilde{\boldsymbol{v}}}{\Delta t} + \frac{1}{2}(\tilde{\boldsymbol{u}}^{n+\frac{1}{2}} \cdot \nabla_h \tilde{\boldsymbol{v}} + \nabla_h \cdot (\tilde{\boldsymbol{u}}^{n+\frac{1}{2}} \tilde{\boldsymbol{v}})) - \nu \Delta_h \tilde{\boldsymbol{v}} + \lambda(\nabla_h \tilde{\boldsymbol{\mu}})\tilde{\boldsymbol{d}}^{n+\frac{1}{2}} + \lambda \nabla_h \cdot (\beta \tilde{\boldsymbol{\mu}}(\tilde{\boldsymbol{d}}^{n+\frac{1}{2}})^T + (\beta+1)\tilde{\boldsymbol{d}}^{n+\frac{1}{2}}\tilde{\boldsymbol{\mu}}^T) = 0. \tag{3.12}$$

In turn, its discrete inner product with $\tilde{\boldsymbol{v}} = \mathcal{L}_h\tilde{\boldsymbol{\mu}}$ yields

$$\frac{2\|\tilde{\boldsymbol{v}}\|^2}{\Delta t} + \nu\|\nabla_h\tilde{\boldsymbol{v}}\|^2 + \lambda\langle(\nabla_h\tilde{\boldsymbol{\mu}})\tilde{\boldsymbol{d}}^{n+\frac{1}{2}}, \tilde{\boldsymbol{v}}\rangle_1 - \lambda\beta\langle\tilde{\boldsymbol{\mu}}(\tilde{\boldsymbol{d}}^{n+\frac{1}{2}})^T, \nabla_h\tilde{\boldsymbol{v}}\rangle_C - \lambda(\beta+1)\langle\tilde{\boldsymbol{d}}^{n+\frac{1}{2}}\tilde{\boldsymbol{\mu}}^T, \nabla_h\tilde{\boldsymbol{v}}\rangle_C = 0, \tag{3.13}$$

where the following summation-by-parts equalities have been applied:

$$\langle\tilde{\boldsymbol{u}}^{n+\frac{1}{2}} \cdot \nabla_h\tilde{\boldsymbol{v}} + \nabla_h \cdot (\tilde{\boldsymbol{u}}^{n+\frac{1}{2}}\tilde{\boldsymbol{v}}), \tilde{\boldsymbol{v}}\rangle_1 = 0,$$
$$\langle -\Delta_h\tilde{\boldsymbol{v}}, \tilde{\boldsymbol{v}}\rangle_1 = \|\nabla_h\tilde{\boldsymbol{v}}\|_2^2.$$

A combination of (3.11) and (3.13) gives

$$\begin{aligned} &\langle\mathcal{G}_h(\tilde{\boldsymbol{\mu}}), \tilde{\boldsymbol{\mu}}\rangle_C = \gamma\|\tilde{\boldsymbol{\mu}}\|^2 + \frac{1}{\lambda}\Big(\frac{2\|\tilde{\boldsymbol{v}}\|^2}{\Delta t} + \nu\|\nabla_h\tilde{\boldsymbol{v}}\|^2\Big), \\ &\text{i.e.} \quad \langle\mathcal{G}_h(\boldsymbol{\mu}^{(1)}) - \mathcal{G}_h(\boldsymbol{\mu}^{(2)}), \boldsymbol{\mu}^{(1)} - \boldsymbol{\mu}^{(2)}\rangle_C = \langle\mathcal{G}_h(\tilde{\boldsymbol{\mu}}), \tilde{\boldsymbol{\mu}}\rangle_C \geq \gamma\|\tilde{\boldsymbol{\mu}}\|_2^2 \geq \gamma\|\boldsymbol{\mu}^{(1)} - \boldsymbol{\mu}^{(2)}\|^2 \geq 0. \end{aligned} \tag{3.14}$$

Inequality (3.9) has been proved, and the equality holds if and only if $\tilde{\boldsymbol{\mu}} = 0$, i.e., $\boldsymbol{\mu}^{(1)} = \boldsymbol{\mu}^{(2)}$. □

Since $\mathcal{G}_h : (\mathbb{R}^{N^2})^2 \to (\mathbb{R}^{N^2})^2$ is a linear operator, the inverse operator $\mathcal{G}_h^{-1}$: $(\mathbb{R}^{N^2})^2 \to (\mathbb{R}^{N^2})^2$ is also linear. Moreover, the monotonicity of $\mathcal{G}_h^{-1}$ will play an important role in the later analysis.

Corollary 3.1. *The linear operator $\mathcal{G}_h^{-1}$ is monotone:*

$$\Big\langle\mathcal{G}_h^{-1}(\boldsymbol{d}^{(1)}) - \mathcal{G}_h^{-1}(\boldsymbol{d}^{(2)}), \boldsymbol{d}^{(1)} - \boldsymbol{d}^{(2)}\Big\rangle_C \geq \gamma\|\mathcal{G}_h^{-1}(\boldsymbol{d}^{(1)} - \boldsymbol{d}^{(2)})\|_2^2 \geq 0, \tag{3.15}$$

for any $\boldsymbol{d}^{(1)}$, $\boldsymbol{d}^{(2)}$, and the equality holds if and only if $\boldsymbol{d}^{(1)} = \boldsymbol{d}^{(2)}$.

Proof. We denote $\boldsymbol{\mu}^{(1)} = \mathcal{G}_h^{-1}(\boldsymbol{d}^{(1)})$, $\boldsymbol{\mu}^{(2)} = \mathcal{G}_h^{-1}(\boldsymbol{d}^{(2)})$, where $\boldsymbol{d}^{(1)} = \mathcal{G}_h\boldsymbol{\mu}^{(1)}$, $\boldsymbol{d}^{(2)} = \mathcal{G}_h\boldsymbol{\mu}^{(2)}$. An application of (3.9) indicates that

$$\begin{aligned} \Big\langle\mathcal{G}_h^{-1}(\boldsymbol{d}^{(1)}) - \mathcal{G}_h^{-1}(\boldsymbol{d}^{(2)}), \boldsymbol{d}^{(1)} - \boldsymbol{d}^{(2)}\Big\rangle_C &= \Big\langle\mathcal{G}_h(\boldsymbol{\mu}^{(1)}) - \mathcal{G}_h(\boldsymbol{\mu}^{(2)}), \boldsymbol{\mu}^{(1)} - \boldsymbol{\mu}^{(2)}\Big\rangle_C \\ &\geq \gamma\|\boldsymbol{\mu}^{(1)} - \boldsymbol{\mu}^{(2)}\|_2^2 = \gamma\|\mathcal{G}_h^{-1}(\boldsymbol{d}^{(1)} - \boldsymbol{d}^{(2)})\|_2^2 \geq 0. \end{aligned}$$

It is obvious that the equality holds only if $\boldsymbol{d}^{(1)} = \boldsymbol{d}^{(2)}$. This finishes the proof of Corollary 3.1. □

The Browder-Minty lemma will be used in the unique solvability analysis.

Lemma 3.3 (Browder-Minty [36, 37])**.** *Let X be a real, reflexive Banach space and suppose X' is its dual. If $T : X \to X'$ is (i) bounded; (ii) continuous; (iii) coercive, that is,*

$$\frac{\langle T(u), u\rangle}{\|u\|_X} \to +\infty \qquad \text{as } \|u\|_X \to +\infty;$$

and (iv) monotone. Then for any $g \in X'$, $u \in X$ of the equation $T(u) = g$ exists. Furthermore, if the operator T is strictly monotone, then the solution u is unique.

Theorem 3.1. *Given the profiles $\boldsymbol{u}^n$, $\boldsymbol{d}^n$, and p^n, the numerical scheme in (2.1)–(2.4) is unconditionally uniquely solvable.*

Proof. According to Eqs (3.7) and (3.8), we see that the numerical solution for the chemical potential vector can be expressed as $\boldsymbol{\mu}^{n+\frac{1}{2}} = -\mathcal{G}_h^{-1}\Big(\frac{\boldsymbol{d}^{n+1}-\boldsymbol{d}^n}{\Delta t}\Big)$. A combination of this representation and the expansion (3.6) reveals that, the numerical system (2.1)–(2.4) is equivalent to

$$\mathcal{G}_h^{-1}\Big(\frac{\boldsymbol{d}^{n+1}-\boldsymbol{d}^n}{\Delta t}\Big)+\varepsilon^{-2}\Big(\frac{|\boldsymbol{d}^{n+1}|^2+|\boldsymbol{d}^n|^2}{2}\boldsymbol{d}^{n+\frac{1}{2}}-\tilde{\boldsymbol{d}}^{n+\frac{1}{2}}\Big)-\Delta_h\boldsymbol{d}^{n+\frac{1}{2}}=0.$$

This turns out to be a closed system of $\boldsymbol{d}^{n+\frac{1}{2}}$, and (2.1)–(2.4) can be rewritten as

$$\mathcal{F}_h(\boldsymbol{d})=\mathcal{G}_h^{-1}\Big(\frac{\boldsymbol{d}-\boldsymbol{d}^n}{\Delta t}\Big)+\varepsilon^{-2}\Big(\frac{|\boldsymbol{d}|^2+|\boldsymbol{d}^n|^2}{2}\cdot\frac{\boldsymbol{d}+\boldsymbol{d}^n}{2}-\frac{3\boldsymbol{d}^n-\boldsymbol{d}^{n-1}}{2}\Big)-\Delta_h\frac{\boldsymbol{d}+\boldsymbol{d}^n}{2}=0. \tag{3.16}$$

Obviously, $\mathcal{F}_h$ is a nonlinear mapping from $(\mathbb{R}^{N^2})^2$ to $(\mathbb{R}^{N^2})^2$, with a prescribed discrete boundary condition. Meanwhile, we see that $X = X' = (\mathbb{R}^{N^2})^2$, with the discrete $\|\cdot\|_2$ norm $\|\boldsymbol{f}\|_X = \|\boldsymbol{f}\|_2$, for $\boldsymbol{f}\in(\mathbb{R}^{N^2})^2$.

Subsequently, we have to prove that the operator $\mathcal{F}_h$ is continuous under the norm $\|\cdot\|_2$, with a fixed Δt and h. Given $\boldsymbol{d}^{(1)},\boldsymbol{d}^{(2)}\in(\mathbb{R}^{N^2})^2$, with $\|\boldsymbol{d}^{(1)}-\boldsymbol{d}^{(2)}\|_2=\delta$. Accordingly, we write $\boldsymbol{\mu}^{(i)}=\mathcal{G}_h^{-1}(\frac{\boldsymbol{d}^{(i)}-\boldsymbol{d}^n}{\Delta t})$, $i=1,2$. By the monotonicity inequality (3.15) in Corollary 3.1, we obtain

$$\Big\langle\boldsymbol{\mu}^{(0)}-\boldsymbol{\mu}^{(1)},\frac{\boldsymbol{d}^{(0)}-\boldsymbol{d}^n}{\Delta t}-\frac{\boldsymbol{d}^{(1)}-\boldsymbol{d}^n}{\Delta t}\Big\rangle_C=\Big\langle\boldsymbol{\mu}^{(0)}-\boldsymbol{\mu}^{(1)},\frac{\boldsymbol{d}^{(0)}-\boldsymbol{d}^{(1)}}{\Delta t}\Big\rangle_C\geq\gamma\|\boldsymbol{\mu}^{(1)}-\boldsymbol{\mu}^{(2)}\|_2^2.$$

In turn, an application of the Cauchy inequality implies that

$$\frac{\gamma}{2}\|\boldsymbol{\mu}^{(1)}-\boldsymbol{\mu}^{(2)}\|_2^2+\frac{1}{2\gamma\Delta t^2}\|\boldsymbol{d}^{(1)}-\boldsymbol{d}^{(2)}\|_2^2\geq\gamma\|\boldsymbol{\mu}^{(1)}-\boldsymbol{\mu}^{(2)}\|_2^2.$$

We then arrive at

$$\|\boldsymbol{\mu}^{(1)}-\boldsymbol{\mu}^{(2)}\|_2^2\leq\gamma^{-2}\Delta t^{-2}\|\boldsymbol{d}^{(1)}-\boldsymbol{d}^{(2)}\|_2^2. \tag{3.17}$$

Therefore, for a fixed Δt, if $\boldsymbol{d}^{(1)}\to\boldsymbol{d}^{(2)}$, under a discrete $\|\cdot\|_2$ norm, then $\boldsymbol{\mu}^{(1)}\to\boldsymbol{\mu}^{(2)}$. This verifies the continuity of the linear operator $\mathcal{G}_h^{-1}$. Regarding the second term in the operator $\mathcal{F}_h$, we begin with its detailed expansion

$$\frac{|\boldsymbol{d}|^2+|\boldsymbol{d}^n|^2}{2}\cdot\frac{\boldsymbol{d}+\boldsymbol{d}^n}{2}=\frac{1}{4}\Big(|\boldsymbol{d}|^2\boldsymbol{d}+|\boldsymbol{d}|^2\boldsymbol{d}^n+|\boldsymbol{d}^n|^2\boldsymbol{d}+|\boldsymbol{d}^n|^2\boldsymbol{d}^n\Big).$$

It is easy to find that

$$\begin{aligned}
\||\boldsymbol{d}^{(1)}|^2\boldsymbol{d}^{(1)}-|\boldsymbol{d}^{(2)}|^2\boldsymbol{d}^{(2)}\|_2&\leq C(\|\boldsymbol{d}^{(1)}\|_6^2+\|\boldsymbol{d}^{(2)}\|_6^2)\|\boldsymbol{d}^{(1)}-\boldsymbol{d}^{(2)}\|_6\\
&\leq Ch^{-3}(\|\boldsymbol{d}^{(1)}\|_2^2+\|\boldsymbol{d}^{(2)}\|_2^2)\|\boldsymbol{d}^{(1)}-\boldsymbol{d}^{(2)}\|_2, &(3.18)\\
\||\boldsymbol{d}^{(1)}|^2\boldsymbol{d}^n-|\boldsymbol{d}^{(2)}|^2\boldsymbol{d}^n\|_2&\leq\|\boldsymbol{d}^n\|_\infty\cdot\|\boldsymbol{d}^{(1)}+\boldsymbol{d}^{(2)}\|_4\cdot\|\boldsymbol{d}^{(1)}-\boldsymbol{d}^{(2)}\|_4\\
&\leq Ch^{-\frac{9}{4}}\|\boldsymbol{d}^n\|_\infty(\|\boldsymbol{d}^{(1)}\|_2+\|\boldsymbol{d}^{(2)}\|_2)\|\boldsymbol{d}^{(1)}-\boldsymbol{d}^{(2)}\|_2, &(3.19)\\
\||\boldsymbol{d}^n|^2\boldsymbol{d}^{(1)}-|\boldsymbol{d}^n|^2\boldsymbol{d}^{(2)}\|_2&\leq\|\boldsymbol{d}^n\|_\infty^2\cdot\|\boldsymbol{d}^{(1)}-\boldsymbol{d}^{(2)}\|_2, &(3.20)
\end{aligned}$$

where the discrete Hölder inequality and three dimensional inverse inequality, $\|f\|_6 \le \frac{C\|f\|_2}{h}$, $\|f\|_4 \le \frac{C\|f\|_2}{h^{\frac{3}{4}}}$, have been used in the derivation. The last term in the expansion of operator $\mathcal{F}_h$ is analyzed as shown below:

$$\|\Delta_h \boldsymbol{d}^{(1)} - \Delta_h \boldsymbol{d}^{(2)}\|_2 \le Ch^{-2}\|\boldsymbol{d}^{(1)} - \boldsymbol{d}^{(2)}\|_2. \tag{3.21}$$

As a result, for fixed values of Δt and h, (3.17)–(3.21) imply that $\mathcal{F}_h(\boldsymbol{d}^{(1)}) \to \mathcal{F}_h(\boldsymbol{d}^{(2)})$ as $\boldsymbol{d}^{(1)} \to \boldsymbol{d}^{(2)}$ under a discrete $\|\cdot\|_2$ norm. This finished the continuity proof of $\mathcal{F}_h$.

In the next step, we need to prove the coercivity of the operator $\mathcal{F}_h$. The following expansion is observed:

$$\begin{aligned}
&\langle \mathcal{F}_h(\boldsymbol{d}), \boldsymbol{d}\rangle_C = I_1 + I_2 + I_3, \quad \text{with} \quad I_1 := \Big\langle \mathcal{G}_h^{-1}(\frac{\boldsymbol{d} - \boldsymbol{d}^n}{\Delta t}), \boldsymbol{d}\Big\rangle_C,\\
&I_2 := \varepsilon^{-2}\Big\langle \frac{\boldsymbol{d}^2 + (\boldsymbol{d}^n)^2}{2}\cdot\frac{\boldsymbol{d} + \boldsymbol{d}^n}{2} - \frac{3\boldsymbol{d}^n - \boldsymbol{d}^{n-1}}{2}, \boldsymbol{d}\Big\rangle_C, \quad I_3 := \Big\langle -\Delta_h\frac{\boldsymbol{d} + \boldsymbol{d}^n}{2}, \boldsymbol{d}\Big\rangle_C.
\end{aligned}$$

By the monotonicity inequality (3.15) and the Cauchy inequality, we see that

$$\begin{aligned}
\Big\langle \mathcal{G}_h^{-1}(\boldsymbol{d} - \boldsymbol{d}^n), \boldsymbol{d} - \boldsymbol{d}^n\Big\rangle_C \ge& \gamma\|\mathcal{G}^{-1}(\boldsymbol{d} - \boldsymbol{d}^n)\|_2^2,\\
\Big\langle \mathcal{G}_h^{-1}(\boldsymbol{d} - \boldsymbol{d}^n), \boldsymbol{d}^n\Big\rangle_C \ge& -\frac{\gamma}{2}\|\mathcal{G}_h^{-1}(\boldsymbol{d} - \boldsymbol{d}^n)\|^2 - \frac{1}{2\gamma}\|\boldsymbol{d}^n\|^2,
\end{aligned}$$

so that the following estimate is valid for the part I_1:

$$\begin{aligned}
I_1 := \Big\langle \mathcal{G}_h^{-1}(\frac{\boldsymbol{d} - \boldsymbol{d}^n}{\Delta t}), \boldsymbol{d}\Big\rangle_C &= \Big\langle \mathcal{G}_h^{-1}(\frac{\boldsymbol{d} - \boldsymbol{d}^n}{\Delta t}), \boldsymbol{d} - \boldsymbol{d}^n\Big\rangle_C + \Big\langle \mathcal{G}_h^{-1}(\frac{\boldsymbol{d} - \boldsymbol{d}^n}{\Delta t}), \boldsymbol{d}^n\Big\rangle_C\\
&\ge \frac{1}{\Delta t}\Big(\frac{\gamma}{2}\|\mathcal{G}_h^{-1}(\boldsymbol{d} - \boldsymbol{d}^n)\|^2 - \frac{1}{2\gamma}\|\boldsymbol{d}^n\|^2\Big).
\end{aligned} \tag{3.22}$$

Meanwhile, a careful application of the quadratic inequality gives $\|\boldsymbol{d}\|_4^4 \ge 2\|\boldsymbol{d}\|_2^2 - |\Omega|$. We then get

$$\begin{aligned}
\varepsilon^{-2}\Big\langle \frac{|\boldsymbol{d}|^2 + |\boldsymbol{d}^n|^2}{2}\cdot\frac{\boldsymbol{d} + \boldsymbol{d}^n}{2}, \boldsymbol{d}\Big\rangle &= \frac{1}{4\varepsilon^2}\Big\langle |\boldsymbol{d}|^2\boldsymbol{d} + |\boldsymbol{d}|^2\boldsymbol{d}^n + |\boldsymbol{d}^n|^2\boldsymbol{d} + |\boldsymbol{d}^n|^2\boldsymbol{d}^n, \boldsymbol{d}\Big\rangle\\
&= \frac{1}{4\varepsilon^2}\Big(\|\boldsymbol{d}\|_4^4 + (\|\boldsymbol{d}\|_2^2 + \|\boldsymbol{d}^n\|_2^2)\langle \boldsymbol{d}^n, \boldsymbol{d}\rangle + \|\boldsymbol{d}^n\|_2^2\|\boldsymbol{d}\|_2^2\Big)\\
&\ge \frac{1}{4\varepsilon^2}\Big(\|\boldsymbol{d}\|_4^4 - \frac{1}{2}(\|\boldsymbol{d}\|_2^2 + \|\boldsymbol{d}^n\|_2^2)^2 + \|\boldsymbol{d}^n\|_2^2\|\boldsymbol{d}\|_2^2\Big)\\
&= \frac{1}{4\varepsilon^2}\Big(\|\boldsymbol{d}\|_4^4 - \frac{1}{2}\|\boldsymbol{d}\|_2^4 - \frac{1}{2}\|\boldsymbol{d}^n\|_2^4\Big)\\
&\ge \frac{1}{4\varepsilon^2}\Big(\frac{1}{2}\|\boldsymbol{d}\|_4^4 - \frac{1}{2}\|\boldsymbol{d}^n\|_2^4\Big) \ge \frac{1}{4\varepsilon^2}\Big(\|\boldsymbol{d}\|_2^2 - |\Omega| - \frac{1}{2}\|\boldsymbol{d}^n\|_2^4\Big),
\end{aligned} \tag{3.23}$$

$$-\frac{1}{2\varepsilon^2}\langle 3\boldsymbol{d}^n - \boldsymbol{d}^{n-1}, \boldsymbol{d}\rangle_C \ge -\frac{1}{2\varepsilon^2}\Big(\|3\boldsymbol{d}^n - \boldsymbol{d}^{n-1}\|_2^2 + \frac{1}{4}\|\boldsymbol{d}\|_2^2\Big). \tag{3.24}$$

A combination of (3.23) and (3.24) leads to an estimate for I_2

$$\begin{aligned}
I_2 :=& \frac{1}{\epsilon^2}\Big\langle \frac{|\boldsymbol{d}|^2 + |\boldsymbol{d}^n|^2}{2}\cdot\frac{\boldsymbol{d} + \boldsymbol{d}^n}{2} - \frac{3\boldsymbol{d}^n - \boldsymbol{d}^{n-1}}{2}, \boldsymbol{d}\Big\rangle_C\\
\ge& \frac{1}{8\varepsilon^2}\|\boldsymbol{d}\|_2^2 - \frac{1}{4\varepsilon^2}\Big(|\Omega| + \frac{1}{2}\|\boldsymbol{d}^n\|_2^4\Big) - \frac{1}{2\varepsilon^2}\|3\boldsymbol{d}^n - \boldsymbol{d}^{n-1}\|_2^2.
\end{aligned} \tag{3.25}$$

The estimate for I_3 is more straightforward

$$I_3 := \Big\langle -\Delta_h \frac{\boldsymbol{d}+\boldsymbol{d}^n}{2}, \boldsymbol{d}\Big\rangle_C = \frac{1}{2}\langle \nabla_h(\boldsymbol{d}+\boldsymbol{d}^n), \nabla_h \boldsymbol{d}\rangle$$
$$= \frac{1}{4}(\|\nabla_h \boldsymbol{d}\|_2^2 - \|\nabla_h \boldsymbol{d}^n\|_2^2 + \|\nabla_h(\boldsymbol{d}+\boldsymbol{d}^n)\|_2^2) \geq -\frac{1}{4}\|\nabla_h \boldsymbol{d}^n\|_2^2. \tag{3.26}$$

As a consequence, a combination of (3.22), (3.25), and (3.26) leads to

$$\frac{\langle \mathcal{F}_h(\boldsymbol{d}), \boldsymbol{d}\rangle}{\|\boldsymbol{d}\|_2} \geq \frac{\frac{1}{8\varepsilon^2}\|\boldsymbol{d}\|_2^2 - Q}{\|\boldsymbol{d}\|_2} \geq \frac{1}{8\varepsilon^2}\|\boldsymbol{d}\|_2 - \frac{Q}{\|\boldsymbol{d}\|_2} \to \infty, \quad (\text{as } \|\boldsymbol{d}\|_2 \to \infty),$$

where $Q = \dfrac{1}{2\gamma\Delta t}\|\boldsymbol{d}^n\|^2 + \dfrac{1}{4\varepsilon^2}\Big(|\Omega| + \dfrac{1}{2}\|\boldsymbol{d}^n\|_2^4\Big) + \dfrac{1}{2\varepsilon^2}\|3\boldsymbol{d}^n - \boldsymbol{d}^{n-1}\|_2^2 + \dfrac{1}{4}\|\nabla_h \boldsymbol{d}^n\|_2^2$ could be viewed as a constant. Thus, the coercivity analysis of $\mathcal{F}_h$ is completed.

Moreover, the monotonicity analysis of $\mathcal{F}_h$ is necessary in the proof of Theorem 3.1. With the given profiles $\boldsymbol{d}^{(1)}$, $\boldsymbol{d}^{(2)}$, let $\tilde{\boldsymbol{d}} = \boldsymbol{d}^{(1)} - \boldsymbol{d}^{(2)}$, and we get

$$\mathcal{F}(\boldsymbol{d}^{(1)}) - \mathcal{F}(\boldsymbol{d}^{(2)}) = \mathcal{G}_h^{-1}\Big(\frac{\boldsymbol{d}^{(1)} - \boldsymbol{d}^{(2)}}{\Delta t}\Big) - \frac{1}{2}\Delta_h(\boldsymbol{d}^{(1)} - \boldsymbol{d}^{(2)})$$
$$+ \varepsilon^{-2}\Big(\frac{|\boldsymbol{d}^{(1)}|^2 + |\boldsymbol{d}^n|^2}{2}\cdot\frac{\boldsymbol{d}^{(1)} + \boldsymbol{d}^n}{2} - \frac{|\boldsymbol{d}^{(2)}|^2 + |\boldsymbol{d}^n|^2}{2}\cdot\frac{\boldsymbol{d}^{(2)} + \boldsymbol{d}^n}{2}\Big). \tag{3.27}$$

The monotonicity for the temporal differentiation and diffusion terms is straightforward:

$$\Big\langle \mathcal{G}_h^{-1}\Big(\frac{\boldsymbol{d}^{(1)} - \boldsymbol{d}^{(2)}}{\Delta t}\Big), \boldsymbol{d}^{(1)} - \boldsymbol{d}^{(2)}\Big\rangle_C \geq 0,$$
$$\langle -\frac{1}{2}\Delta_h(\boldsymbol{d}^{(1)} - \boldsymbol{d}^{(2)}), \boldsymbol{d}^{(1)} - \boldsymbol{d}^{(2)}\rangle_C = \frac{1}{2}\|\nabla_h(\boldsymbol{d}^{(1)} - \boldsymbol{d}^{(2)})\|_2^2 \geq 0.$$

In terms of the inner product with the nonlinear expansion in (3.27) by $\tilde{\boldsymbol{d}}$, it is observed that

$$\Big\langle \frac{|\boldsymbol{d}^{(1)}|^2 + |\boldsymbol{d}^n|^2}{2}\cdot\frac{\boldsymbol{d}^{(1)} + \boldsymbol{d}^n}{2} - \frac{|\boldsymbol{d}^{(2)}|^2 + |\boldsymbol{d}^n|^2}{2}\cdot\frac{\boldsymbol{d}^{(2)} + \boldsymbol{d}^n}{2}, \boldsymbol{d}^{(1)} - \boldsymbol{d}^{(2)}\Big\rangle_C$$
$$= \frac{1}{4}\langle |\boldsymbol{d}^{(1)}|^2\boldsymbol{d}^{(1)} - |\boldsymbol{d}^{(2)}|^2\boldsymbol{d}^{(2)}, \boldsymbol{d}^{(1)} - \boldsymbol{d}^{(2)}\rangle_C + \frac{1}{4}\langle |\boldsymbol{d}^{(1)}|^2\boldsymbol{d}^n - |\boldsymbol{d}^{(2)}|^2\boldsymbol{d}^n, \boldsymbol{d}^{(1)} - \boldsymbol{d}^{(2)}\rangle_C$$
$$+ \frac{1}{4}\langle |\boldsymbol{d}^n|^2\boldsymbol{d}^{(1)} - |\boldsymbol{d}^n|^2\boldsymbol{d}^{(2)}, \boldsymbol{d}^{(1)} - \boldsymbol{d}^{(2)}\rangle_C := J_1 + J_2 + J_3,$$
$$J_1 := \frac{1}{4}\langle |\boldsymbol{d}^{(1)}|^2\boldsymbol{d}^{(1)} - |\boldsymbol{d}^{(2)}|^2\boldsymbol{d}^{(2)}, \boldsymbol{d}^{(1)} - \boldsymbol{d}^{(2)}\rangle_C \geq \frac{1}{8}(\langle |\boldsymbol{d}^{(1)}|^2, |\tilde{\boldsymbol{d}}|^2\rangle_C + \|\boldsymbol{d}^{(2)}\cdot\tilde{\boldsymbol{d}}\|_2^2),$$
$$J_2 := \frac{1}{4}\langle |\boldsymbol{d}^{(1)}|^2\boldsymbol{d}^n - |\boldsymbol{d}^{(2)}|^2\boldsymbol{d}^n, \boldsymbol{d}^{(1)} - \boldsymbol{d}^{(2)}\rangle_C = \frac{1}{4}\langle (\boldsymbol{d}^{(1)} + \boldsymbol{d}^{(2)})\cdot\tilde{\boldsymbol{d}}, \boldsymbol{d}^n\cdot\tilde{\boldsymbol{d}}\rangle_C,$$
$$J_3 := \frac{1}{4}\langle |\boldsymbol{d}^n|^2\boldsymbol{d}^{(1)} - |\boldsymbol{d}^n|^2\boldsymbol{d}^{(2)}, \boldsymbol{d}^{(1)} - \boldsymbol{d}^{(2)}\rangle_C = \frac{1}{4}\langle |\boldsymbol{d}^n|^2, |\tilde{\boldsymbol{d}}|^2\rangle_C.$$

A careful application of the Cauchy inequality reveals that $J_1 + J_2 + J_3 \geq 0$. Finally, for any $\boldsymbol{d}^{(1)}$, $\boldsymbol{d}^{(2)}$, it holds that

$$\langle \mathcal{F}(\boldsymbol{d}^{(1)}) - \mathcal{F}(\boldsymbol{d}^{(2)}), \boldsymbol{d}^{(1)} - \boldsymbol{d}^{(2)}\rangle_C \geq 0,$$

and the equality is true if and only if $\boldsymbol{d}^{(1)} = \boldsymbol{d}^{(2)}$. The proof of the monotonicity of $\mathcal{F}_h$ is finished. By the Browder-Minty lemma, the numerical system (3.16) is uniquely solvable, which is equivalent to the unique solvability of the numerical scheme in (2.1)–(2.4). This completes the proof of Theorem 3.1. □

Theorem 3.2. *(Total energy stability estimate) Given $\boldsymbol{u}^n$, $\boldsymbol{d}^n$, and a fixed $\Delta t > 0, h > 0$, let $(\boldsymbol{u}^{n+1}, \boldsymbol{d}^{n+1}, p^{n+1})$ be the numerical solution of the scheme (2.1)–(2.4) at t_n, the numerical solution at t_{n+1} satisfies $\widetilde{E}_h(\boldsymbol{d}^{n+1}, \boldsymbol{u}^{n+1}, p^{n+1}) \le \widetilde{E}_h(\boldsymbol{d}^n, \boldsymbol{u}^n, p^n)$, where*

$$\widetilde{E}_h(\boldsymbol{d}^n, \boldsymbol{u}^n, p^n) = \lambda E_h(\boldsymbol{d}^n) + \frac{1}{2}\|\boldsymbol{u}^n\|_2^2 + \frac{\lambda}{4\varepsilon^2}\|\boldsymbol{d}^n - \boldsymbol{d}^{n-1}\|_2^2 + \frac{\Delta t^2}{8}\|\nabla_h p^n\|_2^2.$$

Proof. Taking a discrete inner product with (2.4) by $\boldsymbol{\mu}^{n+\frac{1}{2}}$ leads to

$$\begin{aligned}\langle \boldsymbol{d}^{n+1} - \boldsymbol{d}^n, \boldsymbol{\mu}^{n+\frac{1}{2}}\rangle_C + \Delta t\gamma\|\boldsymbol{\mu}^{n+\frac{1}{2}}\|_2^2 &= \Delta t\langle \tilde{\boldsymbol{d}}^{n+\frac{1}{2}}\overline{\boldsymbol{u}}^{n+\frac{1}{2}}, \nabla_h\boldsymbol{\mu}^{n+\frac{1}{2}}\rangle_1 \\ - \Delta t\beta\langle \nabla_h\overline{\boldsymbol{u}}^{n+\frac{1}{2}}\tilde{\boldsymbol{d}}^{n+\frac{1}{2}}, \boldsymbol{\mu}^{n+\frac{1}{2}}\rangle_C &- \Delta t(1+\beta)\langle \nabla_h\overline{\boldsymbol{u}}^{n+\frac{1}{2}})^T\tilde{\boldsymbol{d}}^{n+\frac{1}{2}}, \boldsymbol{\mu}^{n+\frac{1}{2}}\rangle_C, \end{aligned} \tag{3.28}$$

in which the summation-by-parts formulas have been used. The term associated with the temporal differentiation part could be expanded as

$$\langle \boldsymbol{d}^{n+1} - \boldsymbol{d}^n, \boldsymbol{\mu}^{n+\frac{1}{2}}\rangle_C = \Big\langle \boldsymbol{d}^{n+1} - \boldsymbol{d}^n, \varepsilon^{-2}\Big(\frac{|\boldsymbol{d}^{n+1}|^2 + |\boldsymbol{d}^n|^2}{2}\boldsymbol{d}^{n+\frac{1}{2}} - \tilde{\boldsymbol{d}}^{n+\frac{1}{2}}\Big) - \Delta_h\boldsymbol{d}^{n+\frac{1}{2}}\Big\rangle_C,$$

and the following estimates are available:

$$\langle -\Delta_h\boldsymbol{d}^{n+\frac{1}{2}}, \boldsymbol{d}^{n+1} - \boldsymbol{d}^n\rangle_C = \langle \nabla_h\boldsymbol{d}^{n+\frac{1}{2}}, \nabla_h(\boldsymbol{d}^{n+1} - \boldsymbol{d}^n)\rangle_C = \frac{1}{2}(\|\nabla_h\boldsymbol{d}^{n+1}\|^2 - \|\nabla_h\boldsymbol{d}^n\|^2), \tag{3.29}$$

$$\begin{aligned}\langle -\tilde{\boldsymbol{d}}^{n+\frac{1}{2}}, \boldsymbol{d}^{n+1} - \boldsymbol{d}^n\rangle_C &= -\frac{1}{2}\langle 3\boldsymbol{d}^n - \boldsymbol{d}^{n-1}, \boldsymbol{d}^{n+1} - \boldsymbol{d}^n\rangle_C \\ &= -\frac{1}{2}\langle \boldsymbol{d}^{n+1} + \boldsymbol{d}^n, \boldsymbol{d}^{n+1} - \boldsymbol{d}^n\rangle_C + \frac{1}{2}\langle \boldsymbol{d}^{n+1} - 2\boldsymbol{d}^n + \boldsymbol{d}^{n-1}, \boldsymbol{d}^{n+1} - \boldsymbol{d}^n\rangle_C \\ &\ge -\frac{1}{2}(\|\boldsymbol{d}^{n+1}\|_2^2 - \|\boldsymbol{d}^n\|_2^2) + \frac{1}{4}(\|\boldsymbol{d}^{n+1} - \boldsymbol{d}^n\|_2^2 - \|\boldsymbol{d}^n - \boldsymbol{d}^{n-1}\|_2^2), \end{aligned} \tag{3.30}$$

$$\begin{aligned}\langle (|\boldsymbol{d}^{n+1}|^2 + |\boldsymbol{d}^n|^2)\boldsymbol{d}^{n+\frac{1}{2}}, \boldsymbol{d}^{n+1} - \boldsymbol{d}^n\rangle_C &= \frac{1}{2}\langle (|\boldsymbol{d}^{n+1}|^2 + |\boldsymbol{d}^n|^2)(\boldsymbol{d}^{n+1} + \boldsymbol{d}^n), \boldsymbol{d}^{n+1} - \boldsymbol{d}^n\rangle_C \\ &= \frac{1}{2}\langle |\boldsymbol{d}^{n+1}|^2 + |\boldsymbol{d}^n|^2, \boldsymbol{d}^{n+1})^2 - (\boldsymbol{d}^n)^2\rangle_C \\ &= \frac{1}{2}(\|\boldsymbol{d}^{n+1}\|_4^4 - \|\boldsymbol{d}^n\|_4^4). \end{aligned} \tag{3.31}$$

In turn, a combination of (3.29)–(3.31) yields

$$\Big\langle \boldsymbol{d}^{n+1} - \boldsymbol{d}^n, \boldsymbol{\mu}^{n+\frac{1}{2}}\Big\rangle_C \ge E_h(\boldsymbol{d}^{n+1}) - E_h(\boldsymbol{d}^n) + \frac{1}{4\varepsilon^2}(\|\boldsymbol{d}^{n+1} - \boldsymbol{d}^n\|_2^2 - \|\boldsymbol{d}^n - \boldsymbol{d}^{n-1}\|_2^2). \tag{3.32}$$

Meanwhile, taking a discrete inner product with (2.1) by $\overline{\boldsymbol{u}}^{n+\frac{1}{2}}$ reads

$$\begin{aligned}&\frac{1}{2}(\|\overline{\boldsymbol{u}}^{n+1}\|_2^2 - \|\boldsymbol{u}^n\|_2^2) + \Delta t\langle \nabla_h p^n, \overline{\boldsymbol{u}}^{n+\frac{1}{2}}\rangle_1 + \Delta t\nu\|\nabla_h\overline{\boldsymbol{u}}^{n+\frac{1}{2}}\|_2^2 \\ =& -\Delta t\lambda\langle (\nabla_h\boldsymbol{\mu}^{n+\frac{1}{2}})\tilde{\boldsymbol{d}}^{n+\frac{1}{2}}, \overline{\boldsymbol{u}}^{n+\frac{1}{2}}\rangle_1 + \Delta t\lambda\beta\langle \nabla_h\overline{\boldsymbol{u}}^{n+\frac{1}{2}}(\tilde{\boldsymbol{d}}^{n+\frac{1}{2}})^T, \boldsymbol{\mu}^{n+\frac{1}{2}}\rangle_C \\ &+ \Delta t\lambda(\beta+1)\langle \nabla_h\overline{\boldsymbol{u}}^{n+\frac{1}{2}}(\tilde{\boldsymbol{d}}^{n+\frac{1}{2}})^T, \boldsymbol{\mu}^{n+\frac{1}{2}}\rangle_C, \end{aligned} \tag{3.33}$$

in which the following summation-by-parts equalities have been applied:

$$\langle \tilde{\boldsymbol{u}}^{n+\frac{1}{2}} \cdot \nabla_h \overline{\boldsymbol{u}}^{n+\frac{1}{2}} + \nabla_h \cdot (\tilde{\boldsymbol{u}}^{n+\frac{1}{2}} \overline{\boldsymbol{u}}^{n+\frac{1}{2}}), \overline{\boldsymbol{u}}^{n+\frac{1}{2}} \rangle_1 = 0,$$
$$\langle -\Delta_h \overline{\boldsymbol{u}}^{n+\frac{1}{2}}, \overline{\boldsymbol{u}}^{n+\frac{1}{2}} \rangle_1 = \|\nabla_h \overline{\boldsymbol{u}}^{n+\frac{1}{2}}\|_2^2.$$

The term $\langle \nabla_h p^n, \overline{\boldsymbol{u}}^{n+\frac{1}{2}} \rangle_1$ could be derived as follows:

$$\begin{aligned}
\langle \nabla_h p^n, \overline{\boldsymbol{u}}^{n+\frac{1}{2}} \rangle_1 &= -\langle p^n, \nabla_h \cdot \overline{\boldsymbol{u}}^{n+\frac{1}{2}} \rangle_C = -\langle p^n, \frac{1}{2} \nabla_h \cdot (\overline{\boldsymbol{u}}^{n+1} + \boldsymbol{u}^n) \rangle_C \\
&= -\langle p^n, \frac{1}{2} \nabla_h \cdot \overline{\boldsymbol{u}}^{n+1} \rangle_C = -\langle p^n, \frac{\Delta t}{4} \cdot \Delta_h (p^{n+1} - p^n) \rangle_C \\
&= \frac{\Delta t}{4} \langle \nabla_h p^n, \nabla_h (p^{n+1} - p^n) \rangle_1 \\
&= \frac{\Delta t}{8} (\|\nabla_h p^{n+1}\|_2^2 - \|\nabla_h p^n\|_2^2) - \frac{\Delta t}{8} \|\nabla_h (p^{n+1} - p^n)\|_2^2 \\
&= \frac{\Delta t}{8} (\|\nabla_h p^{n+1}\|_2^2 - \|\nabla_h p^n\|_2^2) - \frac{1}{2\Delta t} \|\boldsymbol{u}^{n+1} - \overline{\boldsymbol{u}}^{n+1}\|_2^2.
\end{aligned} \tag{3.34}$$

The identity $\nabla_h \cdot \boldsymbol{u}^n = 0$ has been used. A substitution of (3.34) into (3.33) reads

$$\begin{aligned}
&\frac{1}{2} (\|\overline{\boldsymbol{u}}^{n+1}\|_2^2 - \|\boldsymbol{u}^n\|_2^2) + \frac{\Delta t^2}{8} (\|\nabla_h p^{n+1}\|_2^2 - \|\nabla_h p^n\|_2^2) - \frac{1}{2} \|\boldsymbol{u}^{n+1} - \overline{\boldsymbol{u}}^{n+1}\|_2^2 + \Delta t \nu \|\nabla_h \overline{\boldsymbol{u}}^{n+\frac{1}{2}}\|_2^2 \\
=& -\Delta t \lambda \langle (\nabla_h \boldsymbol{\mu}^{n+\frac{1}{2}}) \tilde{\boldsymbol{d}}^{n+\frac{1}{2}}, \overline{\boldsymbol{u}}^{n+\frac{1}{2}} \rangle_1 + \Delta t \lambda \beta \langle \nabla_h \overline{\boldsymbol{u}}^{n+\frac{1}{2}} (\tilde{\boldsymbol{d}}^{n+\frac{1}{2}})^T, \boldsymbol{\mu}^{n+\frac{1}{2}} \rangle_C \\
&+ \Delta t \lambda (\beta + 1) \langle \nabla_h \overline{\boldsymbol{u}}^{n+\frac{1}{2}} (\tilde{\boldsymbol{d}}^{n+\frac{1}{2}})^T, \boldsymbol{\mu}^{n+\frac{1}{2}} \rangle_C.
\end{aligned} \tag{3.35}$$

On the other hand, taking an inner product with (2.2) by $\boldsymbol{u}^{n+1}$ gives

$$\|\boldsymbol{u}^{n+1}\|_2^2 - \|\overline{\boldsymbol{u}}^{n+1}\|_2^2 + \|\boldsymbol{u}^{n+1} - \overline{\boldsymbol{u}}^{n+1}\|_2^2 = 0. \tag{3.36}$$

A substitution of (3.36) into (3.35) leads to

$$\begin{aligned}
&\frac{1}{2} (\|\boldsymbol{u}^{n+1}\|_2^2 - \|\boldsymbol{u}^n\|_2^2) + \frac{\Delta t^2}{8} (\|\nabla_h p^{n+1}\|_2^2 - \|\nabla_h p^n\|_2^2) + \Delta t \nu \|\nabla_h \overline{\boldsymbol{u}}^{n+\frac{1}{2}}\|_2^2 \\
=& -\Delta t \lambda \langle (\nabla_h \boldsymbol{\mu}^{n+\frac{1}{2}}) \tilde{\boldsymbol{d}}^{n+\frac{1}{2}}, \overline{\boldsymbol{u}}^{n+\frac{1}{2}} \rangle_1 + \Delta t \lambda \beta \langle \nabla_h \overline{\boldsymbol{u}}^{n+\frac{1}{2}} (\tilde{\boldsymbol{d}}^{n+\frac{1}{2}})^T, \boldsymbol{\mu}^{n+\frac{1}{2}} \rangle_C \\
&+ \Delta t \lambda (\beta + 1) \langle \nabla_h \overline{\boldsymbol{u}}^{n+\frac{1}{2}} (\tilde{\boldsymbol{d}}^{n+\frac{1}{2}})^T, \boldsymbol{\mu}^{n+\frac{1}{2}} \rangle_C.
\end{aligned} \tag{3.37}$$

Finally, a combination of (3.28), (3.32), and (3.37) results in

$$\begin{aligned}
E_h(\boldsymbol{d}^{n+1}) - E_h(\boldsymbol{d}^n) + \frac{1}{4\varepsilon^2} (\|\boldsymbol{d}^{n+1} - \boldsymbol{d}^n\|_2^2 - \|\boldsymbol{d}^n - \boldsymbol{d}^{n-1}\|_2^2) + \frac{1}{2} (\|\boldsymbol{u}^{n+1}\|_2^2 - \|\boldsymbol{u}^n\|_2^2) \\
+ \frac{\Delta t^2}{8} (\|\nabla_h p^{n+1}\|_2^2 - \|\nabla_h p^n\|_2^2) + \Delta t \nu \|\nabla_h \overline{\boldsymbol{u}}^{n+\frac{1}{2}}\|_2^2 \le 0,
\end{aligned}$$

which can be rewritten as

$$\begin{aligned}
\lambda E_h(\boldsymbol{d}^{n+1}) + \frac{1}{2} \|\boldsymbol{u}^{n+1}\|_2^2 + \frac{\lambda}{4\varepsilon^2} \|\boldsymbol{d}^{n+1} - \boldsymbol{d}^n\|_2^2 + \frac{\Delta t^2}{8} \|\nabla_h p^{n+1}\|_2^2 \le \\
\lambda E_h(\boldsymbol{d}^n) + \frac{1}{2} \|\boldsymbol{u}^n\|_2^2 + \frac{\lambda}{4\varepsilon^2} \|\boldsymbol{d}^n - \boldsymbol{d}^{n-1}\|_2^2 + \frac{\Delta t^2}{8} \|\nabla_h p^n\|_2^2.
\end{aligned}$$

This completes the proof of Theorem 3.2. □

Remark 3.1. *In the numerical design of a second-order accurate, total energy-stable algorithm of a phase-field-fluid coupled PDE system, the primary difficulty is associated with an appropriate approximation to the nonlinear term and the expansive concave term, with a theoretical justification of all the required mathematical properties. In this work, a modified Crank-Nicolson approximation is derived for the nonlinear vector term, so that its unique solvability is guaranteed by the monotonicity feature, and its free energy dissipation comes from the variational structure. Meanwhile, an explicit Adams-Bashforth extrapolation is applied to the expansive concave term, and a modified energy dissipation could also be carefully established. Moreover, a second-order accurate, semi-implicit approximation is applied to the coupled nonlinear terms, and the monotone property of the corresponding linear operators play an important role in the theoretical analysis.*

In particular, it is noticed that, the dissipation estimate is in terms of a modified total energy functional in Theorem 3.2, composed of the original free energy, the original kinematic energy, and two more numerical correction terms. The first correction term, $\frac{\lambda}{4\varepsilon^2}\|\boldsymbol{d}^n - \boldsymbol{d}^{n-1}\|_2^2$*, comes from the explicit Adams-Bashforth approximation to the concave part; the second correction term,* $\frac{\Delta t^2}{8}\|\nabla_h p^n\|_2^2$*, comes from the pressure correction numerical approach in the decoupled Stokes solver.*

Because of the concave energy part in the free energy expansion, the corresponding dissipation analysis for any multi-step numerical scheme is always in terms of the modified free energy. In contrast, for certain gradient flow without any concave energy part in the free energy expansion, such as the Poisson-Nernst-Planck (PNP) system, a numerical design of a second-order accurate model, the original free energy dissipative numerical algorithm becomes feasible; see the related work [38, 39]. For the reformulated Ericksen-Leslie system (1.5)–(1.7)*, a second-order accurate and original energy dissipative numerical scheme will also be considered in future work.*

4. Optimal rate convergence analysis

The total energy dissipation law implies that the reformulated Ericksen-Leslie system (1.5)–(1.7) takes a similar structure to the Cahn-Hilliard-Navier-Stokes (CHNS) system, with the primary difference between a vector and the scalar phase field energy expansions, combined with a few more coupled terms of rotation and deformation. In fact, the existence of a global-in-time weak solution has been proved in [40], and such an analysis could be extended to the reformulated Ericksen-Leslie system (1.5)–(1.7) in the same fashion. Of course, the regularity of the weak solutions is not sufficient to justify the optimal rate convergence analysis, and a strong solution to the CHNS system, with higher order regularities, is needed in the error estimate. It was proved in [41] that unique strong solutions exist for the CHNS system. In more detail, higher order regularities can be stated as follows: For any initial data $\boldsymbol{u}_0 \in H^m(\Omega)$, $\boldsymbol{d}_0 \in H^{m+1}(\Omega)$, there is an estimate for $\|\boldsymbol{u}(t)\|_{H^m}$ and $\|\boldsymbol{d}(t)\|_{H^{m+1}}$, $m \geq 1$, globally-in-time for two dimensions, and locally-in-time for three dimensions, under appropriate compatibility conditions between the initial data and boundary conditions [42]. Therefore, for the exact solution $(\boldsymbol{d}_e, \boldsymbol{u}_e, p_e)$ to the reformulated Ericksen-Leslie system (1.5)–(1.7), we could always assume that the exact solution has a regularity of class $\mathcal{R}$, with sufficiently regular initial data

$$\boldsymbol{d}_e,\ \boldsymbol{u}_e,\ p_e \in \mathcal{R} := H^4\left(0, T; C_{\text{per}}(\Omega)\right) \cap H^3\left(0, T; C^2_{\text{per}}(\Omega)\right) \cap L^\infty\left(0, T; C^6_{\text{per}}(\Omega)\right). \tag{4.1}$$

4.1. A few preliminary estimates

In this subsection, we will derive the uniform bounds of the solution in H_h^1, L_h^4 and L_h^6 norms, which will be used in the convergence analysis. Some discrete Sobolev inequalities are listed below; a detailed proof could be found in [22].

Lemma 4.1 (Discrete Sobolev inequalities)**.** *[22] For any grid function f, the following inequalities hold:*

$$\|f\|_6 \le C_1\|f\|_{H_h^1}, \quad \|f\|_{H_h^1}^2 := \|f\|_2^2 + \|\nabla_h f\|_2^2, \tag{4.2}$$

$$\|f\|_4 \le C_2(\|f\|_2 + \|f\|_2^{\frac{1}{4}} \cdot \|\nabla_h f\|^{\frac{3}{4}}), \quad \|\nabla_h f\|_4 \le C_2\|\nabla_h f\|_2^{\frac{1}{4}} \cdot \|\Delta_h f\|^{\frac{3}{4}}, \tag{4.3}$$

$$\|f\|_\infty \le C_3(\|f\|_2 + \|\nabla_h f\|_2^{\frac{1}{2}} \cdot \|\Delta_h f\|^{\frac{1}{2}}), \tag{4.4}$$

where C_i is dependent only on Ω, independent of f, with $1 \le i \le 3$.

Proposition 4.1. *Given the initial conditions $\boldsymbol{u}^0 \in \ell^2$, $\boldsymbol{d}^0 \in H_h^1$, the following estimate holds for the numerical solution to the scheme (2.1)–(2.4):*

$$\max_{1\le k\le M} \|\boldsymbol{d}^k\|_{H_h^1} \le M_1, \quad \max_{1\le k\le M} \|\boldsymbol{d}^k\|_4 \le M_4, \quad \max_{1\le k\le M} \|\boldsymbol{d}^k\|_6 \le M_6, \tag{4.5}$$

where M_1, M_4, M_6 are independent of the time step. Furthermore, M_4 is independent of ε, and M_1 and M_6 are of order $O(\varepsilon^{-1})$.

Proof. By the total energy stability estimate in Theorem 3.2, we see that

$$E_h(\boldsymbol{d}^k) \le \widetilde{E}_h(\boldsymbol{d}^k, \boldsymbol{u}^k, p^k) \le \cdots \le \widetilde{E}_h(\boldsymbol{d}^0, \boldsymbol{u}^0, p^0) := M_0, \quad \forall k \ge 0,$$

where M_0 is of order $O(\varepsilon^{-2})$. According to the definition (3.3) for the discrete free energy, we have

$$\frac{1}{4}\|\boldsymbol{d}^k\|_4^4 - \frac{1}{2}\|\boldsymbol{d}^k\|_2^2 + \frac{\varepsilon^2}{2}\|\nabla_h \boldsymbol{d}^k\|_2^2 \le \varepsilon^2 M_0. \tag{4.6}$$

By the point-wise quadratic inequality $\frac{1}{8}|\boldsymbol{d}^k|^4 - \frac{1}{2}|\boldsymbol{d}^k|^2 \ge -\frac{1}{2}$, we obtain

$$\frac{1}{8}\|\boldsymbol{d}^k\|_4^4 - \frac{1}{2}\|\boldsymbol{d}^k\|_2^2 \ge -\frac{1}{2}|\Omega|. \tag{4.7}$$

In turn, a combination of (4.6) and (4.7) gives

$$\frac{1}{8}\|\boldsymbol{d}^k\|_4^4 \le \varepsilon^2 M_0 + \frac{1}{2}|\Omega|, \quad \|\boldsymbol{d}^k\|_4 \le (8\varepsilon^2 M_0 + 4|\Omega|)^{\frac{1}{4}} := M_4, \quad \text{for any } k \ge 0.$$

Because of the fact that $M_0 = O(\varepsilon^{-2})$, we see that $M_4 = O(1)$. Furthermore, subtracting (4.6) from (4.7) implies that

$$\frac{1}{2}\|\boldsymbol{d}^k\|_2^2 + \frac{\varepsilon^2}{2}\|\nabla_h \boldsymbol{d}^k\|_2^2 \le \varepsilon^2 M_0 + |\Omega|, \quad \text{so that } \|\boldsymbol{d}^k\|_2^2 + \|\nabla_h \boldsymbol{d}^k\|_2^2 \le 2(M_0 + \varepsilon^{-2}|\Omega|).$$

We then arrive at

$$\|\boldsymbol{d}^k\|_{H_h^1} = (\|\boldsymbol{d}^k\|_2^2 + \|\nabla_h \boldsymbol{d}^k\|_2^2)^{\frac{1}{2}} \le \sqrt{2}(M_0 + \varepsilon^{-2}|\Omega|)^{\frac{1}{2}} := M_1, \quad M_1 = O(\varepsilon^{-1}).$$

With an discrete Sobolev inequality (4.2), we get

$$\|\boldsymbol{d}^k\|_6 \le C_1\|\boldsymbol{d}^k\|_{H_h^1} \le C_1 M_1 := M_6, \quad M_g = O(\varepsilon^{-1}).$$

The proof of Proposition 4.1 is completed. □

4.2. The consistency analysis

Denote $\boldsymbol{D}$ and P as the exact solutions of the orientation and pressure variables, respectively. Meanwhile, it is noticed that the exact solution $\boldsymbol{u}_e$ (for the velocity vector) does not satisfy the divergence-free condition at a discrete level, namely $\nabla_h \cdot \boldsymbol{u}_e \neq 0$. An approximate velocity U, which is divergence-free at a discrete sense, has to be constructed to overcome this well known difficulty. In fact, for any divergence-free velocity vector $\boldsymbol{u}_e$, there is always a stream function profile $\boldsymbol{\psi}_e = (\psi_{1e}, \psi_{2e}, \psi_{3e})^T$ with $\boldsymbol{u}_e = \nabla^\perp \psi_e$. On the basis of this fact, we define an approximate profile $\boldsymbol{U}$ at the staggered mesh as

$$\boldsymbol{U} = \nabla_h^\perp \boldsymbol{\psi}_e = (D_y\psi_{3e} - D_z\psi_{2e}, D_z\psi_{1e} - D_x\psi_{3e}, D_x\psi_{2e} - D_y\psi_{1e})^T.$$

A careful calculation indicates that $\nabla_h \cdot \boldsymbol{U} = 0$. Moreover, to address the issue of the explicit pressure gradient in the decoupled Stokes solver, we also construct an intermediate velocity vector $\overline{\boldsymbol{U}}$ as follows:

$$\overline{\boldsymbol{U}}^{n+1} = \boldsymbol{U}^{n+1} + \Delta t \nabla_h (P^{n+1} - P^n).$$

Of course, the temporal regularity of the exact pressure profile P implies that

$$\|\overline{\boldsymbol{U}}^{n+1} - \boldsymbol{U}^{n+1}\|_{W_h^{2,\infty}} \le C\Delta t^2, \quad \|f\|_{W_h^{2,\infty}} := \|f\|_\infty + \|\nabla_h f\|_\infty + \|\nabla_h(\nabla_h f)\|_\infty.$$

In term of the vector-valued chemical potential, an approximate profile $\boldsymbol{\Gamma}$ is defined at the intermediate time instant $t^{n+\frac{1}{2}}$

$$\boldsymbol{\Gamma}^{n+\frac{1}{2}} = \varepsilon^{-2}\left(\frac{|\boldsymbol{D}^{n+1}|^2 + |\boldsymbol{D}^n|^2}{2}\boldsymbol{D}^{n+\frac{1}{2}} - \widetilde{\boldsymbol{D}}^{n+\frac{1}{2}}\right) - \Delta_h \boldsymbol{D}^{n+\frac{1}{2}}.$$

The constructed profiles satisfy the following local truncation error estimates:

$$\begin{aligned}
&\frac{\overline{\boldsymbol{U}}^{n+1} - \boldsymbol{U}^n}{\Delta t} + \frac{1}{2}(\widetilde{\boldsymbol{U}}^{n+\frac{1}{2}} \cdot \nabla_h \overline{\boldsymbol{U}}^{n+\frac{1}{2}} + \nabla_h(\widetilde{\boldsymbol{U}}^{n+\frac{1}{2}} \overline{\boldsymbol{U}}^{n+\frac{1}{2}})) + \nabla_h P^n - \nu\Delta_h \overline{\boldsymbol{U}}^{n+\frac{1}{2}} \\
&\quad + \lambda(\nabla_h \boldsymbol{\Gamma}^{n+\frac{1}{2}})\widetilde{\boldsymbol{D}}^{n+\frac{1}{2}} + \lambda\nabla_h \cdot (\beta\boldsymbol{\Gamma}^{n+\frac{1}{2}}(\widetilde{\boldsymbol{D}}^{n+\frac{1}{2}})^T + (\beta+1)\widetilde{\boldsymbol{D}}^{n+\frac{1}{2}}(\boldsymbol{\Gamma}^{n+\frac{1}{2}})^T) = \boldsymbol{\tau}_u^{n+1}, \qquad (4.8)\\
&\frac{\boldsymbol{U}^{n+1} - \overline{\boldsymbol{U}}^{n+1}}{\Delta t} + \frac{1}{2}\nabla_h(P^{n+1} - P^n) = 0, \qquad (4.9)\\
&\nabla_h \cdot \boldsymbol{U}^{n+1} = 0, \qquad (4.10)\\
&\frac{\boldsymbol{D}^{n+1} - \boldsymbol{D}^n}{\Delta t} + \nabla_h \cdot (\widetilde{\boldsymbol{D}}^{n+\frac{1}{2}} \overline{\boldsymbol{U}}^{n+\frac{1}{2}}) + (\beta\nabla_h \overline{\boldsymbol{U}}^{n+\frac{1}{2}} + (1+\beta)(\nabla_h \overline{\boldsymbol{U}}^{n+\frac{1}{2}})^T)\widetilde{\boldsymbol{D}}^{n+\frac{1}{2}} \\
&\quad = -\gamma\boldsymbol{\Gamma}^{n+\frac{1}{2}} + \boldsymbol{\tau}_d^{n+1}, \qquad (4.11)
\end{aligned}$$

where $\|\boldsymbol{\tau}_u^{n+1}\|_2$, $\|\boldsymbol{\tau}_d^{n+1}\|_{H_h^1} \le C(\Delta t^2 + h^2)$, with the help of Taylor expansion.

The numerical errors are defined in the table. Subtracting (2.1)–(2.4) from (4.8)–(4.11) leads to

$$\begin{aligned}
&\frac{\overline{\boldsymbol{e}}_u^{n+1} - \boldsymbol{e}_u^n}{\Delta t} + \frac{1}{2}(\tilde{\boldsymbol{e}}_u^{n+\frac{1}{2}} \cdot \nabla_h \overline{\boldsymbol{U}}^{n+\frac{1}{2}} + \tilde{\boldsymbol{u}}^{n+\frac{1}{2}} \cdot \nabla_h \overline{\boldsymbol{e}}_u^{n+\frac{1}{2}} + \nabla_h(\tilde{\boldsymbol{e}}_u^{n+\frac{1}{2}} \cdot \overline{\boldsymbol{U}}^{n+\frac{1}{2}} + \tilde{\boldsymbol{u}}^{n+\frac{1}{2}} \cdot \overline{\boldsymbol{e}}_u^{n+\frac{1}{2}})) + \nabla_h e_p^n \\
&\quad - \nu\Delta_h \overline{\boldsymbol{e}}_u^{n+\frac{1}{2}} + \lambda(\nabla_h \boldsymbol{e}_\mu^{n+\frac{1}{2}})\tilde{\boldsymbol{d}}^{n+\frac{1}{2}} + \lambda(\nabla_h \boldsymbol{\Gamma}^{n+\frac{1}{2}})\tilde{\boldsymbol{e}}_d^{n+\frac{1}{2}} \\
&\quad + \lambda\nabla_h \cdot (\beta(\boldsymbol{e}_\mu^{n+\frac{1}{2}}\tilde{\boldsymbol{d}}^{n+\frac{1}{2}} + \Gamma^{n+\frac{1}{2}}\tilde{\boldsymbol{e}}_d^{n+\frac{1}{2}}) + (\beta+1)(\boldsymbol{e}_\mu^{n+\frac{1}{2}}\tilde{\boldsymbol{d}}^{n+\frac{1}{2}} + \Gamma^{n+\frac{1}{2}}\tilde{\boldsymbol{e}}_d^{n+\frac{1}{2}})) = \boldsymbol{\tau}_u^{n+1}, \qquad (4.12)
\end{aligned}$$

Numerical solution	Exact solution	Error function
$\boldsymbol{u}^n$	$\boldsymbol{U}^n$	$\boldsymbol{e}_u^n$
$\overline{\boldsymbol{u}}^n$	$\overline{\boldsymbol{U}}^n$	$\overline{\boldsymbol{e}}_u^n$
$\tilde{\boldsymbol{u}}^{n+\frac{1}{2}}$	$\widetilde{\boldsymbol{U}}^{n+\frac{1}{2}}$	$\tilde{\boldsymbol{e}}_u^{n+\frac{1}{2}}$
$\overline{\boldsymbol{u}}^{n+\frac{1}{2}}$	$\overline{\boldsymbol{U}}^{n+\frac{1}{2}}$	$\overline{\boldsymbol{e}}_u^{n+\frac{1}{2}}$
$\boldsymbol{d}^n$	$\boldsymbol{D}^n$	$\boldsymbol{e}_d^n$
$\boldsymbol{d}^{n+\frac{1}{2}}$	$\boldsymbol{D}^{n+\frac{1}{2}}$	$\boldsymbol{e}_d^{n+\frac{1}{2}}$
$\tilde{\boldsymbol{d}}^{n+\frac{1}{2}}$	$\widetilde{\boldsymbol{D}}^{n+\frac{1}{2}}$	$\tilde{\boldsymbol{e}}_d^{n+\frac{1}{2}}$
p^n	P^n	e_p^n
$\boldsymbol{\mu}^{n+\frac{1}{2}}$	$\Gamma^{n+\frac{1}{2}}$	$\boldsymbol{e}_\mu^{n+\frac{1}{2}}$

$$\frac{\boldsymbol{e}_u^{n+1}-\overline{\boldsymbol{e}}_u^{n+1}}{\Delta t}+\frac{1}{2}\nabla_h(e_p^{n+1}-e_p^n)=0, \tag{4.13}$$

$$\nabla_h\cdot\boldsymbol{e}_u^{n+1}=0, \tag{4.14}$$

$$\begin{aligned}&\frac{\boldsymbol{e}_d^{n+1}-\boldsymbol{e}_d^n}{\Delta t}+\nabla_h\cdot(\tilde{\boldsymbol{d}}^{n+\frac{1}{2}}\overline{\boldsymbol{e}}_u^{n+\frac{1}{2}}+\tilde{\boldsymbol{e}}_d^{n+\frac{1}{2}}\overline{\boldsymbol{U}}^{n+\frac{1}{2}})+(\beta\nabla_h\overline{\boldsymbol{U}}^{n+\frac{1}{2}}+(1+\beta)(\nabla_h\overline{\boldsymbol{U}}^{n+\frac{1}{2}})^T)\tilde{\boldsymbol{e}}_d^{n+\frac{1}{2}}\\&\quad+(\beta\nabla_h\overline{\boldsymbol{e}}_u^{n+\frac{1}{2}}+(1+\beta)(\nabla_h\overline{\boldsymbol{e}}_u^{n+\frac{1}{2}})^T)\tilde{\boldsymbol{d}}^{n+\frac{1}{2}}=-\gamma\boldsymbol{e}_\mu^{n+\frac{1}{2}}+\boldsymbol{\tau}_d^{n+1}.\end{aligned} \tag{4.15}$$

for $0\le n\le M$. It is clear that that $\boldsymbol{e}_d^0\equiv 0$, $\boldsymbol{e}_u^0\equiv 0$, and $e_p^0=O(h^2)$.

Of course, the constructed approximate solutions Γ^m and $\overline{U}^m$ preserve the following estimates, which come from the assumed regularity of the exact solution:

$$\|\boldsymbol{\Gamma}^m\|_\infty+\|\nabla_h\boldsymbol{\Gamma}^m\|_\infty\le C^*,\quad \|\overline{\boldsymbol{U}}^m\|_\infty+\|\nabla_h\overline{\boldsymbol{U}}^m\|_\infty\le C^*,\quad \forall m\ge 0. \tag{4.16}$$

Meanwhile, the H_h^1, L_h^4, and L_h^6 bounds for the numerical solution that are uniform in time have been derived in Proposition 4.1.

On the other hand, a more careful look at the numerical error associated with the chemical potential vector is needed. The following expansion is observed:

$$\boldsymbol{e}_\mu^{n+\frac{1}{2}}=\boldsymbol{\Gamma}^{n+\frac{1}{2}}-\boldsymbol{\mu}^{n+\frac{1}{2}}=\mathcal{NLE}^{n+\frac{1}{2}}-\Delta_h\boldsymbol{e}_d^{n+\frac{1}{2}}, \tag{4.17}$$

$$\mathcal{NLE}^{n+\frac{1}{2}}=\mathcal{NLE}_1^{n+\frac{1}{2}}+\mathcal{NLE}_2^{n+\frac{1}{2}}+\mathcal{NLE}_3^{n+\frac{1}{2}}-\varepsilon^{-2}\tilde{\boldsymbol{e}}_d^{n+\frac{1}{2}},$$

$$\mathcal{NLE}_1^{n+\frac{1}{2}}=\frac{1}{2\varepsilon^2}[|\boldsymbol{D}^{n+1}|^2+|\boldsymbol{D}^n|^2]\boldsymbol{e}_d^{n+\frac{1}{2}},\quad \mathcal{NLE}_3^{n+\frac{1}{2}}=\frac{1}{4\varepsilon^2}[(\boldsymbol{D}^n+\boldsymbol{d}^n)\cdot\boldsymbol{e}_d^n](\boldsymbol{D}^{n+1}+\boldsymbol{D}^n), \tag{4.18}$$

$$\mathcal{NLE}_2^{n+\frac{1}{2}}=\frac{1}{4\varepsilon^2}[(\boldsymbol{D}^{n+1}+\boldsymbol{d}^{n+1})\cdot\boldsymbol{e}_d^{n+1}](\boldsymbol{D}^{n+1}+\boldsymbol{D}^n). \tag{4.19}$$

The following preliminary results will be extensively used in the convergence analysis.

Lemma 4.2. *The following estimates hold for the nonlinear error $\mathcal{NLE}^{n+\frac{1}{2}}$:*

$$\|\mathcal{NLE}^{n+\frac{1}{2}}\|_2\le\frac{5}{2\varepsilon^2}((C^*)^2+(M_6)^2)(\|\boldsymbol{e}_d^{n+\frac{1}{2}}\|_2+\|\nabla_h\boldsymbol{e}_d^{n+\frac{1}{2}}\|_2)+\varepsilon^{-2}\|\tilde{\boldsymbol{e}}_d^{n+\frac{1}{2}}\|_2, \tag{4.20}$$

$$\|\mathcal{NLE}^{n+\frac{1}{2}}\|_3 \le \frac{5}{2\varepsilon^2}((C^*)^2+(M_6)^2)\|\boldsymbol{e}_d^{n+\frac{1}{2}}\|_\infty + \varepsilon^{-2}\|\tilde{\boldsymbol{e}}_d^{n+\frac{1}{2}}\|_2, \tag{4.21}$$

$$\|\nabla_h\mathcal{NLE}^{n+\frac{1}{2}}\|_{\frac{3}{2}} \le C\varepsilon^{-2}\Big(((C^*)^2+(M_1)^2+(M_6)^2)(\|\boldsymbol{e}_d^{n+\frac{1}{2}}\|_\infty + \|\nabla_h\boldsymbol{e}_d^{n+\frac{1}{2}}\|_3) + \|\tilde{\boldsymbol{e}}_d^{n+\frac{1}{2}}\|_3\Big). \tag{4.22}$$

Proof. By the nonlinear expansion of $\mathcal{NLE}^{n+\frac{1}{2}}$, we see that

$$\begin{aligned}
\|\mathcal{NLE}^{n+\frac{1}{2}}\|_2 \le{}& \frac{1}{2\varepsilon^2}(\|\boldsymbol{d}^{n+1}\|_6^2+\|\boldsymbol{d}^n\|_6^2)\|\boldsymbol{e}_d^{n+\frac{1}{2}}\|_6\\
&+\frac{1}{4\varepsilon^2}(\|\boldsymbol{D}^{n+1}\|_6+\|\boldsymbol{d}^{n+1}\|_6)(\|\boldsymbol{D}^{n+1}\|_6+\|\boldsymbol{D}^n\|_6)\|\boldsymbol{e}_d^{n+1}\|_6\\
&+\frac{1}{4\varepsilon^2}(\|\boldsymbol{D}^n\|_6+\|\boldsymbol{d}^n\|_6)(\|\boldsymbol{D}^{n+1}\|_6+\|\boldsymbol{D}^n\|_6)\|\boldsymbol{e}_d^n\|_6+\varepsilon^{-2}\|\tilde{\boldsymbol{e}}_d^{n+\frac{1}{2}}\|_2\\
\le{}& \frac{1}{2\varepsilon^2}\{\|\boldsymbol{d}^{n+1}\|_6^2+\|\boldsymbol{d}^n\|_6^2+(\|\boldsymbol{D}^{n+1}\|_6+\|\boldsymbol{d}^{n+1}\|_6)(\|\boldsymbol{D}^{n+1}\|_6+\|\boldsymbol{D}^n\|_6)\\
&+(\|\boldsymbol{D}^n\|_6+\|\boldsymbol{d}^n\|_6)(\|\boldsymbol{D}^{n+1}\|_6+\|\boldsymbol{D}^n\|_6)\}\cdot\|\boldsymbol{e}_d^{n+\frac{1}{2}}\|_6+\varepsilon^{-2}\|\tilde{\boldsymbol{e}}_d^{n+\frac{1}{2}}\|_2\\
\le{}& \frac{5}{4\varepsilon^2}(\|\boldsymbol{D}^{n+1}\|_6^2+\|\boldsymbol{D}^n\|_6^2+\|\boldsymbol{d}^{n+1}\|_6^2+\|\boldsymbol{d}^n\|_6^2)\cdot\|\boldsymbol{e}_d^{n+\frac{1}{2}}\|_6+\varepsilon^{-2}\|\tilde{\boldsymbol{e}}_d^{n+\frac{1}{2}}\|_2\\
\le{}& \frac{5}{2\varepsilon^2}((C^*)^2+(M_6)^2)(\|\boldsymbol{e}_d^{n+\frac{1}{2}}\|_2+\|\nabla_h\boldsymbol{e}_d^{n+\frac{1}{2}}\|_2)+\varepsilon^{-2}\|\tilde{\boldsymbol{e}}_d^{n+\frac{1}{2}}\|_2,
\end{aligned}$$

where the discrete Sobolev inequality and (4.5) in Proposition 4.1 have been used in the last step. Thus the inequality (4.20) is valid. In terms of the discrete $\|\cdot\|_3$ estimate, an application of the discrete Hölder inequality gives

$$\begin{aligned}
\|\mathcal{NLE}^{n+\frac{1}{2}}\|_3 \le{}& \frac{1}{2\varepsilon^2}(\|\boldsymbol{d}^{n+1}\|_6^2+\|\boldsymbol{d}^n\|_6^2)\|\boldsymbol{e}_d^{n+\frac{1}{2}}\|_\infty\\
&+\frac{1}{4\varepsilon^2}(\|\boldsymbol{D}^{n+1}\|_6+\|\boldsymbol{d}^{n+1}\|_6)(\|\boldsymbol{D}^{n+1}\|_6+\|\boldsymbol{D}^n\|_6)\|\boldsymbol{e}_d^{n+1}\|_\infty\\
&+\frac{1}{4\varepsilon^2}(\|\boldsymbol{D}^n\|_6+\|\boldsymbol{d}^n\|_6)(\|\boldsymbol{D}^{n+1}\|_6+\|\boldsymbol{D}^n\|_6)\|\boldsymbol{e}_d^n\|_\infty+\varepsilon^{-2}\|\tilde{\boldsymbol{e}}_d^{n+\frac{1}{2}}\|_3\\
\le{}& \frac{1}{2\varepsilon^2}\{\|\boldsymbol{d}^{n+1}\|_6^2+\|\boldsymbol{d}^n\|_6^2+(\|\boldsymbol{D}^{n+1}\|_6+\|\boldsymbol{d}^{n+1}\|_6)(\|\boldsymbol{D}^{n+1}\|_6+\|\boldsymbol{D}^n\|_6)\\
&+(\|\boldsymbol{D}^n\|_6+\|\boldsymbol{d}^n\|_6)(\|\boldsymbol{D}^{n+1}\|_6+\|\boldsymbol{D}^n\|_6)\}\cdot\|\boldsymbol{e}_d^{n+\frac{1}{2}}\|_\infty+\varepsilon^{-2}\|\tilde{\boldsymbol{e}}_d^{n+\frac{1}{2}}\|_2\\
\le{}& \frac{5}{4\varepsilon^2}(\|\boldsymbol{D}^{n+1}\|_6^2+\|\boldsymbol{D}^n\|_6^2+\|\boldsymbol{d}^{n+1}\|_6^2+\|\boldsymbol{d}^n\|_6^2)\cdot\|\boldsymbol{e}_d^{n+\frac{1}{2}}\|_\infty+\varepsilon^{-2}\|\tilde{\boldsymbol{e}}_d^{n+\frac{1}{2}}\|_2\\
\le{}& \frac{5}{2\varepsilon^2}((C^*)^2+(M_6)^2)\|\boldsymbol{e}_d^{n+\frac{1}{2}}\|_\infty+\varepsilon^{-2}\|\tilde{\boldsymbol{e}}_d^{n+\frac{1}{2}}\|_2,
\end{aligned}$$

which, in turn, yields (4.21). Similarly, a local expansion of $\nabla_h\mathcal{NLE}^{n+\frac{1}{2}}$ implies that

$$\begin{aligned}
\|\nabla_h\mathcal{NLE}^{n+\frac{1}{2}}\|_{\frac{3}{2}} \le{}& \frac{1}{2\varepsilon^2}(\|\boldsymbol{D}^{n+1}\|_6^2+\|\boldsymbol{D}^n\|_6^2)\|\nabla_h\boldsymbol{e}_d^{n+\frac{1}{2}}\|_3\\
&+\frac{1}{\varepsilon^2}(\|\boldsymbol{D}^{n+1}\|_6\|\nabla_h\boldsymbol{D}^{n+1}\|_2+\|\boldsymbol{D}^n\|_6\|\nabla_h\boldsymbol{D}^n\|_2)\|\boldsymbol{e}_d^{n+\frac{1}{2}}\|_\infty\\
&+\frac{1}{4\varepsilon^2}(\|\boldsymbol{D}^{n+1}\|_6+\|\boldsymbol{d}^{n+1}\|_6)(\|\boldsymbol{D}^{n+1}\|_6+\|\boldsymbol{D}^n\|_6)\|\nabla_h\boldsymbol{e}_d^{n+1}\|_3
\end{aligned}$$

$$
\begin{aligned}
&+\frac{1}{4\varepsilon^2}(\|\nabla_h \boldsymbol{D}^{n+1}\|_2+\|\nabla_h \boldsymbol{d}^{n+1}\|_2)(\|\boldsymbol{D}^{n+1}\|_6+\|\boldsymbol{D}^{n}\|_6)\|\boldsymbol{e}_d^{n+1}\|_\infty\\
&+\frac{1}{4\varepsilon^2}(\|\boldsymbol{D}^{n+1}\|_6+\|\boldsymbol{d}^{n+1}\|_6)(\|\nabla_h \boldsymbol{D}^{n+1}\|_2+\|\nabla_h \boldsymbol{D}^{n}\|_2)\|\boldsymbol{e}_d^{n+1}\|_\infty\\
&+\frac{1}{4\varepsilon^2}(\|\nabla_h \boldsymbol{D}^{n}\|_2+\|\nabla_h \boldsymbol{d}^{n}\|_2)(\|\boldsymbol{D}^{n+1}\|_6+\|\boldsymbol{D}^{n}\|_6)\|\boldsymbol{e}_d^{n}\|_\infty\\
&+\frac{1}{4\varepsilon^2}(\|\boldsymbol{D}^{n}\|_6+\|\boldsymbol{d}^{n}\|_6)(\|\nabla_h \boldsymbol{D}^{n+1}\|_2+\|\nabla_h \boldsymbol{D}^{n}\|_2)\|\boldsymbol{e}_d^{n}\|_\infty\\
&+\frac{1}{4\varepsilon^2}(\|\boldsymbol{D}^{n}\|_6+\|\boldsymbol{d}^{n}\|_6)(\|\boldsymbol{D}^{n+1}\|_6+\|\boldsymbol{D}^{n}\|_6)\|\nabla_h \boldsymbol{e}_d^{n}\|_3+\varepsilon^{-2}\|\tilde{\boldsymbol{e}}_d^{n+\frac12}\|_3\\
\le\;& C\varepsilon^{-2}\Big[(\|\boldsymbol{D}^{n+1}\|_6^2+\|\boldsymbol{D}^{n}\|_6^2+\|\boldsymbol{d}^{n+1}\|_6^2+\|\boldsymbol{d}^{n}\|_6^2+\|\nabla_h \boldsymbol{D}^{n+1}\|_2^2+\|\nabla_h \boldsymbol{D}^{n}\|_2^2\\
&+\|\nabla_h \boldsymbol{d}^{n+1}\|_2^2+\|\nabla_h \boldsymbol{d}^{n}\|_2^2)(\|\nabla_h \boldsymbol{e}_d^{n+\frac12}\|_3+\|\boldsymbol{e}_d^{n+\frac12}\|_\infty)+\|\tilde{\boldsymbol{e}}_d^{n+\frac12}\|_3\Big]\\
\le\;& C\varepsilon^{-2}\Big(((C^*)^2+(M_1)^2+(M_6)^2)(\|\nabla_h \boldsymbol{e}_d^{n+\frac12}\|_3+\|\boldsymbol{e}_d^{n+\frac12}\|_\infty)+\|\tilde{\boldsymbol{e}}_d^{n+\frac12}\|_3\Big),
\end{aligned}
$$

which, in turn, gives (4.22). In fact, the Sobolev inequalities (4.2) and (4.5) (in Proposition 4.1) have been recalled. This completes the proof of the Lemma 4.2. □

4.3. Error estimate of the orientation equation in $\ell^\infty(0,T;\ell^2)\cap\ell^2(0,T;H_h^1)$

Taking a discrete inner product with (4.15) by $\boldsymbol{e}_d^{n+\frac12}$ leads to

$$
\begin{aligned}
&\frac12(\|\boldsymbol{e}_d^{n+1}\|_2^2-\|\boldsymbol{e}_d^{n}\|_2^2)+\gamma\Delta t\langle \boldsymbol{e}_\mu^{n+\frac12},\boldsymbol{e}_d^{n+\frac12}\rangle_C-\Delta t\langle \tilde{\boldsymbol{d}}^{n+\frac12}\overline{\boldsymbol{e}}_u^{n+\frac12}+\tilde{\boldsymbol{e}}_d^{n+\frac12}\overline{\boldsymbol{U}}^{n+\frac12},\nabla \boldsymbol{e}_d^{n+\frac12}\rangle_C\\
&\quad+\Delta t\langle(\beta\nabla_h\overline{\boldsymbol{U}}^{n+\frac12}+(1+\beta)(\nabla_h\overline{\boldsymbol{U}}^{n+\frac12})^T)\tilde{\boldsymbol{e}}_d^{n+\frac12},\boldsymbol{e}_d^{n+\frac12}\rangle_C\\
&\quad+\Delta t\langle(\beta\nabla_h\overline{\boldsymbol{e}}_u^{n+\frac12}+(1+\beta)(\nabla_h\overline{\boldsymbol{e}}_u^{n+\frac12})^T)\tilde{\boldsymbol{d}}^{n+\frac12},\boldsymbol{e}_d^{n+\frac12}\rangle_C=\Delta t\langle\boldsymbol{\tau}_d^{n+1},\boldsymbol{e}_d^{n+\frac12}\rangle_C.
\end{aligned}\tag{4.23}
$$

The term associated with the local truncation error could be bounded as

$$
\langle\boldsymbol{\tau}_d^{n+1},\boldsymbol{e}_d^{n+\frac12}\rangle_C\le\frac12(\|\boldsymbol{\tau}_d^{n+1}\|_2^2+\|\boldsymbol{e}_d^{n+\frac12}\|_2^2)\le\frac12\|\boldsymbol{\tau}_d^{n+1}\|_2^2+\frac14(\|\tilde{\boldsymbol{d}}^{n}\|_2^2+\|\tilde{\boldsymbol{d}}^{n+1}\|_2^2).
$$

In terms of of the chemical potential vector error, the nonlinear expansion (4.17) indicates that

$$
\begin{aligned}
-\langle\boldsymbol{e}_\mu^{n+\frac12},\boldsymbol{e}_d^{n+\frac12}\rangle_C&=\varepsilon^{-2}\langle\tilde{\boldsymbol{e}}_d^{n+\frac12},\boldsymbol{e}_d^{n+\frac12}\rangle_C-\langle\mathcal{NLE}^{n+\frac12},\boldsymbol{e}_d^{n+\frac12}\rangle_C\\
&\le\frac{1}{2\varepsilon^2}\Big(\|\tilde{\boldsymbol{e}}_d^{n+\frac12}\|_2^2+\|\boldsymbol{e}_d^{n+\frac12}\|_2^2\Big)+\frac12\|\mathcal{NLE}^{n+\frac12}\|_2^2+\frac12\|\boldsymbol{e}_d^{n+\frac12}\|_2^2\\
&\le\frac{5}{2\varepsilon^2}\|\tilde{\boldsymbol{e}}_d^{n+\frac12}\|_2^2+D_1\|\boldsymbol{e}_d^{n+\frac12}\|_2^2+D_2\|\nabla_h\boldsymbol{e}_d^{n+\frac12}\|_2^2,\quad\text{with}\\
D_1&=\frac{25}{\varepsilon^2}\Big((C^*)^2+(M_6)^2\Big)^2+\frac{1}{2\varepsilon^2}+\frac12,\quad D_2=\frac{25}{\varepsilon^2}\Big((C^*)^2+(M_6)^2\Big)^2.
\end{aligned}\tag{4.24}
$$

Regarding the nonlinear coupled terms, the regularity estimate (4.16) implies the following bounds:

$$
\langle\tilde{\boldsymbol{e}}_d^{n+\frac12}\overline{\boldsymbol{U}}^{n+\frac12},\nabla\boldsymbol{e}_d^{n+\frac12}\rangle_C\le C^*\cdot\|\tilde{\boldsymbol{e}}_d^{n+\frac12}\|_2\cdot\|\nabla\boldsymbol{e}_d^{n+\frac12}\|_2\le\frac{2(C^*)^2}{\gamma}\|\tilde{\boldsymbol{e}}_d^{n+\frac12}\|_2^2+\frac{\gamma}{8}\|\nabla\boldsymbol{e}_d^{n+\frac12}\|_2^2,\tag{4.25}
$$

$$\beta\langle\nabla_h\overline{\boldsymbol{U}}^{n+\frac{1}{2}}\tilde{\boldsymbol{e}}_d^{n+\frac{1}{2}},\boldsymbol{e}_d^{n+\frac{1}{2}}\rangle_C\le\beta C^*\|\tilde{\boldsymbol{e}}_d^{n+\frac{1}{2}}\|_2\cdot\|\boldsymbol{e}_d^{n+\frac{1}{2}}\|_2\le\frac{\beta C^*}{2}(\|\tilde{\boldsymbol{e}}_d^{n+\frac{1}{2}}\|_2^2+\|\boldsymbol{e}_d^{n+\frac{1}{2}}\|_2^2),\tag{4.26}$$

$$\begin{aligned}(1+\beta)\langle(\nabla_h\overline{\boldsymbol{U}}^{n+\frac{1}{2}})^T\tilde{\boldsymbol{e}}_d^{n+\frac{1}{2}},\boldsymbol{e}_d^{n+\frac{1}{2}}\rangle_C&\le(1+\beta)C^*\|\tilde{\boldsymbol{e}}_d^{n+\frac{1}{2}}\|_2\cdot\|\boldsymbol{e}_d^{n+\frac{1}{2}}\|_2\\&\le\frac{(1+\beta)C^*}{2}(\|\tilde{\boldsymbol{e}}_d^{n+\frac{1}{2}}\|_2^2+\|\boldsymbol{e}_d^{n+\frac{1}{2}}\|_2^2).\end{aligned}\tag{4.27}$$

Meanwhile, the following bound is obvious:

$$\|\tilde{\boldsymbol{d}}^{n+\frac{1}{2}}\|_4=\|\frac{1}{2}(3\boldsymbol{d}^n-\boldsymbol{d}^{n-1})\|_4\le\frac{3}{2}\|\boldsymbol{d}^n\|_4+\frac{1}{2}\|\boldsymbol{d}^{n-1}\|_4\le 2M_4,\tag{4.28}$$

where the uniform $\|\cdot\|_4$ bound (4.5) for the numerical solution is recalled. With the help of this bound, we get the estimates for the three other nonlinear coupled terms:

$$\begin{aligned}\langle\tilde{\boldsymbol{d}}^{n+\frac{1}{2}}\overline{\boldsymbol{e}}_u^{n+\frac{1}{2}},\nabla\boldsymbol{e}_d^{n+\frac{1}{2}}\rangle_C&\le\|\tilde{\boldsymbol{d}}^{n+\frac{1}{2}}\|_4\cdot\|\overline{\boldsymbol{e}}_u^{n+\frac{1}{2}}\|_4\cdot\|\nabla\boldsymbol{e}_d^{n+\frac{1}{2}}\|_2\\&\le M_4\cdot\|\overline{\boldsymbol{e}}_u^{n+\frac{1}{2}}\|_4\cdot\|\nabla\boldsymbol{e}_d^{n+\frac{1}{2}}\|_2\le\frac{2M_4^2}{\gamma}\|\overline{\boldsymbol{e}}_u^{n+\frac{1}{2}}\|_4^2+\frac{\gamma}{8}\|\nabla\boldsymbol{e}_d^{n+\frac{1}{2}}\|_2^2,\end{aligned}\tag{4.29}$$

$$\begin{aligned}\beta\langle\nabla_h\overline{\boldsymbol{e}}_u^{n+\frac{1}{2}}\tilde{\boldsymbol{d}}^{n+\frac{1}{2}},\boldsymbol{e}_d^{n+\frac{1}{2}}\rangle_C&\le\beta\|\nabla_h\overline{\boldsymbol{e}}_u^{n+\frac{1}{2}}\|_2\cdot\|\tilde{\boldsymbol{d}}^{n+\frac{1}{2}}\|_4\cdot\|\boldsymbol{e}_d^{n+\frac{1}{2}}\|_4\\&\le\beta M_4\|\nabla_h\overline{\boldsymbol{e}}_u^{n+\frac{1}{2}}\|_2\cdot\|\boldsymbol{e}_d^{n+\frac{1}{2}}\|_4\le\frac{2\beta^2M_4^2\lambda}{\nu}\|\boldsymbol{e}_d^{n+\frac{1}{2}}\|_4^2+\frac{\nu}{8\lambda}\|\nabla_h\overline{\boldsymbol{e}}_u^{n+\frac{1}{2}}\|_2^2,\end{aligned}\tag{4.30}$$

$$\begin{aligned}(1+\beta)\langle(\nabla_h\overline{\boldsymbol{e}}_u^{n+\frac{1}{2}})^T\tilde{\boldsymbol{d}}^{n+\frac{1}{2}},\boldsymbol{e}_d^{n+\frac{1}{2}}\rangle&\le(1+\beta)\|\nabla_h\overline{\boldsymbol{e}}_u^{n+\frac{1}{2}}\|_2\cdot\|\tilde{\boldsymbol{d}}^{n+\frac{1}{2}}\|_4\cdot\|\boldsymbol{e}_d^{n+\frac{1}{2}}\|_4\\&\le(1+\beta)M_4\|\nabla_h\overline{\boldsymbol{e}}_u^{n+\frac{1}{2}}\|_2\cdot\|\boldsymbol{e}_d^{n+\frac{1}{2}}\|_4\\&\le\frac{2(1+\beta)^2M_4^2\lambda}{\nu}\|\boldsymbol{e}_d^{n+\frac{1}{2}}\|_4^2+\frac{\nu}{8\lambda}\|\nabla_h\overline{\boldsymbol{e}}_u^{n+\frac{1}{2}}\|_2^2.\end{aligned}\tag{4.31}$$

Finally, a substitution of (4.24)–(4.31) into (4.23) yields

$$\begin{aligned}&\|\boldsymbol{e}_d^{n+1}\|_2^2-\|\boldsymbol{e}_d^n\|_2^2+\frac{3}{2}\gamma\Delta t\|\nabla_h\boldsymbol{e}_d^{n+\frac{1}{2}}\|_2^2-\frac{\nu\Delta t}{4\lambda}\|\nabla_h\overline{\boldsymbol{e}}_u^{n+\frac{1}{2}}\|_2^2\\&\le D_1^n\Delta t(\|\boldsymbol{e}_d^n\|_2^2+\|\boldsymbol{e}_d^{n+1}\|_2^2)+D_2^n\Delta t\|\overline{\boldsymbol{e}}_u^{n+\frac{1}{2}}\|_4^2+D_3^n\Delta t\|\boldsymbol{e}_d^{n+\frac{1}{2}}\|_4^2+\Delta t\|\boldsymbol{\tau}_d^{n+1}\|_2^2,\quad\text{with}\\&D_1^n:=\gamma\epsilon^{-2}+4(C^*)^2\gamma^{-1}+\beta C^*+(1+\beta)C^*+\frac{1}{2},\ \ D_2^n:=\frac{4M_4^2}{\gamma},\ \ D_3^n:=\frac{4(2\beta^2+2\beta+1)M_4^2\lambda}{\nu}.\end{aligned}\tag{4.32}$$

4.4. Error estimate of the momentum equation in $\ell^\infty(0,T;\ell^2)\cap\ell^2(0,T;H_h^1)$

Taking an inner product with (4.12) by $\overline{\boldsymbol{e}}_u^{n+\frac{1}{2}}$ leads to

$$\begin{aligned}&\frac{1}{2}(\|\overline{\boldsymbol{e}}_u^{n+1}\|_2^2-\|\boldsymbol{e}_u^n\|_2^2)+\nu\Delta t\|\nabla_h\overline{\boldsymbol{e}}_u^{n+\frac{1}{2}}\|_2^2+\Delta t\langle\nabla_he_p^n,\overline{\boldsymbol{e}}_u^{n+\frac{1}{2}}\rangle_1-\Delta t\langle\boldsymbol{\tau}_u^{n+1},\overline{\boldsymbol{e}}_u^{n+\frac{1}{2}}\rangle_1\\&+\frac{1}{2}\Delta t\langle\tilde{\boldsymbol{e}}_u^{n+\frac{1}{2}}\cdot\nabla_h\overline{\boldsymbol{U}}^{n+\frac{1}{2}}+\tilde{\boldsymbol{u}}^{n+\frac{1}{2}}\cdot\nabla_h\overline{\boldsymbol{e}}_u^{n+\frac{1}{2}}+\nabla_h\cdot(\tilde{\boldsymbol{e}}_u^{n+\frac{1}{2}}\cdot\overline{\boldsymbol{U}}^{n+\frac{1}{2}}+\tilde{\boldsymbol{u}}^{n+\frac{1}{2}}\cdot\overline{\boldsymbol{e}}_u^{n+\frac{1}{2}}),\overline{\boldsymbol{e}}_u^{n+\frac{1}{2}}\rangle_1\\&+\lambda\Delta t\langle(\nabla_h\boldsymbol{e}_\mu^{n+\frac{1}{2}})\tilde{\boldsymbol{d}}^{n+\frac{1}{2}},\overline{\boldsymbol{e}}_u^{n+\frac{1}{2}}\rangle_1-\lambda\Delta t\langle(\beta\boldsymbol{e}_\mu^{n+\frac{1}{2}}\tilde{\boldsymbol{d}}^{n+\frac{1}{2}}+(1+\beta)\Gamma^{n+\frac{1}{2}}\tilde{\boldsymbol{e}}_d^{n+\frac{1}{2}}),\nabla_h\overline{\boldsymbol{e}}_u^{n+\frac{1}{2}}\rangle_1\end{aligned}$$

$$+ \lambda\Delta t\langle(\nabla_h\boldsymbol{\Gamma}^{n+\frac{1}{2}})\tilde{\boldsymbol{e}}_d^{n+\frac{1}{2}}, \overline{\boldsymbol{e}}_u^{n+\frac{1}{2}}\rangle_1 - \lambda\Delta t\langle(\beta\Gamma^{n+\frac{1}{2}}\tilde{\boldsymbol{e}}_d^{n+\frac{1}{2}} + (\beta+1)\boldsymbol{e}_\mu^{n+\frac{1}{2}}\tilde{\boldsymbol{d}}^{n+\frac{1}{2}}), \nabla_h\overline{\boldsymbol{e}}_u^{n+\frac{1}{2}}\rangle_1 = 0, \tag{4.33}$$

with repeated application of the summation-by-parts formulas (3.1)–(3.2). A bound for the truncation term is similar

$$\langle\boldsymbol{\tau}_u^{n+1}, \overline{\boldsymbol{e}}_u^{n+\frac{1}{2}}\rangle_1 \le \frac{1}{2}(\|\boldsymbol{\tau}_u^{n+1}\|_2^2 + \|\overline{\boldsymbol{e}}_u^{n+\frac{1}{2}}\|_2^2). \tag{4.34}$$

The analysis for the explicit the pressure gradient term includes more technical details

$$\begin{aligned}
\langle\nabla_h e_p^n, \overline{\boldsymbol{e}}_u^{n+\frac{1}{2}}\rangle_1 &= -\langle e_p^n, \nabla_h\cdot\overline{\boldsymbol{e}}_u^{n+\frac{1}{2}}\rangle_C = -\langle e_p^n, \frac{1}{2}\nabla_h\cdot(\overline{\boldsymbol{e}}_u^{n+1} + \boldsymbol{e}_u^n)\rangle_C = -\langle e_p^n, \frac{1}{2}\nabla_h\cdot\overline{\boldsymbol{e}}_u^{n+1}\rangle_C \\
&= -\langle e_p^n, \frac{\Delta t}{4}\Delta_h(e_p^{n+1} - e_p^n)\rangle_C = \frac{\Delta t}{4}\langle\nabla_h e_p^n, \nabla_h(e_p^{n+1} - e_p^n)\rangle_1 \\
&= \frac{\Delta t}{8}(\|\nabla_h e_p^{n+1}\|_2^2 - \|\nabla_h e_p^n\|_2^2) - \frac{\Delta t}{8}\|\nabla_h e_p^{n+1} - \nabla_h e_p^n\|_2^2 \\
&= \frac{\Delta t}{8}(\|\nabla_h e_p^{n+1}\|_2^2 - \|\nabla_h e_p^n\|_2^2) - \frac{1}{2\Delta t}\|\boldsymbol{e}_u^{n+1} - \overline{\boldsymbol{e}}_u^{n+1}\|_2^2,
\end{aligned} \tag{4.35}$$

where the error equation (4.13) plays an important role. Regarding the linearized convection term, we begin with the following identity, which comes from the summation-by-parts formula:

$$\begin{aligned}
&\langle\tilde{\boldsymbol{u}}^{n+\frac{1}{2}}\cdot\nabla_h\overline{\boldsymbol{e}}_u^{n+\frac{1}{2}} + \nabla_h\cdot(\tilde{\boldsymbol{u}}^{n+\frac{1}{2}}\cdot\overline{\boldsymbol{e}}_u^{n+\frac{1}{2}}), \overline{\boldsymbol{e}}_u^{n+\frac{1}{2}}\rangle_1 \\
&= \langle\tilde{\boldsymbol{u}}^{n+\frac{1}{2}}\cdot\nabla_h\overline{\boldsymbol{e}}_u^{n+\frac{1}{2}}, \overline{\boldsymbol{e}}_u^{n+\frac{1}{2}}\rangle_1 - \langle\tilde{\boldsymbol{u}}^{n+\frac{1}{2}}\cdot\overline{\boldsymbol{e}}_u^{n+\frac{1}{2}}, \nabla_h\overline{\boldsymbol{e}}_u^{n+\frac{1}{2}}\rangle_1 = 0.
\end{aligned} \tag{4.36}$$

The two remaining terms in the convection part could be analyzed as follows:

$$-\langle\tilde{\boldsymbol{e}}_u^{n+\frac{1}{2}}\cdot\nabla_h\overline{\boldsymbol{U}}^{n+\frac{1}{2}}, \overline{\boldsymbol{e}}_u^{n+\frac{1}{2}}\rangle_1 \le C^*\|\tilde{\boldsymbol{e}}_u^{n+\frac{1}{2}}\|_2\cdot\|\overline{\boldsymbol{e}}_u^{n+\frac{1}{2}}\|_2 \le \frac{C^*}{2}(\|\tilde{\boldsymbol{e}}_u^{n+\frac{1}{2}}\|_2^2 + \|\overline{\boldsymbol{e}}_u^{n+\frac{1}{2}}\|_2^2), \tag{4.37}$$

$$\begin{aligned}
-\langle\nabla_h\cdot(\tilde{\boldsymbol{e}}_u^{n+\frac{1}{2}}\cdot\overline{\boldsymbol{U}}^{n+\frac{1}{2}}), \overline{\boldsymbol{e}}_u^{n+\frac{1}{2}}\rangle_1 &= \langle\tilde{\boldsymbol{e}}_u^{n+\frac{1}{2}}\cdot\overline{\boldsymbol{U}}^{n+\frac{1}{2}}, \nabla_h\overline{\boldsymbol{e}}_u^{n+\frac{1}{2}}\rangle_1 \le C^*\|\tilde{\boldsymbol{e}}_u^{n+\frac{1}{2}}\|_2\cdot\|\nabla_h\overline{\boldsymbol{e}}_u^{n+\frac{1}{2}}\|_2 \\
&\le \frac{2(C^*)^2}{\nu}\|\tilde{\boldsymbol{e}}_u^{n+\frac{1}{2}}\|_2^2 + \frac{\nu}{8}\|\nabla_h\overline{\boldsymbol{e}}_u^{n+\frac{1}{2}}\|_2^2,
\end{aligned} \tag{4.38}$$

with the help of the regularity estimate (4.16). The three other nonlinear terms could be bounded in a similar manner:

$$-\lambda\langle(\nabla_h\boldsymbol{\Gamma}^{n+\frac{1}{2}})\tilde{\boldsymbol{e}}_d^{n+\frac{1}{2}}, \overline{\boldsymbol{e}}_u^{n+\frac{1}{2}}\rangle_1 \le C^*\lambda\|\tilde{\boldsymbol{e}}_d^{n+\frac{1}{2}}\|_2\cdot\|\overline{\boldsymbol{e}}_u^{n+\frac{1}{2}}\|_2 \le \frac{C^*\lambda}{2}(\|\tilde{\boldsymbol{e}}_d^{n+\frac{1}{2}}\|_2^2 + \|\overline{\boldsymbol{e}}_u^{n+\frac{1}{2}}\|_2^2), \tag{4.39}$$

$$\begin{aligned}
\lambda\beta\langle\tilde{\boldsymbol{e}}_d^{n+\frac{1}{2}}(\Gamma^{n+\frac{1}{2}})^T, \nabla_h\overline{\boldsymbol{e}}_u^{n+\frac{1}{2}}\rangle_1 &\le \lambda\beta C^*\|\tilde{\boldsymbol{e}}_d^{n+\frac{1}{2}}\|_2\cdot\|\nabla_h\overline{\boldsymbol{e}}_u^{n+\frac{1}{2}}\|_2 \\
&\le \frac{4(\lambda\beta C^*)^2}{\nu}\|\tilde{\boldsymbol{e}}_d^{n+\frac{1}{2}}\|_2^2 + \frac{\nu}{16}\|\nabla_h\overline{\boldsymbol{e}}_u^{n+\frac{1}{2}}\|_2^2,
\end{aligned} \tag{4.40}$$

$$\begin{aligned}
\lambda(1+\beta)\langle\boldsymbol{\Gamma}^{n+\frac{1}{2}}(\tilde{\boldsymbol{e}}_d^{n+\frac{1}{2}})^T, \nabla_h\overline{\boldsymbol{e}}_u^{n+\frac{1}{2}}\rangle_1 &\le \lambda(1+\beta)C^*\|\tilde{\boldsymbol{e}}_d^{n+\frac{1}{2}}\|_2\cdot\|\nabla_h\overline{\boldsymbol{e}}_u^{n+\frac{1}{2}}\|_2 \\
&\le \frac{4(\lambda(1+\beta)C^*)^2}{\nu}\|\tilde{\boldsymbol{e}}_d^{n+\frac{1}{2}}\|_2^2 + \frac{\nu}{16}\|\nabla_h\overline{\boldsymbol{e}}_u^{n+\frac{1}{2}}\|_2^2.
\end{aligned} \tag{4.41}$$

The estimates of the three remaining three nonlinear coupled terms contain more technical details. The chemical potential vector's error expansion (4.17) leads to the following decomposition of the first nonlinear coupled term:

$$-\lambda\langle(\nabla_h \boldsymbol{e}_\mu^{n+\frac{1}{2}})\tilde{\boldsymbol{d}}^{n+\frac{1}{2}}, \overline{\boldsymbol{e}}_u^{n+\frac{1}{2}}\rangle_1 = \lambda\langle\nabla_h(\Delta_h \boldsymbol{e}_d^{n+\frac{1}{2}})\tilde{\boldsymbol{d}}^{n+\frac{1}{2}}, \overline{\boldsymbol{e}}_u^{n+\frac{1}{2}}\rangle_2 - \lambda\langle(\nabla_h \mathcal{NLE}^{n+\frac{1}{2}})\tilde{\boldsymbol{d}}^{n+\frac{1}{2}}, \overline{\boldsymbol{e}}_u^{n+\frac{1}{2}}\rangle_2. \tag{4.42}$$

In particular, a bound for the second part on the right hand side is straightforward:

$$\begin{aligned}
-\lambda\langle(\nabla_h \mathcal{NLE}^{n+\frac{1}{2}})\tilde{\boldsymbol{d}}^{n+\frac{1}{2}}, \overline{\boldsymbol{e}}_u^{n+\frac{1}{2}}\rangle_1 &\le \lambda\|\nabla_h \mathcal{NLE}^{n+\frac{1}{2}}\|_{\frac{3}{2}} \cdot \|\tilde{\boldsymbol{d}}^{n+\frac{1}{2}}\|_6 \cdot \|\overline{\boldsymbol{e}}_u^{n+\frac{1}{2}}\|_6 \\
&\le C_1\lambda M_6(\|\overline{\boldsymbol{e}}_u^{n+\frac{1}{2}}\|_2 + \|\nabla_h \overline{\boldsymbol{e}}_u^{n+\frac{1}{2}}\|_2)\|\nabla_h \mathcal{NLE}^{n+\frac{1}{2}}\|_{\frac{3}{2}} \\
&\le \frac{C_1\lambda M_6}{2}\|\overline{\boldsymbol{e}}_u^{n+\frac{1}{2}}\|_2^2 + \frac{\nu}{16}\|\nabla_h \overline{\boldsymbol{e}}_u^{n+\frac{1}{2}}\|_2^2 + C_5\|\nabla_h \mathcal{NLE}^{n+\frac{1}{2}}\|_{\frac{3}{2}}^2,
\end{aligned}$$

with $C_5 = \dfrac{C_1\lambda M_6}{2} + 4\nu^{-1}(C_1\lambda M_6)^2$, and the discrete Sobolev inequality (4.2) has been applied in the derivation. Going back (4.42), we see that

$$\begin{aligned}
-\lambda\langle(\nabla_h \boldsymbol{e}_\mu^{n+\frac{1}{2}})\tilde{\boldsymbol{d}}^{n+\frac{1}{2}}, \overline{\boldsymbol{e}}_u^{n+\frac{1}{2}}\rangle_1 &\le \lambda\langle\nabla_h(\Delta_h \boldsymbol{e}_d^{n+\frac{1}{2}})\tilde{\boldsymbol{d}}^{n+\frac{1}{2}}, \overline{\boldsymbol{e}}_u^{n+\frac{1}{2}}\rangle_1 \\
&\quad + \frac{C_1\lambda M_6}{2}\|\overline{\boldsymbol{e}}_u^{n+\frac{1}{2}}\|_2^2 + \frac{\nu}{16}\|\nabla_h \overline{\boldsymbol{e}}_u^{n+\frac{1}{2}}\|_2^2 + C_5\|\nabla_h \mathcal{NLE}^{n+\frac{1}{2}}\|_{\frac{3}{2}}^2 \\
&\le \lambda\langle\nabla_h(\Delta_h \boldsymbol{e}_d^{n+\frac{1}{2}})\tilde{\boldsymbol{d}}^{n+\frac{1}{2}}, \overline{\boldsymbol{e}}_u^{n+\frac{1}{2}}\rangle_1 + \frac{C_1\lambda M_6}{2}\|\overline{\boldsymbol{e}}_u^{n+\frac{1}{2}}\|_2^2 + \frac{\nu}{16}\|\nabla_h \overline{\boldsymbol{e}}_u^{n+\frac{1}{2}}\|_2^2 \\
&\quad + C_6\varepsilon^{-4}(\|\boldsymbol{e}_d^{n+\frac{1}{2}}\|_\infty^2 + \|\nabla_h \boldsymbol{e}_d^{n+\frac{1}{2}}\|_3^2) + 2C^2\varepsilon^{-4}\|\tilde{\boldsymbol{e}}_d^{n+\frac{1}{2}}\|_3^2,
\end{aligned} \tag{4.43}$$

with $C_6 = 4C^2((C^*)^2 + (M_1)^2 + (M_6)^2)^2$, and the estimate (4.22) (in Lemma 4.2) has been recalled. A similar argument could be applied to the second nonlinear coupled term:

$$\begin{aligned}
&\lambda\beta\langle\mathcal{NLE}^{n+\frac{1}{2}}\tilde{\boldsymbol{d}}^{n+\frac{1}{2}}, \nabla_h \overline{\boldsymbol{e}}_u^{n+\frac{1}{2}}\rangle_1 \le \lambda\beta\|\mathcal{NLE}^{n+\frac{1}{2}}\|_3 \cdot \|\tilde{\boldsymbol{d}}^{n+\frac{1}{2}}\|_6 \cdot \|\nabla_h \overline{\boldsymbol{e}}_u^{n+\frac{1}{2}}\|_2 \\
\le&\lambda\beta M_6\|\mathcal{NLE}^{n+\frac{1}{2}}\|_3 \cdot \|\nabla_h \overline{\boldsymbol{e}}_u^{n+\frac{1}{2}}\|_2 \le \frac{2(\lambda\beta M_6)^2}{\nu}\|\mathcal{NLE}^{n+\frac{1}{2}}\|_3^2 + \frac{\nu}{8}\|\nabla_h \overline{\boldsymbol{e}}_u^{n+\frac{1}{2}}\|_2^2,
\end{aligned} \tag{4.44}$$

$$\begin{aligned}
&\lambda\beta\langle\boldsymbol{e}_\mu^{n+\frac{1}{2}}\tilde{\boldsymbol{d}}^{n+\frac{1}{2}}, \nabla_h \overline{\boldsymbol{e}}_u^{n+\frac{1}{2}}\rangle_1 = -\lambda\beta\langle\Delta_h \boldsymbol{e}_d^{n+\frac{1}{2}}\tilde{\boldsymbol{d}}^{n+\frac{1}{2}}, \nabla_h \overline{\boldsymbol{e}}_u^{n+\frac{1}{2}}\rangle_1 + \lambda\beta\langle\mathcal{NLE}^{n+\frac{1}{2}}\tilde{\boldsymbol{d}}^{n+\frac{1}{2}}, \nabla_h \overline{\boldsymbol{e}}_u^{n+\frac{1}{2}}\rangle_1 \\
\le& -\lambda\beta\langle\Delta_h \boldsymbol{e}_d^{n+\frac{1}{2}}\tilde{\boldsymbol{d}}^{n+\frac{1}{2}}, \nabla_h \overline{\boldsymbol{e}}_u^{n+\frac{1}{2}}\rangle_1 + \frac{2(\lambda\beta M_6)^2}{\nu}\|\mathcal{NLE}^{n+1}\|_3^2 + \frac{\nu}{8}\|\nabla_h \overline{\boldsymbol{e}}_u^{n+\frac{1}{2}}\|_2^2 \\
\le& -\lambda\beta\langle\Delta_h \boldsymbol{e}_d^{n+\frac{1}{2}}\tilde{\boldsymbol{d}}^{n+\frac{1}{2}}, \nabla_h \overline{\boldsymbol{e}}_u^{n+\frac{1}{2}}\rangle_1 + \frac{\nu}{8}\|\nabla_h \overline{\boldsymbol{e}}_u^{n+\frac{1}{2}}\|_2^2 + \varepsilon^{-4}(C_7\|\boldsymbol{e}_d^{n+\frac{1}{2}}\|_\infty^2 + C_8\|\tilde{\boldsymbol{e}}_d^{n+\frac{1}{2}}\|_3^2),
\end{aligned} \tag{4.45}$$

with $C_7 = 25(\lambda\beta M_6)^2((C^*)^2 + (M_6)^2)^2\nu^{-1}$, $C_8 = 4(\lambda\beta M_6)^2\nu^{-1}$. The third nonlinear coupled term could be analyzed as follows:

$$\begin{aligned}
&\lambda(1+\beta)\langle\mathcal{NLE}^{n+\frac{1}{2}}\tilde{\boldsymbol{d}}^{n+\frac{1}{2}}, \nabla_h \overline{\boldsymbol{e}}_u^{n+\frac{1}{2}}\rangle_1 \le \lambda(1+\beta)\|\mathcal{NLE}^{n+\frac{1}{2}}\|_3 \cdot \|\tilde{\boldsymbol{d}}^{n+\frac{1}{2}}\|_6 \cdot \|\nabla_h \overline{\boldsymbol{e}}_u^{n+\frac{1}{2}}\|_2 \\
\le&\lambda(1+\beta)M_6\|\mathcal{NLE}^{n+\frac{1}{2}}\|_3 \cdot \|\nabla_h \overline{\boldsymbol{e}}_u^{n+\frac{1}{2}}\|_2 \le \frac{2(\lambda(1+\beta)M_6)^2}{\nu}\|\mathcal{NLE}^{n+\frac{1}{2}}\|_3^2 + \frac{\nu}{8}\|\nabla_h \overline{\boldsymbol{e}}_u^{n+\frac{1}{2}}\|_2^2, \\
&\lambda(1+\beta)\langle\boldsymbol{e}_\mu^{n+\frac{1}{2}}\tilde{\boldsymbol{d}}^{n+\frac{1}{2}}, \nabla_h \overline{\boldsymbol{e}}_u^{n+\frac{1}{2}}\rangle_1
\end{aligned}$$

$$
\begin{aligned}
&= -\lambda(1+\beta)\langle\Delta_h \boldsymbol{e}_d^{n+\frac{1}{2}}\tilde{\boldsymbol{d}}^{n+\frac{1}{2}}, \nabla_h \overline{\boldsymbol{e}}_u^{n+\frac{1}{2}}\rangle_1 + \lambda(1+\beta)\langle \mathcal{NLE}^{n+1}\tilde{\boldsymbol{d}}^{n+\frac{1}{2}}, \nabla_h \overline{\boldsymbol{e}}_u^{n+\frac{1}{2}}\rangle_1 \\
&\le -\lambda(1+\beta)\langle\Delta_h \boldsymbol{e}_d^{n+\frac{1}{2}}\tilde{\boldsymbol{d}}^{n+\frac{1}{2}}, \nabla_h \overline{\boldsymbol{e}}_u^{n+\frac{1}{2}}\rangle_1 + \frac{2(\lambda(1+\beta)M_6)^2}{\nu}\|\mathcal{NLE}^{n+\frac{1}{2}}\|_3^2 + \frac{\nu}{8}\|\nabla_h \overline{\boldsymbol{e}}_u^{n+\frac{1}{2}}\|_2^2 \\
&\le -\lambda(1+\beta)\langle\Delta_h \boldsymbol{e}_d^{n+\frac{1}{2}}\tilde{\boldsymbol{d}}^{n+\frac{1}{2}}, \nabla_h \overline{\boldsymbol{e}}_u^{n+\frac{1}{2}}\rangle_1 + \frac{\nu}{8}\|\nabla_h \overline{\boldsymbol{e}}_u^{n+\frac{1}{2}}\|_2^2 + \varepsilon^{-4}(C_9\|\boldsymbol{e}_d^{n+\frac{1}{2}}\|_\infty^2 + C_{10}\|\tilde{\boldsymbol{e}}_d^{n+\frac{1}{2}}\|_3^2),
\end{aligned} \tag{4.46}
$$

where $C_9 = 25(\lambda(1+\beta)M_6)^2((C^*)^2 + (M_6)^2)^2\nu^{-1}$, $C_{10} = 4(\lambda(1+\beta)M_6)^2\nu^{-1}$.

Meanwhile, taking a discrete inner product with the error equation (4.13) by $\boldsymbol{e}_u^{n+1}$ yields

$$
\|\boldsymbol{e}_u^{n+1}\|_2^2 - \|\overline{\boldsymbol{e}}_u^{n+1}\|_2^2 + \|\boldsymbol{e}_u^{n+1} - \overline{\boldsymbol{e}}_u^{n+1}\|_2^2 = 0, \qquad \langle e_u^{n+1}, \nabla_h(e_p^{n+1} - e_p^n)\rangle = 0. \tag{4.47}
$$

Finally, a substitution of (4.34), (4.35), and (4.37)–(4.46) into (4.33), combined with (4.47), gives

$$
\begin{aligned}
&\|\overline{\boldsymbol{e}}_u^{n+1}\|_2^2 - \|\boldsymbol{e}_u^n\|_2^2 + \nu\Delta t\|\nabla_h \overline{\boldsymbol{e}}_u^{n+\frac{1}{2}}\|_2^2 + \frac{\Delta t^2}{4}(\|\nabla_h e_p^{n+1}\|_2^2 - \|\nabla_h e_p^n\|_2^2) \\
\le& 2\lambda\Delta t\langle\nabla_h(\Delta_h \boldsymbol{e}_d^{n+\frac{1}{2}})\tilde{\boldsymbol{d}}^{n+\frac{1}{2}}, \overline{\boldsymbol{e}}_u^{n+\frac{1}{2}}\rangle_1 - 2\lambda\Delta t\langle(1+\beta)\Delta_h \boldsymbol{e}_d^{n+\frac{1}{2}}\tilde{\boldsymbol{d}}^{n+\frac{1}{2}} + \beta\Delta_h \boldsymbol{e}_d^{n+\frac{1}{2}}\tilde{\boldsymbol{d}}^{n+\frac{1}{2}}, \nabla_h \overline{\boldsymbol{e}}_u^{n+\frac{1}{2}}\rangle_1 \\
&+ \Delta t\|\boldsymbol{\tau}_u^{n+1}\|_2^2 + D_6^n\Delta t\|\overline{\boldsymbol{e}}_u^{n+\frac{1}{2}}\|_2^2 + D_7^n\Delta t\|\tilde{\boldsymbol{e}}_u^{n+\frac{1}{2}}\|_2^2 + \|\boldsymbol{e}_u^{n+\frac{1}{2}} - \overline{\boldsymbol{e}}_u^{n+\frac{1}{2}}\|_2^2 + D_8^n\Delta t\|\tilde{\boldsymbol{e}}_d^{n+\frac{1}{2}}\|_2^2 \\
&+ 2\varepsilon^{-4}\Delta t\Big((C_6 + C_7 + C_9)\|\boldsymbol{e}_d^{n+\frac{1}{2}}\|_\infty^2 + (2C^2 + C_8 + C_{10})\|\tilde{\boldsymbol{e}}_d^{n+\frac{1}{2}}\|_3^2 + C_6\|\nabla_h \boldsymbol{e}_d^{n+\frac{1}{2}}\|_3^2\Big), \\
&D_6^n = C^*(1+\lambda) + C_1\lambda M_6 + 1, \quad D_7^n = C^*/2 + 2C^*\nu^{-1}, \\
&D_8^n = C^*\lambda + 8(2\beta^2 + 2\beta + 1)(\lambda C^*)^2\nu^{-1}.
\end{aligned} \tag{4.48}
$$

4.5. Error estimate of the orientation equation in $\ell^\infty(0,T;H_h^1)\cap\ell^2(0,T;H_h^2)$

Taking a discrete inner product with (4.15) by $-\Delta_h \boldsymbol{e}_d^{n+\frac{1}{2}}$, we get

$$
\begin{aligned}
&\frac{1}{2}(\|\nabla_h \boldsymbol{e}_d^{n+1}\|_2^2 - \|\nabla_h \boldsymbol{e}_d^n\|_2^2) - \gamma\Delta t\langle\tilde{\boldsymbol{\mu}}^{n+\frac{1}{2}}, \Delta_h \boldsymbol{e}_d^{n+\frac{1}{2}}\rangle_C \\
&\quad - \Delta t\langle\nabla_h\cdot(\tilde{\boldsymbol{e}}_d^{n+\frac{1}{2}}\overline{\boldsymbol{U}}^{n+\frac{1}{2}}), \Delta_h \boldsymbol{e}_d^{n+\frac{1}{2}}\rangle_C + \Delta t\langle\tilde{\boldsymbol{d}}^{n+\frac{1}{2}}\overline{\boldsymbol{e}}_u^{n+\frac{1}{2}}, \nabla_h\Delta_h \boldsymbol{e}_d^{n+\frac{1}{2}}\rangle_1 \\
&\quad - \Delta t\langle(\beta\nabla_h\overline{\boldsymbol{U}}^{n+\frac{1}{2}} + (1+\beta)(\nabla_h\overline{\boldsymbol{U}}^{n+\frac{1}{2}})^T)\tilde{\boldsymbol{e}}_d^{n+\frac{1}{2}}, \Delta_h \boldsymbol{e}_d^{n+\frac{1}{2}}\rangle_C \\
&\quad - \Delta t\langle(\beta\nabla_h\overline{\boldsymbol{e}}_u^{n+\frac{1}{2}} + (1+\beta)(\nabla_h\overline{\boldsymbol{e}}_u^{n+\frac{1}{2}})^T)\tilde{\boldsymbol{d}}^{n+\frac{1}{2}}, \Delta_h \boldsymbol{e}_d^{n+\frac{1}{2}}\rangle_C = -\Delta t\langle\boldsymbol{\tau}_d^{n+1}, \Delta_h \boldsymbol{e}_d^{n+\frac{1}{2}}\rangle_C.
\end{aligned} \tag{4.49}
$$

A bound for the truncation error term is standard:

$$
-\langle\boldsymbol{\tau}_d^{n+1}, \Delta_h \boldsymbol{e}_d^{n+\frac{1}{2}}\rangle_C = \langle\nabla_h\boldsymbol{\tau}_d^{n+1}, \nabla_h \boldsymbol{e}_d^{n+\frac{1}{2}}\rangle_1 \le \frac{1}{2}(\|\nabla_h\boldsymbol{\tau}_d^{n+1}\|^2 + \|\nabla_h \boldsymbol{e}_d^{n+\frac{1}{2}}\|^2).
$$

A combination of the chemical potential error expansion (4.17) and inequality (4.20) (in Lemma 4.2) reveals that

$$
\begin{aligned}
&-\langle\tilde{\boldsymbol{\mu}}^{n+\frac{1}{2}}, \Delta_h \boldsymbol{e}_d^{n+\frac{1}{2}}\rangle_C = \langle-\mathcal{NLE}^{n+\frac{1}{2}} + \Delta_h \boldsymbol{e}_d^{n+\frac{1}{2}}, \Delta_h \boldsymbol{e}_d^{n+\frac{1}{2}}\rangle_C = \|\Delta_h \boldsymbol{e}_d^{n+\frac{1}{2}}\|_2^2 - \langle\mathcal{NLE}^{n+\frac{1}{2}}, \Delta_h \boldsymbol{e}_d^{n+\frac{1}{2}}\rangle_C \\
\ge& \|\Delta_h \boldsymbol{e}_d^{n+\frac{1}{2}}\|_2^2 - \frac{1}{8}\|\Delta_h \boldsymbol{e}_d^{n+\frac{1}{2}}\|_2^2 - 2\|\mathcal{NLE}^{n+\frac{1}{2}}\|_2^2 \\
\ge& \frac{7}{8}\|\Delta_h \boldsymbol{e}_d^{n+\frac{1}{2}}\|_2^2 - \frac{5}{\varepsilon^2}((C^*)^2 + (M_6)^2)(\|\overline{\boldsymbol{d}}^{n+\frac{1}{2}}\|_2^2 + \|\nabla_h\overline{\boldsymbol{d}}^{n+\frac{1}{2}}\|_2^2) - 2\varepsilon^{-2}\|\tilde{\boldsymbol{d}}^{n+\frac{1}{2}}\|_2^2.
\end{aligned} \tag{4.50}
$$

Meanwhile, the discrete gradient term could be analyzed as follows, with the help of the regularity estimate (4.16):

$$\begin{aligned}\|\nabla_h \cdot (\tilde{\boldsymbol{e}}_d^{n+\frac{1}{2}} \overline{\boldsymbol{U}}^{n+\frac{1}{2}})\|_2 &\le C(\|\overline{\boldsymbol{U}}^{n+\frac{1}{2}}\|_\infty + \|\nabla_h \overline{\boldsymbol{U}}^{n+\frac{1}{2}}\|_\infty)(\|\tilde{\boldsymbol{e}}_d^{n+\frac{1}{2}}\|_2 + \|\nabla_h \tilde{\boldsymbol{e}}_d^{n+\frac{1}{2}}\|_2) \\ &\le CC^*(\|\tilde{\boldsymbol{e}}_d^{n+\frac{1}{2}}\|_2 + \|\nabla_h \tilde{\boldsymbol{e}}_d^{n+\frac{1}{2}}\|_2).\end{aligned}$$

In turn, a bound for the nonlinear term $\langle \nabla_h \cdot (\tilde{\boldsymbol{e}}_d^{n+\frac{1}{2}} \overline{\boldsymbol{U}}^{n+\frac{1}{2}}), \Delta_h \boldsymbol{e}_d^{n+\frac{1}{2}} \rangle$ could be derived as

$$\begin{aligned}\langle \nabla_h \cdot (\tilde{\boldsymbol{e}}_d^{n+\frac{1}{2}} \overline{\boldsymbol{U}}^{n+\frac{1}{2}}), \Delta_h \boldsymbol{e}_d^{n+\frac{1}{2}} \rangle_C &\le \|\nabla_h \cdot (\tilde{\boldsymbol{e}}_d^{n+\frac{1}{2}} \overline{\boldsymbol{U}}^{n+\frac{1}{2}})\|_2 \cdot \|\Delta_h \boldsymbol{e}_d^{n+\frac{1}{2}}\|_2 \\ &\le \frac{2}{\gamma}\|\nabla_h \cdot (\tilde{\boldsymbol{e}}_d^{n+\frac{1}{2}} \overline{\boldsymbol{U}}^{n+\frac{1}{2}})\|_2^2 + \frac{\gamma}{8}\|\Delta_h \boldsymbol{e}_d^{n+\frac{1}{2}}\|_2^2 \\ &\le \frac{2CC^*}{\gamma}(\|\tilde{\boldsymbol{e}}_d^{n+\frac{1}{2}}\|_2^2 + \|\nabla_h \tilde{\boldsymbol{e}}_d^{n+\frac{1}{2}}\|_2^2) + \frac{\gamma}{8}\|\Delta_h \boldsymbol{e}_d^{n+\frac{1}{2}}\|_2^2. \end{aligned} \tag{4.51}$$

The estimate for the remaining terms turns out to be more straightforward:

$$\begin{aligned}\beta\langle \nabla_h \overline{\boldsymbol{U}}^{n+\frac{1}{2}} \tilde{\boldsymbol{e}}_d^{n+\frac{1}{2}}, \Delta_h \boldsymbol{e}_d^{n+\frac{1}{2}} \rangle_C &\le \beta C^* \|\tilde{\boldsymbol{e}}_d^{n+\frac{1}{2}}\|_2 \cdot \|\Delta_h \boldsymbol{e}_d^{n+\frac{1}{2}}\|_2 \\ &\le \frac{2(\beta C^*)^2}{\gamma}\|\tilde{\boldsymbol{e}}_d^{n+\frac{1}{2}}\|_2^2 + \frac{\gamma}{8}\|\Delta_h \boldsymbol{e}_d^{n+\frac{1}{2}}\|_2^2, \end{aligned} \tag{4.52}$$

$$\begin{aligned}(1+\beta)\langle (\nabla_h \overline{\boldsymbol{U}}^{n+\frac{1}{2}})^T \tilde{\boldsymbol{e}}_d^{n+\frac{1}{2}}, \Delta_h \boldsymbol{e}_d^{n+\frac{1}{2}} \rangle_C &\le (1+\beta) C^* \|\tilde{\boldsymbol{e}}_d^{n+\frac{1}{2}}\|_2 \cdot \|\Delta_h \boldsymbol{e}_d^{n+\frac{1}{2}}\|_2 \\ &\le \frac{2(1+\beta)^2 (C^*)^2}{\gamma}\|\tilde{\boldsymbol{e}}_d^{n+\frac{1}{2}}\|_2^2 + \frac{\gamma}{8}\|\Delta_h \boldsymbol{e}_d^{n+\frac{1}{2}}\|_2^2. \end{aligned} \tag{4.53}$$

The other three nonlinear coupled terms in (4.49) will be canceled by the associated inner products in the moment equation. As a result, a substitution of (4.50)–(4.53) into (4.49) leads to

$$\begin{aligned}&(\|\nabla_h \boldsymbol{e}_d^{n+1}\|^2 - \|\nabla_h \boldsymbol{e}_d^n\|^2) + \gamma\Delta t\|\Delta_h \boldsymbol{e}_d^{n+\frac{1}{2}}\|_2^2 + 2\Delta t\langle \tilde{\boldsymbol{d}}^{n+\frac{1}{2}} \overline{\boldsymbol{e}}_u^{n+\frac{1}{2}}, \nabla_h \Delta_h \boldsymbol{e}_d^{n+\frac{1}{2}} \rangle_1 \\ &\quad - 2\Delta t\langle (\beta \nabla_h \overline{\boldsymbol{e}}_u^{n+\frac{1}{2}} + (1+\beta)(\nabla_h \overline{\boldsymbol{e}}_u^{n+\frac{1}{2}})^T)\tilde{\boldsymbol{d}}^{n+\frac{1}{2}}, \Delta_h \boldsymbol{e}_d^{n+\frac{1}{2}} \rangle_C \\ \le &\Delta t\|\nabla_h \boldsymbol{\tau}_d^{n+1}\|_2^2 + D_9^n \Delta t\|\boldsymbol{e}_d^{n+\frac{1}{2}}\|_2^2 + D_{10}^n \Delta t\|\tilde{\boldsymbol{e}}_d^{n+\frac{1}{2}}\|_2^2 \\ &+ D_{11}^n \Delta t\|\nabla_h \boldsymbol{e}_d^{n+\frac{1}{2}}\|_2^2 + D_{12}^n \Delta t\|\nabla_h \tilde{\boldsymbol{e}}_d^{n+\frac{1}{2}}\|_2^2, \quad \text{with} \\ &D_9^n = 50\varepsilon^{-4}((C^*)^2 + (M_6)^2)^2, \quad D_{10}^n = 4(CC^* + (2\beta^2 + 2\beta + 1)(C^*)^2)\gamma^{-1} + 4\varepsilon^{-4}, \\ &D_{11}^n = 50\varepsilon^{-4}((C^*)^2 + (M_6)^2)^2 + 1, \quad D_{12}^n = 4CC^*\gamma^{-1}. \end{aligned} \tag{4.54}$$

4.6. The convergence estimate

The optimal rate convergence result is stated in the following theorem.

Theorem 4.1. *Assume the homogeneous boundary condition and initial data $\boldsymbol{d}^0, \boldsymbol{u}^0 \in C^6(\overline{\Omega})$ are given, and suppose the unique solution to the Ericksen-Leslie system has the required regularity. If Δt and h are sufficiently small enough with $n\Delta t \le T$, the following the error estimate holds:*

$$\|\boldsymbol{e}_d^n\|_2 + \|\nabla_h \boldsymbol{e}_d^n\|_2 + \|\boldsymbol{e}_u^n\|_2 + \Big(\Delta t \sum_{m=1}^{n} \|\Delta_h \tilde{\boldsymbol{d}}^{n+\frac{1}{2}}\|_2^2\Big)^{\frac{1}{2}} \le C(\Delta t^2 + h^2), \tag{4.55}$$

where $C > 0$ is independent of Δt and h.

Proof. A combination of (4.32), (4.48) and (4.54) yields

$$\begin{aligned}
&\|\boldsymbol{e}_u^{n+1}\|_2^2-\|\boldsymbol{e}_u^{n}\|_2^2+\lambda(\|\boldsymbol{e}_d^{n+1}\|_2^2+\|\nabla_h\boldsymbol{e}_d^{n+1}\|_2^2-\|\boldsymbol{e}_d^{n}\|_2^2-\|\nabla_h\boldsymbol{e}_d^{n}\|_2^2)+\|\boldsymbol{e}_u^{n+1}-\overline{\boldsymbol{e}}_u^{n+1}\|_2^2\\
&\quad+\frac{\nu\Delta t}{2}\|\nabla_h\overline{\boldsymbol{e}}_u^{n+\frac{1}{2}}\|_2^2+\gamma\lambda\Delta t\|\Delta_h\boldsymbol{e}_d^{n+\frac{1}{2}}\|_2^2\\
&\le\lambda\Delta t\|\boldsymbol{\tau}_d^{n+1}\|_2^2+\Delta t\|\boldsymbol{\tau}_u^{n+1}\|_2^2+\lambda\Delta t\|\nabla_h\boldsymbol{\tau}_d^{n+1}\|_2^2\\
&\quad+\lambda\Delta t(D_1^n+D_9^n)\|\boldsymbol{e}_d^{n+\frac{1}{2}}\|_2^2+\Delta t(\lambda D_3^n+D_8^n+\lambda D_{10}^n)\|\tilde{\boldsymbol{e}}_d^{n+\frac{1}{2}}\|_2^2\\
&\quad+\lambda\Delta t(D_2^n+D_{11}^n)\|\nabla_h\boldsymbol{e}_d^{n+\frac{1}{2}}\|_2^2+\lambda D_{12}^n\Delta t\|\nabla_h\tilde{\boldsymbol{e}}_d^{n+\frac{1}{2}}\|_2^2\\
&\quad+D_6^n\Delta t\|\overline{\boldsymbol{e}}_u^{n+\frac{1}{2}}\|_2^2+D_7^n\Delta t\|\tilde{\boldsymbol{e}}_u^{n+\frac{1}{2}}\|_2^2\\
&\quad+\lambda D_4^n\Delta t\|\overline{\boldsymbol{e}}_u^{n+\frac{1}{2}}\|_4^2+D_{12}^n\Delta t\|\boldsymbol{e}_d^{n+\frac{1}{2}}\|_\infty^2+D_{13}^n\Delta t\|\tilde{\boldsymbol{e}}_d^{n+\frac{1}{2}}\|_3^2+D_{14}^n\Delta t\|\nabla_h\boldsymbol{e}_d^{n+\frac{1}{2}}\|_3^2,
\end{aligned}\tag{4.56}$$

with $D_{12}^n=2\varepsilon^{-4}(C_6+C_7+C_9)$, $D_{13}^n=2\varepsilon^{-4}(2C^2+C_8+C_{10})$, $D_{14}^n=2\varepsilon^{-4}C_6$. In particular, we notice that the nonlinear and coupled inner product terms, namely, $2\Delta t\langle\tilde{\boldsymbol{d}}^{n+\frac{1}{2}}\overline{\boldsymbol{e}}_u^{n+\frac{1}{2}},\nabla_h\Delta_h\boldsymbol{e}_d^{n+\frac{1}{2}}\rangle_1$, $-2\Delta t\langle\beta\nabla_h\overline{\boldsymbol{e}}_u^{n+\frac{1}{2}},\Delta_h\boldsymbol{e}_d^{n+\frac{1}{2}}\rangle_C$, and $\langle(1+\beta)(\nabla_h\overline{\boldsymbol{e}}_u^{n+\frac{1}{2}})^T\tilde{\boldsymbol{d}}^{n+\frac{1}{2}},\Delta_h\boldsymbol{e}_d^{n+\frac{1}{2}}\rangle_C$, have been cancelled between (4.48) and (4.54). This subtle fact is very important in the following analysis.

Recalling the Sobolev inequalities in Lemma 4.1, $\|f\|_3\le C\|f\|_4$, and $\|\nabla_h f\|_3\le C\|\nabla_h f\|_4$, we are able to derive the following estimates, with the help of Young's inequality

$$\begin{aligned}
\lambda D_4^n\|\overline{\boldsymbol{e}}_u^{n+\frac{1}{2}}\|_4^2&\le 2C_2^2\lambda D_4^n(\|\overline{\boldsymbol{e}}_u^{n+\frac{1}{2}}\|_2^2+\|\overline{\boldsymbol{e}}_u^{n+\frac{1}{2}}\|_2^{\frac{1}{2}}\cdot\|\nabla_h\overline{\boldsymbol{e}}_u^{n+\frac{1}{2}}\|_2^{\frac{3}{2}})\\
&\le Q_{C_2,D_4^n,\lambda,\nu}\|\overline{\boldsymbol{e}}_u^{n+\frac{1}{2}}\|_2^2+\frac{\nu}{4}\|\nabla_h\overline{\boldsymbol{e}}_u^{n+\frac{1}{2}}\|_2^2,\\
D_{12}^n\|\boldsymbol{e}_d^{n+\frac{1}{2}}\|_\infty^2&\le 2C_3^2D_{12}^n(\|\boldsymbol{e}_d^{n+\frac{1}{2}}\|_2^2+\|\nabla_h\boldsymbol{e}_d^{n+\frac{1}{2}}\|_2\cdot\|\Delta_h\boldsymbol{e}_d^{n+\frac{1}{2}}\|_2)\\
&\le Q_{C_3,D_{12}^n,\lambda,\gamma}(\|\boldsymbol{e}_d^{n+\frac{1}{2}}\|_2^2+\|\nabla_h\boldsymbol{e}_d^{n+\frac{1}{2}}\|_2^2)+\frac{\lambda\gamma}{4}\|\Delta_h\boldsymbol{e}_d^{n+\frac{1}{2}}\|_2^2,\\
D_{13}^n\|\tilde{\boldsymbol{e}}_d^{n+\frac{1}{2}}\|_3^2&\le C^2D_{13}^n\|\tilde{\boldsymbol{e}}_d^{n+\frac{1}{2}}\|_4^2\\
&\le 2C_2^2C^2D_{13}^n(\|\tilde{\boldsymbol{e}}_d^{n+\frac{1}{2}}\|_2^2+\|\tilde{\boldsymbol{e}}_d^{n+\frac{1}{2}}\|_2^{\frac{1}{2}}\cdot\|\nabla_h\tilde{\boldsymbol{e}}_d^{n+\frac{1}{2}}\|_2^{\frac{3}{2}})\\
&\le Q_{C_2,D_{13}^n,C,\nu}\|\tilde{\boldsymbol{e}}_d^{n+\frac{1}{2}}\|_2^2+\frac{\nu}{4}\|\nabla_h\tilde{\boldsymbol{e}}_d^{n+\frac{1}{2}}\|_2^2,\\
D_{14}^n\|\nabla_h\boldsymbol{e}_d^{n+\frac{1}{2}}\|_3^2&\le C^2D_{14}^n\|\nabla_h\boldsymbol{e}_d^{n+\frac{1}{2}}\|_4^2\\
&\le 2C^2C_2^2D_{14}^n\|\nabla_h\boldsymbol{e}_d^{n+\frac{1}{2}}\|_2^{\frac{1}{2}}\cdot\|\Delta_h\boldsymbol{e}_d^{n+\frac{1}{2}}\|_2^{\frac{3}{2}}\\
&\le Q_{C_2,D_{14}^n,C,\lambda,\gamma}\|\nabla_h\boldsymbol{e}_d^{n+\frac{1}{2}}\|_2^2+\frac{\lambda\gamma}{4}\|\Delta_h\boldsymbol{e}_d^{n+\frac{1}{2}}\|_2^2.
\end{aligned}$$

A substitution of the above inequalities into (4.56) reveals that

$$\begin{aligned}
&\|\boldsymbol{e}_u^{n+1}\|_2^2-\|\boldsymbol{e}_u^{n}\|_2^2+\lambda(\|\boldsymbol{e}_d^{n+1}\|_2^2+\|\nabla_h\boldsymbol{e}_d^{n+1}\|_2^2-\|\boldsymbol{e}_d^{n}\|_2^2-\|\nabla_h\boldsymbol{e}_d^{n}\|_2^2)+\|\boldsymbol{e}_u^{n+1}-\overline{\boldsymbol{e}}_u^{n+1}\|_2^2\\
&+\frac{\nu\Delta t}{4}\|\nabla_h\overline{\boldsymbol{e}}_u^{n+\frac{1}{2}}\|_2^2+\frac{\gamma\lambda\Delta t}{2}\|\Delta_h\boldsymbol{e}_d^{n+\frac{1}{2}}\|_2^2\\
&\le\lambda\Delta t\|\boldsymbol{\tau}_d^{n+1}\|_2^2+\Delta t\|\boldsymbol{\tau}_u^{n+1}\|_2^2+\lambda\Delta t\|\nabla_h\boldsymbol{\tau}_d^{n+1}\|_2^2+H_1^n\Delta t\|\boldsymbol{e}_d^{n+\frac{1}{2}}\|_2^2+H_2^n\Delta t\|\tilde{\boldsymbol{e}}_d^{n+\frac{1}{2}}\|_2^2
\end{aligned}$$

$$+ H_3^n \Delta t \|\nabla_h \boldsymbol{e}_d^{n+\frac{1}{2}}\|_2^2 + H_4^n \Delta t \|\nabla_h \tilde{\boldsymbol{e}}_d^{n+\frac{1}{2}}\|_2^2 + H_5^n \Delta t \|\overline{\boldsymbol{e}}_u^{n+\frac{1}{2}}\|_2^2 + D_7^n \Delta t \|\tilde{\boldsymbol{e}}_u^{n+\frac{1}{2}}\|_2^2, \tag{4.57}$$

with $H_1^n = \lambda(D_1^n + D_9^n) + Q_{C_3,D_{12}^n,\lambda,\gamma}$, $H_2^n = \lambda D_3^n + D_8^n + \lambda D_{10}^n + Q_{C_2,D_{13}^n,C,\nu}$, $H_3^n = \lambda(D_2^n + D_{11}^n) + Q_{C_3,D_{12}^n,\lambda,\gamma} + Q_{C_2,D_{14}^n,C,\lambda,\gamma}$, $H_4^n = \lambda D_{12}^n + \frac{\nu}{4}$, $H_5^n = D_6^n + Q_{C_2,D_4^n,\lambda,\nu}$. Meanwhile, an application of Minkowsiki's inequality could be applied to the numerical errors at time instant $n + \frac{1}{2}$:

$$\begin{aligned}
&\|\boldsymbol{e}_d^{n+\frac{1}{2}}\|_2^2 = \|\frac{1}{2}(\boldsymbol{e}_d^{n+1} + \boldsymbol{e}_d^n)\|_2^2 \le \frac{1}{2}(\|\boldsymbol{e}_d^{n+1}\|_2^2 + \|\boldsymbol{e}_d^n\|_2^2),\ \ \|\nabla_h \boldsymbol{e}_d^{n+\frac{1}{2}}\|_2^2 \le \frac{1}{2}(\|\nabla_h \boldsymbol{e}_d^{n+1}\|_2^2 + \|\nabla_h \boldsymbol{e}_d^n\|_2^2),\\
&\|\tilde{\boldsymbol{e}}_d^{n+\frac{1}{2}}\|_2^2 = \|\frac{3}{2}\boldsymbol{e}_d^n - \frac{1}{2}\boldsymbol{e}_d^{n-1}\|_2^2 \le \frac{9}{2}\|\boldsymbol{e}_d^n\|_2^2 + \frac{1}{2}\|\boldsymbol{e}_d^{n-1}\|_2^2,\ \ \|\nabla_h \tilde{\boldsymbol{e}}_d^{n+\frac{1}{2}}\|_2^2 \le \frac{9}{2}\|\nabla_h \boldsymbol{e}_d^n\|_2^2 + \frac{1}{2}\nabla_h\|\boldsymbol{e}_d^{n-1}\|_2^2,\\
&\|\overline{\boldsymbol{e}}_u^{n+\frac{1}{2}}\|_2^2 = \frac{1}{2}(\|\overline{\boldsymbol{e}}_u^{n+1}\|_2^2 + \|\boldsymbol{e}_u^n\|_2^2) \le \|\boldsymbol{e}_u^{n+1}\|_2^2 + \|\boldsymbol{e}_u^{n+1} - \overline{\boldsymbol{e}}_u^{n+1}\|_2^2 + \frac{1}{2}\|\boldsymbol{e}_u^n\|_2^2,\\
&\|\tilde{\boldsymbol{e}}_u^{n+\frac{1}{2}}\|_2^2 = \|\frac{3}{2}\boldsymbol{e}_u^n - \frac{1}{2}\boldsymbol{e}_u^{n-1}\|_2^2 \le \frac{9}{2}\|\boldsymbol{e}_u^n\|_2^2 + \frac{1}{2}\|\boldsymbol{e}_u^{n-1}\|_2^2.
\end{aligned}$$

As a result, (4.57) could be rewritten as

$$\begin{aligned}
&\lambda(\|\boldsymbol{e}_d^{n+1}\|_2^2 + \|\nabla_h \boldsymbol{e}_d^{n+1}\|_2^2 - \|\boldsymbol{e}_d^n\|_2^2 - \|\nabla_h \boldsymbol{e}_d^n\|_2^2) + \|\boldsymbol{e}_u^{n+1}\|_2^2 - \|\boldsymbol{e}_u^n\|_2^2 + \|\boldsymbol{e}_u^{n+1} - \overline{\boldsymbol{e}}_u^{n+1}\|_2^2\\
&+ \frac{\nu\Delta t}{4}\|\nabla_h \overline{\boldsymbol{e}}_u^{n+\frac{1}{2}}\|_2^2 + \frac{\gamma\lambda\Delta t}{2}\|\Delta_h \boldsymbol{e}_d^{n+\frac{1}{2}}\|_2^2\\
\le& H_1^n \Delta t\|\boldsymbol{e}_d^{n+1}\|_2^2 + (H_1^n + \frac{9}{2}H_2^n)\Delta t\|\boldsymbol{e}_d^n\|_2^2 + \frac{1}{2}H_2^n\Delta t\|\boldsymbol{e}_d^{n-1}\|_2^2\\
&+ H_3^n \Delta t\|\nabla_h \boldsymbol{e}_d^{n+1}\|_2^2 + (H_3^n + \frac{9}{2}H_4^n)\Delta t\|\nabla_h \boldsymbol{e}_d^n\|_2^2 + \frac{1}{2}H_4^n\Delta t\|\nabla_h \boldsymbol{e}_d^{n-1}\|_2^2\\
&+ H_5^n \Delta t\|\boldsymbol{e}_u^{n+1}\|_2^2 + (H_5^n + \frac{9}{2}D_7^n)\Delta t\|\boldsymbol{e}_u^n\|_2^2 + \frac{1}{2}D_7^n\Delta t\|\boldsymbol{e}_u^{n-1}\|_2^2 + H_5^n\Delta t\|\boldsymbol{e}_u^{n+1} - \overline{\boldsymbol{e}}_u^{n+1}\|_2^2\\
&+ \lambda\Delta t\|\boldsymbol{\tau}_d^{n+1}\|_2^2 + \Delta t\|\boldsymbol{\tau}_u^{n+1}\|_2^2 + \lambda\Delta t\|\nabla_h \boldsymbol{\tau}_d^{n+1}\|_2^2.
\end{aligned}$$

Consequently, under the constraint that $H_5^n \Delta t \le 1$, an application of the discrete Gronwall inequality yields the desired convergence estimate (4.55). This completes the proof of Theorem 4.1. □

Remark 4.1. *For simplicity of presentation, we focus on the finite difference scheme over a regular rectangular domain in this work. If an irregular geometric domain is taken into consideration, the finite differenced spatial discretization is not appropriate any more, and the mixed finite element method could be a more appropriate choice. Such a mixed finite element approach has been carefully applied and analyzed for various coupled physical systems [28, 31–33, 35], and its application to the reformulated Ericksen-Leslie system* (1.5)–(1.7) *will be considered in future work.*

Remark 4.2. *If a three dimensional domain* $\Omega = (0, 1)^3$ *is taken into consideration, the numerical scheme* (2.1)–(2.4) *will take the same form; the unique solvability and modified total energy stability analysis will also follow exactly the same process. In the optimal rate convergence analysis and error estimate, it is observed that the discrete Sobolev inequalities in Lemma 4.1 are valid for both the two-dimensional (2D) and three-dimensional (3D) domains. Therefore, we have use the 3-D Sobolev interpolation coefficients, although the mathematical presentation is 2-D, for simplicity of presentation.*

Therefore, all the subsequent estimates are available for both the 2-D and 3-D cases, so that the the convergence result (4.55) *could be carefully derived for the 3-D numerical scheme without essential difficulty. The technical details are left to interested readers.*

5. Numerical experiments

5.1. A preconditioned steepest descent (PSD) iteration solver

By the unique solvability analysis presented in Section 3, the discrete system (2.1)–(2.4) could be reformulated as

$$\mathcal{F}_h(\boldsymbol{d}) = \mathcal{G}_h^{-1}\Big(\frac{\boldsymbol{d}-\boldsymbol{d}^n}{\Delta t}\Big) + \varepsilon^{-2}\Big(\frac{(\boldsymbol{d})^2+(\boldsymbol{d}^n)^2}{2}\cdot\frac{\boldsymbol{d}+\boldsymbol{d}^n}{2} - \frac{3\boldsymbol{d}^n-\boldsymbol{d}^{n-1}}{2}\Big) - \Delta_h\frac{\boldsymbol{d}+\boldsymbol{d}^n}{2} = 0, \tag{5.1}$$

with the discrete linear operators $\mathcal{L}_h$ and $\mathcal{G}_h$ defined as

$$\begin{aligned}\frac{2\mathcal{L}_h(\boldsymbol{\mu})-2\boldsymbol{u}^n}{\Delta t} &+ \frac{1}{2}(\tilde{\boldsymbol{u}}^{n+\frac{1}{2}}\cdot\nabla_h\mathcal{L}_h(\boldsymbol{\mu}) + \nabla_h\cdot(\tilde{\boldsymbol{u}}^{n+\frac{1}{2}}\mathcal{L}_h(\boldsymbol{\mu}))) + \nabla_h p^n - \nu\Delta_h(\mathcal{L}_h(\boldsymbol{\mu})) + \lambda(\nabla_h\boldsymbol{\mu})\tilde{\boldsymbol{d}}^{n+\frac{1}{2}}\\ &+ \lambda\nabla_h\cdot(\beta\boldsymbol{\mu}(\tilde{\boldsymbol{d}}^{n+\frac{1}{2}})^T + (\beta+1)\tilde{\boldsymbol{d}}^{n+\frac{1}{2}}(\boldsymbol{\mu})^T) = 0,\\ \mathcal{G}_h(\boldsymbol{\mu}) &:= \nabla_h\cdot(\tilde{\boldsymbol{d}}^{n+\frac{1}{2}}\mathcal{L}_h(\boldsymbol{\mu})) + (\beta\nabla_h\mathcal{L}_h(\boldsymbol{\mu}) + (1+\beta)(\nabla_h\mathcal{L}_h(\boldsymbol{\mu}))^T)\tilde{\boldsymbol{d}}^{n+\frac{1}{2}} + \gamma\boldsymbol{\mu}.\end{aligned}$$

Notice that $\mathcal{L}_h$ and $\mathcal{G}_h$ are non-symmetric operators with positive eigenvalues (as discussed in Section 3). The following linear iteration could be proposed to solve $\boldsymbol{\mu} = \mathcal{G}_h^{-1}(\boldsymbol{g})$:

$$(\gamma+\omega)\boldsymbol{\mu}^{(k+1)} = -\nabla_h\cdot(\tilde{\boldsymbol{d}}^{n+\frac{1}{2}}\mathcal{L}_h\boldsymbol{\mu}^{(k)}) - (\beta\nabla_h(\mathcal{L}_h\boldsymbol{\mu}^{(k)}) + (1+\beta)(\nabla_h(\mathcal{L}_h\boldsymbol{\mu}^{(k)})^T))\tilde{\boldsymbol{d}}^{n+\frac{1}{2}} + \omega\boldsymbol{\mu}^{(k)} + \boldsymbol{g},$$

where ω is relaxation parameter, $\boldsymbol{\mu}^{(k)}$ and $\boldsymbol{\mu}^{(k+1)}$ denote the k-th and $(k+1)$-th approximate solution to $\mathcal{G}_h(\boldsymbol{\mu}) = \boldsymbol{g}$.

Of course, $\frac{(\boldsymbol{d})^2+(\boldsymbol{d}^n)^2}{2}\cdot\frac{\boldsymbol{d}+\boldsymbol{d}^n}{2}$ in (5.1) is nonlinear, and $\varepsilon^{-2}|\boldsymbol{d}|^2\boldsymbol{d} - \Delta_h\boldsymbol{d}$ is implicit in (5.1), corresponding to the convex part of the free energy functional. On the basis of this fact, we apply the preconditioned steepest descent (PSD) method [43] to solve for (3.16). The key point is to make use of a linearized version of the nonlinear operator as a pre-conditioner. In more details, the preconditioner $\mathcal{J}_h$ is defined as

$$\mathcal{J}_h[\boldsymbol{\psi}] := \frac{1}{\Delta t}\mathcal{G}_h^{-1}(\boldsymbol{\psi}) + \frac{3}{4\varepsilon^2}\boldsymbol{\psi} - \frac{1}{2}\Delta_h\boldsymbol{\psi}.$$

Of course, $\mathcal{J}_h$ is a linear operator with positive eigenvalues. Given the current $\boldsymbol{d}^{(k)}$, we define the following search direction $\boldsymbol{q}^{(k)}$ such that:

$$\mathcal{J}_h\boldsymbol{q}^{(k)} = \boldsymbol{r}^{(k)}, \qquad \boldsymbol{r}^{(k)} := \mathcal{F}_h(\boldsymbol{d}^{(k)}),$$

where $\boldsymbol{r}^{(k)}$ is the nonlinear residual at the $k-$th iteration stage. In fact, this equation can be efficiently implemented by an fast Fourier transformation (FFT) solver. Subsequently, the next iterative stage's solution can be obtained by

$$\boldsymbol{d}^{(k+1)} := \boldsymbol{d}^{(k)} + \boldsymbol{\alpha}^{(k)}\boldsymbol{q}^{(k)} = (d_1^{(k)} + \alpha_1^{(k)}q_1^{(k)}, d_2^{(k)} + \alpha_2^{(k)}q_2^{(k)})^T,$$

where $\boldsymbol{\alpha}^{(k)} = (\alpha_1^{(k)}, \alpha_2^{(k)}) \in \mathbb{R}^2$ is the unique solution of the following $\boldsymbol{q}^{(k)}$:

$$\Big((\mathcal{F}_h(\boldsymbol{d}^{(k)} + \boldsymbol{\alpha}^{(k)}\boldsymbol{q}^{(k)}))_1, q_1^{(k)}\Big) = 0,$$
$$\Big((\mathcal{F}_h(\boldsymbol{d}^{(k)} + \boldsymbol{\alpha}^{(k)}\boldsymbol{q}^{(k)}))_2, q_2^{(k)}\Big) = 0.$$

which is a nonlinear problem with respect to $(\alpha_1^{(k)}, \alpha_2^{(k)})$. In more details, the linear part corresponds to a matrix with positive eigenvalues, and the nonlinear part has a positive definite Jacobian matrix (because of the convex energy for the nonlinear implicit part). In turn, such a 2×2 nonlinear system could be very efficiently solved by the Newton iteration:

$$\boldsymbol{\alpha}^{(k+1)} = \boldsymbol{\alpha}^{(k)} - \nabla_\alpha^{-1} \left\langle \mathcal{F}_h(\boldsymbol{d}^{(k)} + \boldsymbol{\alpha}^{(k)}\boldsymbol{q}^{(k)}), \boldsymbol{q}^{(k)} \right\rangle_C \left\langle \mathcal{F}_h(\boldsymbol{d}^{(k)} + \boldsymbol{\alpha}^{(k)}\boldsymbol{q}^{(k)}), \boldsymbol{q}^{(k)} \right\rangle_C .$$

Fortran code was used in the numerical implementation of the proposed scheme. At each time step, only a few Poisson-like solvers are needed at each PSD iteration stage to obtain the search direction $\boldsymbol{q}^{(k)}$. Meanwhile, the solver for the parameter vector $\boldsymbol{\alpha}^{(k)}$ is only involved with two monotone algebraic equations, so that the computation cost is almost negligible. In addition, a few Poisson-like solvers correspond to the most computation costs at each PSD iteration stage. On the other hand, a geometric iteration convergence rate has been theoretically justified in [43] for the PSD iteration to the regularized convex optimization problems, and we expect a similar geometric convergence rate for the PSD iteration used in this article. As a result, only 10–15 Poisson-like solvers are needed in the numerical implementation of the proposed numerical scheme at each time step, which turns out to be a very efficient approach for such a highly nonlinear and coupled numerical system.

5.2. Convergence test and numerical examples

Example 5.1. We will test the numerical accuracy for the numerical scheme in (2.1)–(2.4). The domain is taken as $\Omega = (-1, 1)^2$, and the exact solutions $\boldsymbol{d}_e$, $\boldsymbol{u}_e$, p_e are chosen as follows:

$$\boldsymbol{d}_e(x, y, t) = \frac{1}{2\pi}\Big(\sin(2\pi x)\cos(2\pi y), \cos(2\pi x)\sin(2\pi y)\Big)^T \cos(t),$$
$$\boldsymbol{u}_e(x, y, t) = \frac{1}{2\pi}\Big(-\sin(2\pi x)\cos(2\pi y), \cos(2\pi x)\sin(2\pi y)\Big)^T \cos(t),$$
$$p_e(x, y, t) = \frac{1}{2\pi}\cos(2\pi x)\cos(2\pi y)\cos(t).$$

The physical parameters are set as $\varepsilon = 0.5$, $\nu = 0.5$, $\lambda = 1$, $\beta = -0.5$, and $\gamma = 2$, and a periodic boundary condition is taken. Moreover, an artificial time-dependent forcing term has to be added to make $(\boldsymbol{d}_e, \boldsymbol{\mu}_e, \boldsymbol{u}_e, p_e)$ satisfy the original Erickson-Leslie system (1.1)–(1.3). In the numerical implementation, the numerical system in (2.1)–(2.4) is solved in the equivalent form (5.1). The PSD iteration algorithm, introduced in the previous subsection, will be used, combined with the linear iterative solver (5.1) to obtain $\mathcal{G}^{-1}\boldsymbol{g}$.

In this example, we set time step size as $\Delta t = Ch$ with $h = \frac{1}{N}$, so that the time step and spacial mesh sizes are of the same order. The final time is taken to be $T = 0.1$, and the numerical resolution is given with $N = 16, 32, 64, 128, 256$.

Table 1 displays the numerical errors of d_1, d_2, u, v in the ℓ^2 norm; an almost perfect second-order numerical accuracy is clearly observed. The associated ℓ^∞ numerical errors are presented Table 2, which also indicates an almost perfect second-order accuracy.

Table 1. Errors of $\boldsymbol{d}$, $\boldsymbol{u}$, and p in the ℓ^2 norm ($\Delta t = 0.1h$, $T = 0.1$).

mesh	$\|\boldsymbol{d} - \boldsymbol{d}_e\|_2$	rate	$\|\boldsymbol{u} - \boldsymbol{u}_e\|_2$	rate	$\|p - p_e\|_2$	rate
16^2	2.13E-03		2.05E-03		7.74E-03	
32^2	5.56E-04	1.935703	5.29E-04	1.951707	2.03E-03	1.930202
64^2	1.46E-04	1.929653	1.39E-04	1.930576	5.13E-04	1.985084
128^2	3.96E-05	1.880546	3.78E-05	1.875682	1.28E-04	1.997667
256^2	1.15E-05	1.789707	1.10E-05	1.780659	3.21E-05	2.000128

Table 2. Errors of $\boldsymbol{d}$, $\boldsymbol{u}$, and p in the ℓ^∞ norm ($\Delta t = 0.1h$, $T = 0.1$).

mesh	$\|\boldsymbol{d} - \boldsymbol{d}_e\|_\infty$	rate	$\|\boldsymbol{u} - \boldsymbol{u}_e\|_\infty$	rate	$\|p - p_e\|_\infty$	rate
16^2	1.10E-03		1.04E-03		3.41E-03	
32^2	2.81E-04	1.976774	2.66E-04	1.972873	8.32E-04	2.033039
64^2	7.31E-05	1.93969	6.95E-05	1.935811	2.07E-04	2.006647
128^2	1.98E-05	1.88298	1.89E-05	1.876942	5.19E-05	1.995021
256^2	5.73E-06	1.790305	5.50E-06	1.780907	1.32E-05	1.980892

In the next three examples, we will perform a numerical simulation of liquid crystal defects under various parameter settings.

Example 5.2. Annihilation of singularities. We pick this example from the reference works [20, 44]. The domain is given by $\Omega = (-1, 1)^2$, and the parameters are taken as $\lambda = \nu = \gamma = 1$, and $\varepsilon = 0.05$. The temporal and spatial numerical resolutions are set as: $\Delta t = 10^{-4}$, $N_x = N_y = 64$. Initially, the phase variable $\boldsymbol{d}$ has two singularities at $\pm\frac{1}{2}$. The initial velocity is set as $\mathbf{0}$. Specially, the initial and boundary conditions are listed as follows:

$$\begin{aligned}
&\boldsymbol{d}_0 = \hat{\boldsymbol{d}}/\sqrt{|\hat{\boldsymbol{d}}|^2 + 0.05^2}, \quad \hat{\boldsymbol{d}} = (x^2 + y^2 - 0.25, y),\\
&\boldsymbol{u}_0 = (0, 0),\\
&\boldsymbol{d}|_{\partial\Omega} = \boldsymbol{d}_0/|\boldsymbol{d}_0|, \quad \boldsymbol{u}|_{\partial\Omega} = 0, \quad \nabla_h p|_{\partial\Omega} = 0.
\end{aligned}$$

In Figure 1, the orientation field $\boldsymbol{d}$ of the liquid crystal molecule is displayed at some selected time instants. It is observed that the two singularities at $\pm\frac{1}{2}$ move close to the origin with the evolution of time, until they finally vanish. The annihilation time instant is around $t = 0.2759$. The velocity vector field presented in Figure 2 also reveals that the velocity field is driven by the orientation field, though the initial velocity is zero, and the two swirls are formed afterwards. In addition, the contour plot of the speed field, defined as $|\boldsymbol{u}| = \sqrt{u^2 + v^2}$, is displayed in Figure 3. It is noticed that the velocity vectors presented in Figure 2 have different lengths and directions; in Figure 1, the orientation direction vectors have the same length, i.e., $|\boldsymbol{d}| = 1$.

In Figure 4, we plot the energy curves including the total energy, kinetic energy, elastic energy, and penalty energy. It is observed that the total energy always decays, which agrees with the theoretical result in Theorem 3.2. The total energy has a quick descent at around the time of annihilation, which indicates a phase transition. The kinetic energy increases in the early stage, since the orientation field drives the velocity field (with trivial zero initial data) until the time of annihilation, then it tends to decrease until the orientation field reaches a steady state. The elastic energy denotes the interaction

among the liquid crystal molecules, and it decreases because of the stretching or contraction of the molecules caused by the flow. The penalty energy has a significant descent at around the time of annihilation, which implies that the constraint $|\boldsymbol{d}| = 1$ is well approximated.

Example 5.3. The effects of β and ν on the annihilation time. The parameter β denotes the ratio of the length to the width of the liquid crystal molecule. Because of the different shapes of the molecules, different elastic stress may be produced in the movement. Thus the annihilation time may be affected by the molecular shape. In Table 3, we discover that a bigger β may lead to a longer annihilation time, which indicates that the annihilation time of disc-like molecules is larger than that of rod-like molecules. In Table 4, we list the annihilation times for different viscosities. It is easy to find that a smaller viscosity may cause shorter annihilation time.

Table 3. Annihilation times under different values of β.

β	-1	-0.75	-0.5	-0.25	-0.1
Annihilation time	0.2509	0.2626	0.2759	0.2873	0.2921

Table 4. Annihilation times under different levels of viscosity ν.

ν	1	0.1	0.01	0.001	0.0001
Annihilation time	0.2758	0.2268	0.2145	0.2131	0.2130

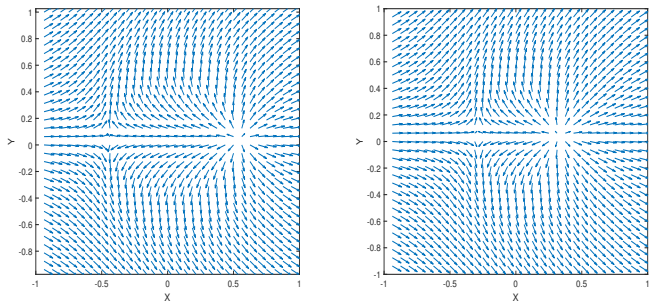

(a) $t = 0$ (b) $t = 0.15$

(c) $t = 0.26$ (d) $t = 0.4$

Figure 1. In Example 5.2, the singularities at $\pm\frac{1}{2}$ move closer to each other until they vanish.

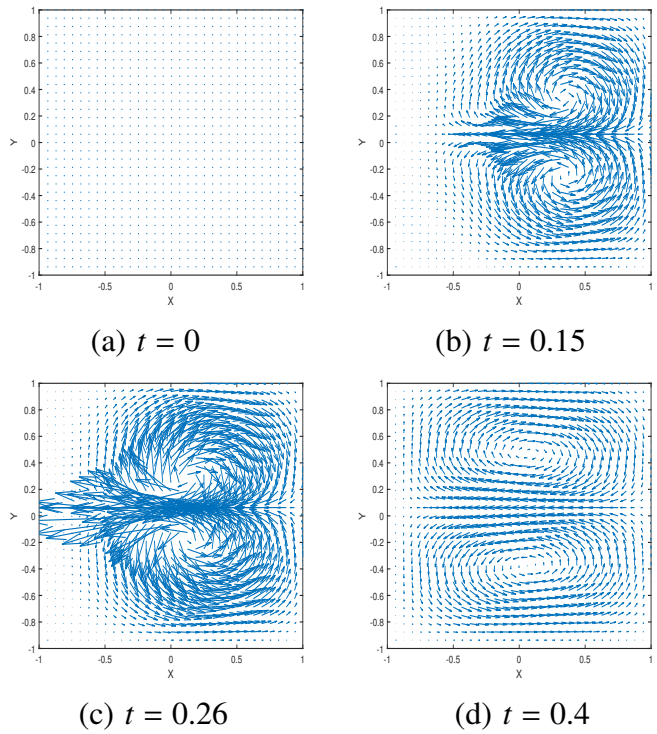

(a) $t = 0$ (b) $t = 0.15$

(c) $t = 0.26$ (d) $t = 0.4$

Figure 2. In Example 5.2, the velocity field is driven by the phase field at different time instants.

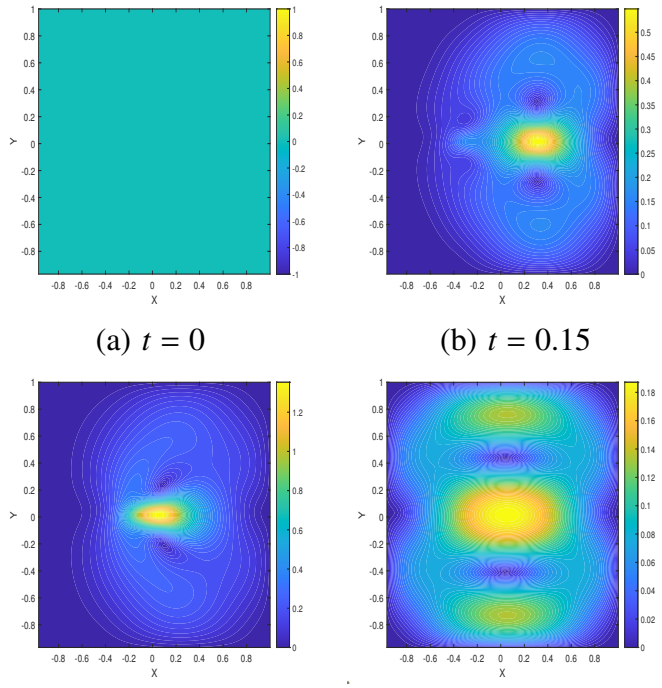

(a) $t = 0$ (b) $t = 0.15$

(c) $t = 0.26$ (d) $t = 0.4$

Figure 3. The contour plot of the speed field in Example 5.2.

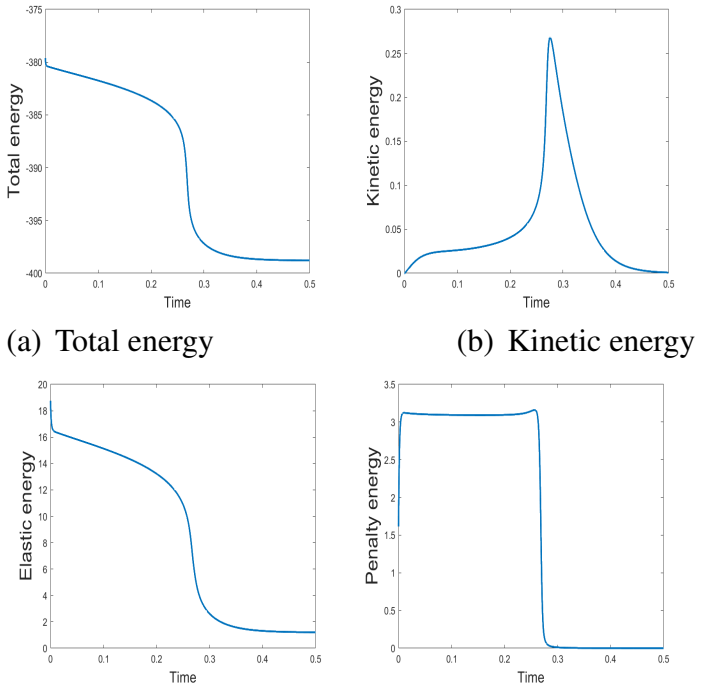

(a) Total energy (b) Kinetic energy

(c) Elastic energy (d) Penalty energy

Figure 4. Example 5.2: The development of energy.

In Figure 5, we see that the total energy and elastic energy decay faster with smaller viscosity $\nu = 1/Re$, while the kinetic energy becomes larger with smaller ν.

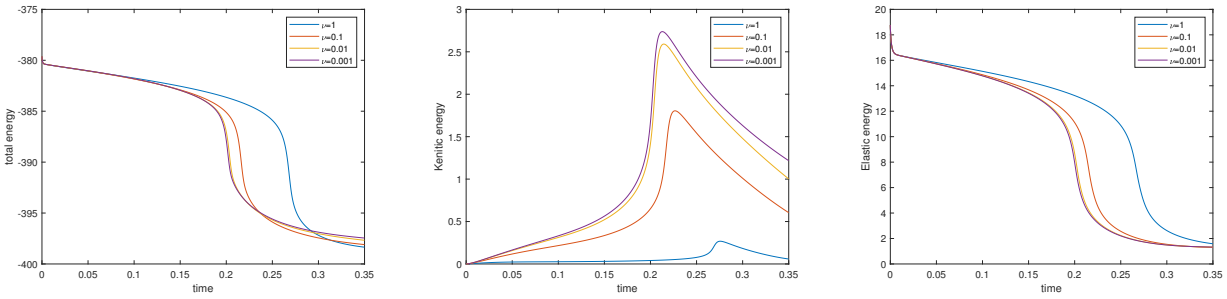

(a) Total energy (b) Kinetic energy (c) Elastic energy

Figure 5. Energy curves with different viscosity ν in Example 5.3.

Example 5.4. Annihilation of singularities in a rotating flow

$$\boldsymbol{d}_0 = \hat{\boldsymbol{d}}/\sqrt{|\hat{\boldsymbol{d}}|^2 + 0.05^2}, \quad \text{where } \hat{\boldsymbol{d}} = (x^2 + y^2 - 0.25, y),$$
$$\text{rotating flow: } \boldsymbol{u} = (-\omega y, \omega x),$$
$$\boldsymbol{d}|_{\partial\Omega} = \boldsymbol{d}_0/|\boldsymbol{d}_0|, \quad \boldsymbol{u}|_{\partial\Omega} = 0, \quad \nabla_h p|_{\partial\Omega} = 0.$$

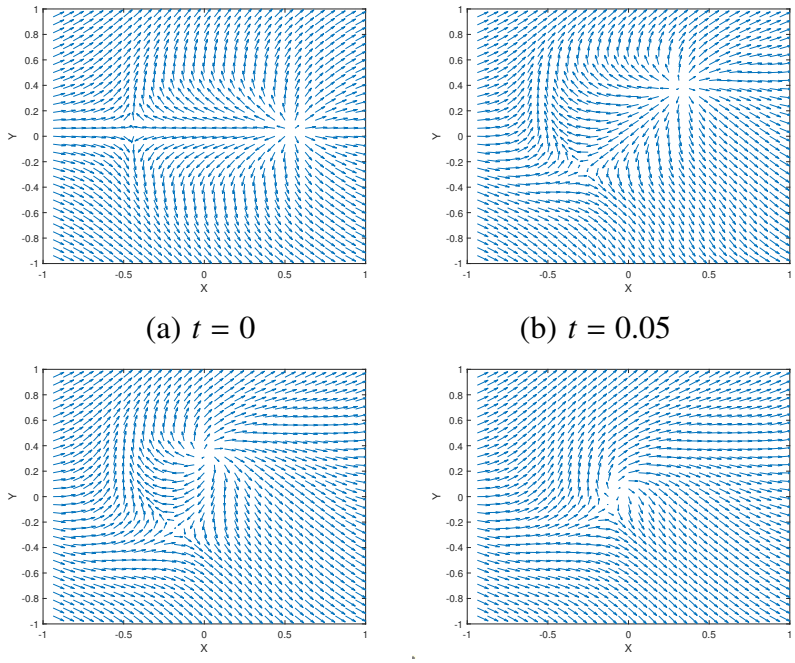

(a) $t = 0$ (b) $t = 0.05$

(c) $t = 0.12$ (d) $t = 0.2$

Figure 6. Orientation field of the liquid crystal molecules under the initial rotating flow $\boldsymbol{u}(\omega = 20)$, in Example 5.4.

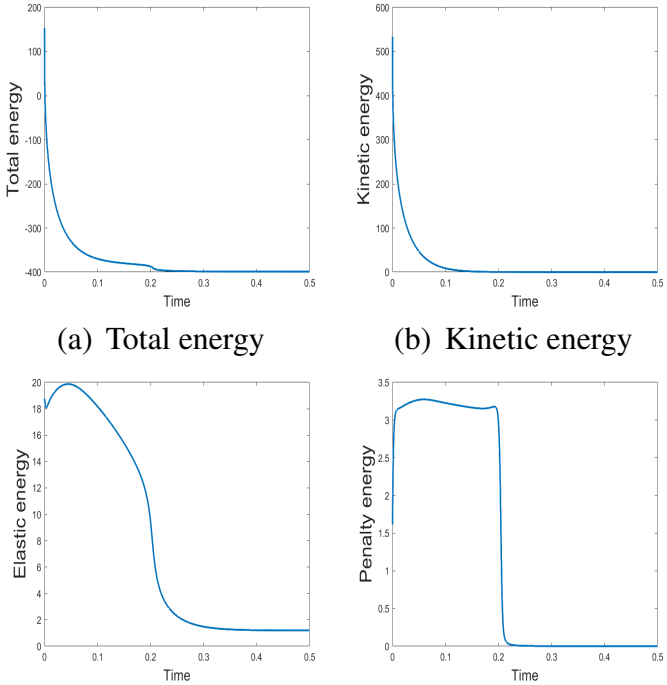

(a) Total energy (b) Kinetic energy

(c) Elastic energy (d) Penalty energy

Figure 7. Energy curves with the rotating flow ($\omega = 20$) in Example 5.4.

Figure 6 displays the annihilation of singularities under rotating flow with ($\omega = 20$). The two singularities move close each other and rotate anticlockwise until the annihilation time $t = 0.2$. In comparison with the case of $\boldsymbol{u}_0 = (0, 0)$, it takes shorter time to reach the annihilation time under the rotating flow.

Energy curves are displayed in Figure 7. It is observed that the total energy and the kinetic energy have the same tendency and there is no significant change around the annihilation time. Initially, the kinetic energy determined by the rotating flow is nonz-ero, and then it decays until the system reaches a steady state accompanying $\boldsymbol{u} = \mathbf{0}$. The elastic energy and the penalty energy display a rather large change at the early stage because the molecular shape is deformed by the rotating flow. These phenomena agree well agreement with the physical law of the liquid crystals' dynamics.

6. Concluding remarks

A second-order accurate Crank-Nicolson style numerical scheme is proposed for the Ericksen-Leslie model, a governing PDE system of nematic liquid crystals. The proposed scheme is based on the convex splitting form of the corresponding free energy functional, while the convection terms in the orientation's evolutionary equation and the momentum equation are treated by semi-implicit approximations. The incompressible Navier-Stokes equation is discretized via the conventional frame of velocity correction method to preserve the divergence-free property at the numerical level. The finite difference spatial approximation is adopted over staggered mesh points, in which the orientation variables are defined over the cell center, the related gradient vectors are defined over the edges of the mesh, and the velocity components are located at the grid points. The unique solvability analysis of the numerical system is theoretically derived, with the help of Browder-Minty lemma. An unconditional stability in terms of the total energy is proved, with a second-order correction of the original energy. Moreover, we provide an optimal rate convergence analysis and error estimate for the fully discrete scheme. The numerical test results have demonstrated the second-order accuracy in both time and space. Some numerical simulations are carried out to demonstrate the effectiveness and robustness of the proposed scheme.

Use of AI tools declaration

The authors declare they have not used Artificial Intelligence (AI) tools in the creation of this article.

Acknowledgments

C. Wang is partially supported by the NSF DMS-2012669 and DMS 2309548. Z. R. Zhang is partially supported by the NSFC No.11871105 and 12231003.

Conflict of interest

The authors declare there are no conflicts of interest.

References

1. P. G. De Gennes, J. Prost, *The Physics of Liquid Crystal*, Oxford University Press, 1993. https://doi.org/10.1093/oso/9780198520245.001.0001
2. J. L. Ericksen, Equilibrium theory of liquid crystals, *Adv. Liq. Cryst.*, **2** (1976), 233–298. https://doi.org/10.1016/B978-0-12-025002-8.50012-9
3. G. Friedel, Les états mésomorphes de la matière, *Ann. Phys.*, **9** (1922), 273–474. https://doi.org/10.1051/anphys/192209180273
4. F. M. Leslie, Theory of flow phenomena in liquid crystals, *Adv. Liq. Cryst.*, **4** (1979), 1–81. https://doi.org/10.1016/B978-0-12-025004-2.50008-9
5. L. Liu, *The Oseen-Frank theory of liquid crystals*, Ph.D thesis, University of Oxford, 2019.
6. M. Doi, Molecular dynamics and rheological properties of concentrated solutions of rod-like polymers in isotropic and liquid crystalline phases, *J. Polym Sci.*, **19** (1981), 229–243. https://doi.org/10.1002/pol.1981.180190205
7. B. Tjipto-Margo, G. T. Evans, The Onsager theory of the isotropic-nematic liquid-crystal transition: Biaxial particles in uniaxial phases, *J. Chem. Phys.*, **94** (1991), 4546–4556. https://doi.org/10.1063/1.460609
8. F. C. Frank, I. Liquid crystals. On the theory of liquid crystals, *Discuss. Faraday Soc.*, **25** (1958), 19–28. https://doi.org/10.1039/df9582500019
9. C. W. Oseen, The theory of liquid crystals, *Trans. Faraday Soc.*, **29** (1933), 883–899. https://doi.org/10.1039/tf9332900883
10. F. H. Lin, C. Y. Wang, Recent developments of analysis for hydrodynamic flow of nematic liquid crystals, *Philos. Trans. R. Soc. London, Ser. A*, **372** (2014), 20130361. https://doi.org/10.1098/rsta.2013.0361
11. H. Wu, X. Xu, C. Liu, Asymptotic behavior for a nematic liquid crystal model with different kinematic transport properties, *Calc. Var.*, **45** (2012), 319–345. https://doi.org/10.1007/s00526-011-0460-5
12. J. R. Huang, F. H. Lin, C. Y. Wang, Regularity and existence of global solutions to the Ericksen-Leslie system in $\mathbb{R}^2$, *Commun. Math. Phys.*, **331** (2014), 805–850. https://doi.org/10.1007/s00220-014-2079-9
13. J. Zhao, X. F. Yang, J. Shen, Q. Wang, A decoupled energy stable scheme for a hydrodynamic phase-field model of mixtures of nematic liquid crystals and viscous fluids, *J. Comput. Phys.*, **305** (2016), 539–556. https://doi.org/10.1016/j.jcp.2015.09.044
14. C. F. Zhou, P. T. Yue, J. J. Feng, The rise of Newtonian drops in a nematic liquid crystal, *J. Fluid Mech.*, **593** (2007), 385–404. https://doi.org/10.1017/S0022112007008889
15. C. F. Zhou, P. T. Yue, J. J. Feng, Dynamic simulation of droplet interaction and self-assembly in a nematic liquid crystal, *Langmuir*, **24** (2008), 3099–3110. https://doi.org/10.1021/la703312f
16. K. Maryna, T. Denis, J. Zhao, W. Timothy, X. F. Yang, C. Alex, et al., Modeling the excess cell surface stored in a complex morphology of bleb-like protrusions, *PLoS Comput. Biol.*, **12** (2016), e1004841. https://doi.org/10.1371/journal.pcbi.1004841

17. R. Chen, W. Z. Bao, H. Zhang, The kinematic effects of the defects in liquid crystal dynamics, *Commun. Comput. Phys.*, **20** (2016), 234—249. https://doi.org/10.4208/cicp.120115.071215a

18. S. P. Zhang, C. Liu, H. Zhang, Numerical simulations of hydrodynamics of nematic liquid crystals: Effects of kinematic transports, *Commun. Comput. Phys.*, **9** (2011), 974–993. https://doi.org/10.4208/cicp.160110.290610a

19. J. Zhao, X. F. Yang, J. Li, Q. Wang, Energy stable numerical schemes for a hydrodynamic model of nematic liquid crystals, *SIAM J. Sci. Comput.*, **38** (2016), A326—A3290. https://doi.org/10.1137/15M1024093

20. P. Lin, C. Liu, H. Zhang, An energy law preserving C^0 finite element scheme for simulating the kinematic effects in liquid crystal dynamics, *J. Comput. Phys.*, **227** (2007), 1411–1427. https://doi.org/10.1016/j.jcp.2007.09.005

21. F. M. Guillén-González, J. V. Gutiérrez-Santacreu, A linear mixed finite element scheme for a nematic Ericksen-Leslie liquid crystal model, *Esaim Math. Model. Numer. Anal.*, **47** (2013), 1433–1464. https://doi.org/10.1051/m2an/2013076

22. K. L. Cheng, C. Wang, S. Wise, An energy stable finite difference scheme for the Ericksen-Leslie system with penalty function and its optimal rate convergence analysis, *Commun. Math. Sci.*, **21** (2023), 1135–1169. https://doi.org/10.4310/CMS.2023.v21.n4.a10

23. C. Liu, J. Shen, X. F. Yang, Dynamics of defect motion in nematic liquid crystal flow: Modeling and numerical simulation, *Commun. Comput. Phys.*, **2** (2007), 1184–1198.

24. J. L. Guermond, P. Minev, J. Shen, An overview of projection methods for incompressible flows, *Comput. Methods Appl. Mech. Eng.*, **195** (2006), 6011–6045. https://doi.org/10.1016/j.cma.2005.10.010

25. Z. Zheng, G. Zou, B. Wang, W. Zhao, A fully-decoupled discontinuous Galerkin method for the nematic liquid crystal flows with SAV approach, *J. Comput. Appl. Math.*, **429** (2023), 115207. https://doi.org/10.1016/j.cam.2023.115207

26. G. Zou, X. Wang, J. Li, An extrapolated Crank-Nicolson virtual element scheme for the nematic liquid crystal flows, *Adv. Comput. Math.*, **49** (2023), 30. https://doi.org/10.1007/s10444-023-10028-0

27. W. B. Chen, W. Q. Feng, Y. Liu, C. Wang, S. M. Wise, A second-order energy stable scheme for the Cahn-Hilliard-Hele-Shaw equation, *Discrete Contin. Dyn. Syst. Ser. B*, **24** (2019), 149–182. https://doi.org/10.3934/dcdsb.2018090

28. W. B. Chen, D. Z. Han, C. Wang, S. F. wang, X. M. Wang, S. M. Wise, Error estimate of a decoupled numerical scheme for the Cahn-Hilliard-Stokes-Darcy system, *IMA J. Numer. Anal.*, **42** (2022), 2621–2655. https://doi.org/10.1093/imanum/drab046

29. W. B. Chen, J. Y. Jing, Q. Q. Liu, C. Wang, X. M. Wang, Convergence analysis of a second-order numerical scheme for the Flory-Huggins-Cahn-Hilliard-Navier-Stokes system, *J. Comput. Appl. Math.*, **450** (2024), 115981. https://doi.org/10.1016/j.cam.2024.115981

30. W. B. Chen, Y. Liu, C. Wang, S. M. Wise, An optimal-rate convergence analysis of a fully discrete finite difference scheme for Cahn-Hilliard-Hele-Shaw equation, *Math. Comp.*, **85** (2016), 2231–2257. https://doi.org/10.1090/mcom3052

31. A. Diegel, C. Wang, X. M. Wang, S. M. Wise, Convergence analysis and error estimates for a second-order accurate finite element method for the Cahn-Hilliard-Navier-Stokes system, *Numer. Math.*, **137** (2017), 495–534. https://doi.org/10.1007/s00211-017-0887-5
32. Y. Liu, W. B. Chen, Y. Liu, C. Wang, S. M. Wise, Error analysis of a mixed finite element method for a Cahn-Hilliard-Hele-Shaw system, *Numer. Math.*, **135** (2017), 679–709. https://doi.org/10.1007/s00211-016-0813-2
33. L. M. Ma, C. Wang, Z. Y. Xia, Convergence analysis of a BDF finite element method for the resistive magnetohydrodynamic equations, *Adv. Appl. Math. Mech.*, **17** (2025), 633–662. https://doi.org/10.4208/aamm.OA-2023-0118
34. C. Wang, J. L. Wang, Z. Y. Xia, L. W. Xu, Optimal error estimates of a second-order projection finite element method for magnetohydrodynamic equations, *Math. Model. Numer. Anal.*, **56** (2022), 767–789. https://doi.org/10.1051/m2an/2022020
35. C. Wang, J. L. Wang, S. M. Wise, Z. Y. Xia, L. W. Xu, Convergence analysis of a temporally second-order accurate finite element scheme for the Cahn-Hilliard-magnetohydrodynamics system of equations, *J. Comput. Appl. Math.*, **436** (2023), 115409. https://doi.org/10.1016/j.cam.2023.115409
36. F. E. Browder, Semigroup approach to nonlinear diffusion equations, in *Nonlinear Elliptic Boundary Value Problems*, (1963), 81–136. https://doi.org/10.1090/S0002-9904-1963-11068-X
37. G. J. Minty, On a "monotonicity" method for the solution of nonlinear equations in Banach spaces, *Proc. Natl. Acad. Sci. U.S.A.*, **50** (1963), 1038–1041. https://doi.org/10.1073/pnas.50.6.1038
38. J. Ding, S. Zhou, Second-order, positive, and unconditional energy dissipative scheme for modified Poisson-Nernst-Planck equations, *J. Comput. Phys.*, **510** (2024), 113094. https://doi.org/10.1016/j.jcp.2024.113094
39. C. Liu, C. Wang, S. Wise, X. Yue, S. Zhou, A second order accurate, positivity preserving numerical method for the Poisson-Nernst-Planck system and its convergence analysis, *J. Sci. Comput.*, **97** (2023), 23. https://doi.org/10.1007/s10915-023-02345-9
40. C. Liu, J. Shen, A phase field model for the mixture of two incompressible fluids and its approximation by a Fourier-spectral method, *Phys. D*, **179** (2003), 211–228. https://doi.org/10.1016/S0167-2789(03)00030-7
41. H. Abels, On a diffuse interface model for two-phase flows of viscous, incompressible fluids with matched densities, *Arch. Ration. Mech. Anal.*, **194** (2009), 463–506. https://doi.org/10.1007/s00205-008-0160-2
42. R. Temam, *Navier-Stokes Equations: Theory and Numerical Analysis*, AMS Chelsea Publishing, **343** (1984). https://doi.org/10.1090/chel/343
43. W. Q. Feng, A. J. Salgado, C. Wang, S. M. Wise, Preconditioned steepest descent methods for some nonlinear elliptic equations involving p-Laplacian terms, *J. Comput. Phys.*, **334** (2017), 45—67. https://doi.org/10.1016/j.jcp.2016.12.046
44. C. Liu, N. J. Walkington, Approximation of liquid crystal flows, *SIAM J. Numer. Anal.*, **37** (2000), 725–741. https://doi.org/10.1137/S0036142997327282
45. W. Wang, L. Zhang, P. W. Zhang, Modelling and computation of liquid crystals, *Acta Numer.*, **30** (2021), 765–851. https://doi.org/10.1017/S0962492921000088

AIMS Press